UNIVERSITÀ DEGLI STUDI DI PADOVA

DIPARTIMENTO DI INGEGNERIA INDUSTRIALE

CORSO DI LAUREA MAGISTRALE IN INGEGNERIA CHIMICA E DEI PROCESSI INDUSTRIALI

Tesi di Laurea Magistrale in Ingegneria

Chimica e dei Processi Industriali

A hybrid chemical and biological process for CO_2 fixation: an analysis based on process simulation

Relatore: Prof. Alberto Bertucco

Correlatore: Prof.ssa Elena Barbera

Laureanda: LUCREZIA PERNA

ANNO ACCADEMICO 2021 - 2022

A mio padre, il cui ricordo resterà
sempre vivo nel mio cuore.

A mio zio Sergio, che mi ha insegnato a scorgere
un delfino in una noce.

Abstract

This thesis is focused on verifying large-scale feasibility of a hybrid chemical and biological process for CO2-fixation, combining carbon dioxide absorption by means of a carbonate-based solvent with microalgal sequestration, where CO2 is fed to the culture in bicarbonates form. A rigorous simulation is carried out using Aspen Plus process simulator to solve material and energy balances, and to check whether this process can be scaled-up at industrial level. The steam methane reforming plant data are taken as the starting point to set up the process simulation. The plant layout includes a first section where the carbon dioxide in the steam methane reforming tail gas is chemically absorbed by using a sodium carbonate aqueous solution. The liquid from the bottom of the column is then fed to the photobioreactor, microalgae are separated from water, which is recycled to the absorption column, after a suitable make up. The model kinetic parameters are obtained from experimental growth data of *Arthrospira Platensis* species measured in laboratory continuous cultivation systems, and takes into account the effect of temperature and light. Simulation results are used to calculate the volume of the photobioreactor and the irradiated area required, as a function of light intensity. Photosynthetic efficiency and electrical energy consumption are also evaluated. Eventually, a reactor design proposal is suggested, and costs related to energy supply to microalgae culture are presented.

Index

Introduction

Nowadays, capturing CO_2 is fundamental in the industrial practice in order to reduce greenhouse gas emissions, which are the main cause of global warming. According to the European Union legislation, the goal is to achieve zero net greenhouse gas emissions by 2050. In this perspective, all industrial sectors have the obligation to set up dedicated sections for carbon dioxide capture and storage. The drawback of storing CO_2 underground or in oceanic depths is that it is an expensive procedure, in terms of both capital and operating costs. In addition, the possibility that carbon dioxide may escape from reservoirs is still to be checked. Another option is that, after capturing it, CO_2 can be employed for other applications. (CCUS, Carbon Capture and Utilization Systems). Recently, among other possibilities, research is strongly focused on carbon dioxide biological fixation by means of microalgae, in order to produce biomass. The assessment of the technical and economic feasibility of this carbon sequestration route is still under investigation.

The purpose of this thesis is to simulate an integrated process that consists in CO_2 absorption by means of a sodium carbonate aqueous solution, and its biological fixation using an *Arthrospira Platensis* culture, where the absorbing solution is recycled. Process simulations are carried out with Aspen Plus® process simulator, while a Fortran® subroutine is employed to account for biomass production reaction, whose parameters are based on experimental measurements at laboratory scale. The industrial scale applicability and the economic evaluation of the energy supply to microalgae culture are assessed.

This thesis is composed by four chapters.

The first chapter describes the state of the art concerning industrial operations for carbon dioxide capture. A comparison among carbon capture and storage (CCS) and carbon capture and utilization (CCU) systems is carried out by an extensive literature search. Eventually, microalgae current research proposals and results as a potential way to fix CO_2 in biomass structure are summarised.

The second chapter is about the thermodynamic and the kinetic model that are employed for process simulations. Specifically, components that are present in the system and the involved equilibria, together with the selected thermodynamic model are considered in detail.

Afterwards, the kinetic model used for biomass production reaction is explained, and the procedure to retrieve parameters values from experimental data is developed and presented.

The third chapter concerns the results of a base case of the integrated process simulations. Four industrial case studies are considered for quantifying the required area using an open pond, namely a gas-fired power plant, a cement production plant, a steel mill and a stream-methane reforming plant. For each case, it is assumed that the flue gas stream is fed to the absorption unit, where at least 90% of CO_2 is captured to be fed to a microalgal cultivation plant. Both the open pond and the closed photobioreactor (PBR) options are considered. For each process unit, simulations set up and results are reported. Then, the integrated process with the nutrients solution recycle operation is simulated and results are given for the base case. Finally, the importance to run the PBR under light compensation condition is discussed.

The fourth chapter is dedicated to propose a possible design for the photobioreactor, and to assess operating costs related to the energy supply for the microalgae culture as a function of the incident light intensity. A comparison among CSTR and PFR performances is also carried out. Following the photobioreactor design proposal results of process simulations using different incident light intensities are presented. For each case, the photosynthetic efficiency, the total irradiated area and the required power are computed, as well as the energy operating costs.

I would like to kindly thank Professor Elena Barbera, whose help and support have been fundamental for this thesis development.

Chapter 1 - CO_2 capture: state of the art and new perspectives

This chapter aims to present the current state of the art concerning CO_2 biological sequestration by microalgae, after describing more mature technologies for carbon dioxide capture briefly. Moreover, microalgal growth conditions, cultivation medium, nutrients and harvesting procedures are discussed. Eventually, the aim of the thesis is explained in the last paragraph.

1.1 Why reducing carbon dioxide emissions?

Several countries have pledged to reach net-zero emissions by 2050, according to the current environmental policy, since nowadays the main challenge is to manage the climate crisis (IEA 2021). Despite renewable sources spread, particularly in the power sector (Barbera *et al*., 2022), carbon dioxide emissions still mostly arise from energy production (JRC science for policy report. Global energy and climate outlook, 2019). Indeed, a decade ago it was already found that human activities are the major cause of global warming (Ring *et al*., 2012). Hence, the energy sector plays a fundamental role in preventing the worst effect of global warming. Reducing carbon dioxide emissions to net-zero by 2050 implies making efforts to phase out the use of fossil fuel, in order to avoid the long-term average global temperature growth of 1.5°C (IEA, 2021). To translate this perspective into reality, the way in which energy is produced, transported and consumed has to be transformed completely (IEA, 2021).

1.2 Carbon dioxide capture traditional technologies

For the afore mentioned reasons, the carbon dioxide produced by industrial activities must first be captured. To do so, several techniques are available, like physical absorption, chemical absorption, membrane filtration, cryogenic distillation or adsorption. Some of them, namely physical and chemical absorption are more mature applications and they have been implemented at industrial scale for years, while the others are less used, since they require high costs or also because they need to be improved.

1.2.1 Physical absorption

In the review written by Ban *et al*., 2014, the main operating conditions and features of CO_2 physical absorption are described: this process consists of a first step which is carried out in the absorber, where the CO_2-rich gas stream is put into counter-current contact with the liquid solvent stream, which must be able to absorb carbon dioxide physically, hence no chemical reactions are involved. In figure 1.1 the process PFD is shown.

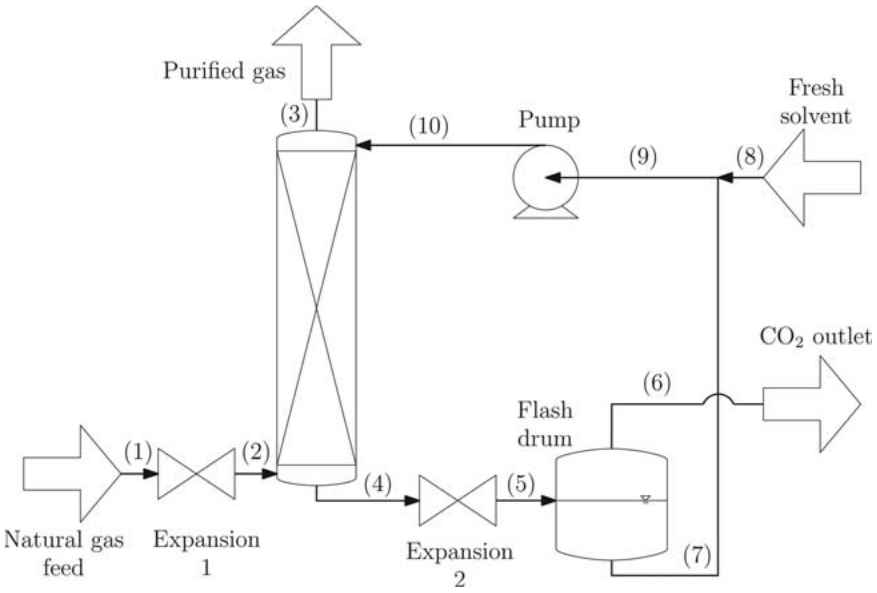

Figure 1.1. *CO_2 physical absorption process scheme (Burger et al., 2015)*

According to this rationale, the carbon dioxide-rich gas stream enters the absorber, where it meets the solvent stream; the driving force that enables CO_2 transfer from the gas phase to the liquid one is its solubility, which is enhanced by operating at high CO_2 partial pressure and low solvent temperature, and it's ruled by Henry's law. The absorption step is followed by the solvent regeneration: in fact, while the purified gas comes out from the top of the absorber, the enriched solution exits at the bottom. It is firstly depressurized and then it is sent to a flash tank or a series of flash tanks, where the absorbed CO_2 is released and the solvent is recovered and, together with some fresh make up, recycled back to the absorption column. The main advantages of this very mature industrial practice are the absence of chemical reactions, that allows for a simple solvent regeneration step by depressurization, in addition to a quite low energy demand, since the significant energy requirement is needed for solvent recycle only (Ban *et al*., 2014). There are several commercial options, concerning the solvents that are

available on the market, such as SELEXOL™ (Dimethyl ether of polyethylene glycol or DEPG), RECTISOL™ (Methanol), IFPEXOL™ (Methanol), PURISOL™ (Normal methyl pyrrolidone or NMP), and so on. All these types of solvents are not only quite selective towards carbon dioxide, but also non-corrosive, which translates into a lower capital cost, since no alloy steel is required as constructing material for pipelines. However, there are some disadvantages, like the loss of lighter hydrocarbons in the solvent regeneration step, since they are inevitably vented together with carbon dioxide (Ban *et al*., 2014).

1.2.2 Chemical absorption

CO_2 chemical absorption can be carried out either using, for example, amines or carbonates solutions as solvents. Chemical absorption is suitable when CO_2 partial pressure is relatively low, as is typically the case with flue gas streams, where CO_2 volume fraction is usually below 10% (Asif *et al*., 2018).

1.2.2.1 Alkanolamines solutions

Carbon dioxide chemical absorption can be achieved by using amine-based solvents. Similarly, to the case of physical absorption, the gaseous stream to be treated enters at the bottom of the absorption column, which is usually a packed one, and is put into contact, according to a counter-current configuration, with the solvent stream fed from the top. Here, absorption takes place through a set of reversible reactions, which are reported in equations 1.1 to 1.4 (Asif *et al*., 2018):

$$2H_2O \leftrightarrows H_3O^+ + OH^- \quad (1.1)$$

$$CO_2 + 2H_2 \leftrightarrows HCO_3^- + H_3O^+ \quad (1.2)$$

$$RNH_2 + H^+ \leftrightarrows RNH_3^+ \quad (1.3)$$

$$2RNH_2 + CO_2 \leftrightarrows RNHCOO^- + RNH_3^+ \quad (1.4)$$

Equation 1.1 shows water ionization, 1.2 represents hydrolysis and ionization of carbon dioxide that is dissolved, 1.3 is the protonation of alkanolamine, and 1.4 displays the carbamate formation. As shown in figure 1.2, after being heated up due to the absorption process, the CO_2-

rich solution is sent to a stripping column, where the reverse mechanism occurs, so that the solvent is regenerated and can be sent back to the absorber (Asif *et al*., 2018).

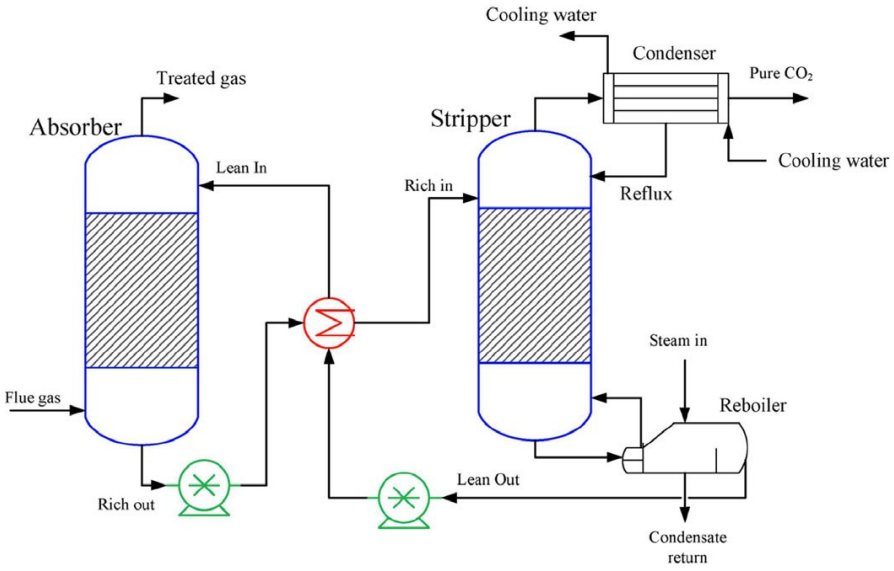

Figure 1.2. *CO_2 chemical absorption by alkanolamines process scheme (Asif et al., 2018)*

Therefore, this configuration translates into an integrated absorption and stripping process for CO_2 capture. Concerning the solvent choice, an alkanolamine aqueous solution is employed, like MEA (mono-ethanolamine) or DGA (diglycolamine), typically at 30%wt; since the previous reactions take place in the absorber, bonds between amines and carbon dioxide build up, but because they are weak, they can be broken by simply heating the rich-out solution (typical reboiler temperatures are up to 120°C). Finally, the purified CO_2 is recovered from the top of the stripper, while the regenerated solvent (lean solution) is recycled back to the absorption column (Bertucco and Barbera, 2019-2020). Some issues related to amine-based solvents include possible thermal degradation, corrosion to equipment and high energy demand for regeneration (Borhani *et al*., 2015), losses through evaporation and, hence, negative environmental impacts (Yamada, 2020), considering that they are toxic compounds (Bertucco and Barbera, 2019-2020). Moreover, assuming that MEA is used as solvent, the energy duty that is required to regenerate it ranges around 4 MJ kg^{-1} of CO_2 captured, which translates into 80% of the total energy consumption related to the process (Asif *et al*., 2018).

1.2.2.2 Carbonate solutions

Another way to carry out chemical absorption of carbon dioxide is to use potassium carbonate in aqueous solution rather than amine-based solvents. The plant section layout is similar to the previous one and it is represented in figure 1.3 (Borhani *et al*., 2015).

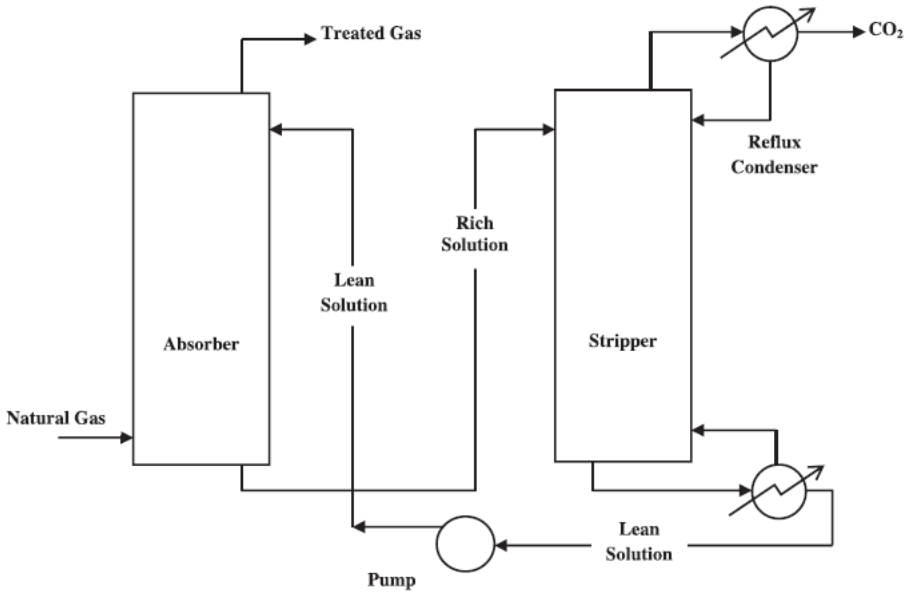

Figure 1.3. *CO_2 chemical absorption by hot potassium carbonate solution process scheme (Borhani et al., 2015)*

The gas stream to be treated enters at the bottom of the absorption column, where it meets the solvent in a counter-current fashion (Borhani *et al*., 2015). As for the amines case, first of all carbon dioxide mass transfer takes place, after which the following reversible reactions take place:

$$CO_2 + H_2O + K_2CO_3 \leftrightarrows 2KHCO_3 \quad (1.5)$$

$$CO_2 + 2H_2O \leftrightarrows HCO_3^- + H_3O^+ \quad (1.6)$$

$$CO_3^{2-} + H_2O \leftrightarrows HCO_3^- + OH^- \quad (1.7)$$

$$CO_2 + CO_3^{2-} + H_2O \leftrightarrows 2HCO_3^- \quad (1.8)$$

Equations from 1.5 to 1.8 (Borhani *et al*., 2015) show what happens in the absorption cycle: the potassium carbonate is transformed into bicarbonate (non-ionic form), as can be seen from the global reaction, which goes through a sequence of elementary steps displayed in the subsequent

equations; the controlling step is the hydration of dissolved CO_2, since its mass transfer is very slow (Borhani *et al*., 2015). While the decarbonised gas goes out from the top of the absorber, the carbon dioxide-rich solution exits from the bottom and goes to the stripper, which works at lower pressure: here, the solvent is regenerated, and it is recycled back to the absorber, while purified CO_2 goes out from the top of the column. Typically, the most suitable potassium carbonate concentration in water ranges between 20 and 40%wt; in addition, in order to avoid precipitation issues, conversion to bicarbonate must be kept under control (Isa *et al*., 2018). The main advantages of this process are enhanced solubility of carbon dioxide in carbonate/bicarbonate solution, together with low solvent toxicity, costs and degradation tendency; on the other hand, in addition to the afore mentioned precipitation issues, there is still the corrosion problem, although it is less remarkable with respect to the amine-based solvent (Borhani *et al*., 2015). As an alternative to potassium carbonate, a sodium carbonate aqueous solution could be used as solvent, but it was found that the latter one shows a less performing absorption rate than K_2CO_3 (Knuutila *et al*., 2010). In the case of potassium carbonate solution, the heat duty at the reboiler that is required to regenerate the solvent is about 2 MJ kg^{-1} of CO_2 captured (Isa *et al*., 2018).

Although carbon dioxide capture by carbonate solution requires less energy than the amines-based process in order to achieve solvent regeneration, the duty at the reboiler is still very high, that is the reason why this thesis focuses on the perspective of capturing CO_2 emitted by industrial activities by using microalgae, since the solvent recovery will be much less energy demanding, as it is going to be explained later on.

1.2.3 Adsorption

Another carbon dioxide capture technology is adsorption, which exploits the formation of physical and chemical bonds between CO_2 and the surface of the adsorbent material (Wilberforce *et al*., 2019). The adsorbent material selection must meet several criteria such as high CO_2 adsorption capacity and selectivity, tolerance to impurities that could be present in the gas to be treated, high kinetics and stability. In addition, the way to regenerate the adsorbent must be taken into account. Depending on the adsorbent nature and on its chemical structure, the adsorption-desorption cycle can be implemented via temperature, pressure or concentration swing (Sayari *et al*., 2011). Focusing on pressure-swing adsorption, the usual configuration

consists in a series of fixed-bed columns that operate at high and low pressure alternatively. At high pressure, carbon dioxide is adsorbed on the adsorbent surface, while at low pressure the regeneration step occurs; it's a cyclical, unsteady-state process, where complete adsorbent regeneration is hardly achieved (Bertucco and Barbera, 2019-2020).

1.2.4 Cryogenic separation

There are several proposals concerning cryogenic CO_2 separation, either from flue gas or natural gas, allowing for high carbon dioxide recovery and purity up to 99.99%, but their industrial application is not so feasible, since they are very high energy demanding. An example could be cryogenic distillation, that is shown in figure 1.4 (Song *et al*., 2019).

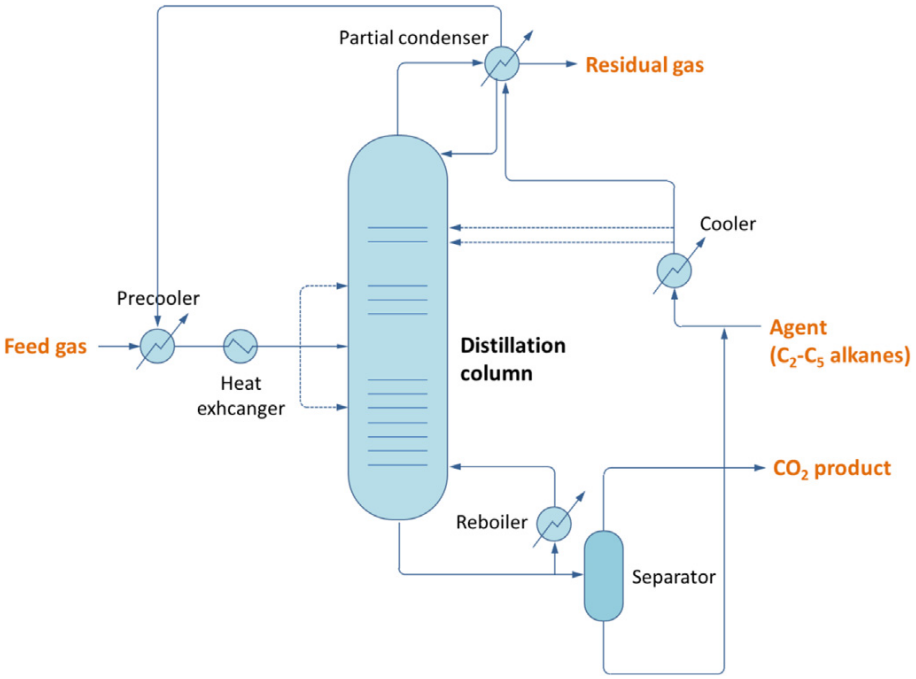

Figure 1.4. *CO_2 capture by cryogenic distillation (Song et al., 2019)*

According to such configuration, the feed stream is cooled and then chilled at low temperature before entering the distillation tower. Here, the condensed carbon dioxide is collected at the bottom of the column, and it is sent to a further separation step, from which purified CO_2 is obtained. Since very low temperatures are reached, the energy required to achieve them

translates into 50% of the plant operating costs (Song *et al*., 2019). It is estimated that the related energy consumption is almost 2 MJ kg^{-1} of CO_2 captured (Shen *et al*., 2022). Due to the fact that high product purity can be attained, further investigations are still going on to make this practice more feasible from the industrial point of view (Song *et al*., 2019). In the review written by Shen et al., 2022, the operating temperature and pressure in the distillation section are -87.43°C and 40 bar respectively, just to purify methane from CO_2, and it is stated that this practice is not suitable for capturing carbon dioxide from flue gases, since its concentration would be too low to make this process feasible (Shen *et al*., 2022).

1.2.5 Membrane separation

According to the review written by Norahim *et al*., 2018, CO_2 removal by membrane separation at industrial scale is mainly implemented to natural gas sweetening. This technique is based on the fact that some of the species present in the gaseous feed are able to permeate the membrane. So, carbon dioxide will diffuse through the membrane pores thanks to the concentration gradient that is guaranteed by a difference in pressure: indeed, on the gas side CO_2 partial pressure is kept high, while on the permeate side it is low. This ensures that a suitable extent of mass transfer occurs, in order to achieve the desired separation. Anyway, there is the need to have a membrane that has both high selectivity and permeability towards carbon dioxide, which results to be quite challenging. The membranes that can be employed for this purpose can be either inorganic, such as zeolites o ceramic-made, or organic, like polymer-made ones. The first ones are more performing, but they are more expensive than the latter ones, and that is the reason why polymeric membranes are used at industrial scale (Norahim *et al*., 2018). Even though membranes are environmental friendly applications and there is quite a big variety of materials that can be used for their construction, there are still some open issues, such as swelling, degradation and fouling, mainly caused by the pollutants that are present in the stream to be treated (Ziobrowski and Rotkegel, 2022).

1.2.6 Innovative carbon capture technologies: X-Prize winners

Very recently, Elon Musk held a competition - XPRIZE Carbon Removal project- aiming to gather ideas for extracting and sequestering carbon dioxide from the atmosphere or oceans (X-Price Foundation, 2022). A brief description of the 23 winning ideas, picked up by X-Price Foundation official web-site follows:

- ACIDD project from the University of Miami - This solution aims to create and distribute "green hydroxide", a form of alkalinity that when added to the ocean, both removes CO_2 and buffers against acid, actively fighting ocean acidification. In creating this hydroxide, hydrogen gas and carbon credits are generated as byproducts. This team is supported by Planetary Hydrogen, the producers of this alkalinity. Their labs based out of the Rosenstiel School for Marine and Atmospheric Sciences will be used to test the effects of alkalinity enhancement on the environment, specifically on coral and fish health. The team mentor, Dr. Chris Langdon has already seen promising results in preliminary testing.
- BJU global challenges from Bob Jones University – This team will develop a verification technology to ensure that carbon that is removed from the air and stored in soil remains in the soil. Starting with a low-cost sensor prototype described in the literature, they will add longer battery life, wireless data logging, and weatherproofing to produce a commercially viable and more widely useful product. Multiple sensors in a field will send data on CO_2 respiration levels wirelessly to a central database. By collecting data from multiple sensors distributed throughout a field, the system can display a contour map of the field's CO_2 levels.
- Environmental sensing from the University of Wyoming – This project affordably measures CO_2 in the natural world to find any changes that could occur at carbon storage sites. These changes could indicate human-caused change in the area from carbon storage as well as any natural changes that could affect the sites used for carbon storage. There is risk in carbon capture and storage if the sites leak, and this technology can detect any potential leaks immediately to allow rapid responses to any carbon storage sites.
- Plant village from Pennsylvania State University – Terrestrial carbon sequestration requires a transparent, low cost system that results in both an accurate and transparent

system to measure not only how much carbon is being pulled down but which areas of the world are our best bets for cost effective drawdown. This use the global platform, PlantVillage, which is an award winning tool used by the UN across 60 countries. This platform integrates phone based AI systems based on computer vision and cloud based systems that integrate multiple satellite streams and soil databases.

- Working trees from Stanford University - Working Trees mission is to deploy trees where the interests of farmers and the climate overlap. This team is developing a technology platform that democratizes access to carbon markets for landowners of all sizes by leveraging smartphone LiDAR, satellite remote sensing data, and machine learning models. The starting focus is on the potential for establishing trees on pasture land in the US Southeast.
- Answer of Biochar (AOB), Northeastern University, China – This group proposes a process route that can significantly improve the economics and scalability of biochar preparation by converting the by-products of biochar production into high value added products with a large market.
- BioCORE, Technical University of Munich, Germany - The BioCORE process employs a novel system design for high-temperature Solid Oxide Cells with complete fuel utilization and CO_2-separation. It can operate either as fuel cell, producing electricity, or as electrolysis unit in the first economically viable Power-to-Gas process. It can switch between both modes within seconds and stabilizes future net-zero energy systems based on non-reliable photovoltaic and wind power. As fuel cell, the innovative BioCORE technology converts valuable biogas into electricity with record-breaking efficiency (80% electrical), while separating pure CO_2, thereby enabling negative emissions at large scale. During electrolysis, BioCORE plants produce hydrogen and solve long-term energy storage issues.
- Biosorra, Iese Business School, Fuqua School of Business Spain - In Sub-Saharan Africa the soil is sick, having supply shortage and hence a direct impact in malnutrition. Burning fields is a quick way to clear farm waste and provide some nutrients to the soil, but it degrades the land. Farmers' lands in Ghana and Kenya are becoming less fertile and producing fewer crops, meaning lower income for the farmers, to spend in modern equipment or sustainable farming techniques. This is the vicious cycle of land degradation. The work of this team is based on transforming crop waste into crop yield by creating a soil improver, that leads to healthier and sustainable soil.

- Bison Underground independent from, but affiliated with University of Oklahoma United States - Farming produces a large amount of carbon, adding to the mounting levels in our atmosphere. This project takes unusable organic material, like stalks and leaves, and turns it in a nutrient-rich mix to add back deep into farming soil. This limits the addition of new carbon to the atmosphere, and also helps farmers to have better yields (facilitating new plants to capture carbon more efficiently), supports communities to be more resilient against extreme weather events (which will intensify with climate change), and promotes food diversity and security for all.
- Blue Symbiosis, University of Tasmania, IMAS, AMC, Australia, Launceston, Tasmania - Blue Symbiosis repurposes oil and gas infrastructure as a stepping stone to scaling seaweed production offshore. The team has a data-driven approach and believes in facing challenging conditions in order to learn to scale seaweed growth beyond the coast. Carbon will be stored in by using seaweed as the basis for fireproof building materials.
- C2 (C-Squared), Virginia Tech, Max Planck Institute, United States, Germany – this team has proposed to capture carbon by crowd-farming bamboo, to store it by building bamboo houses, and to transform the World's housing deficit into a Giga Carbon Warehouse. In the team platform, Farmers find Know-how, Know-where (to grow bamboo) data. Additionally, it provides them access to local Manufacturing units and the marketplace, improving their income. Architects, Designers, Engineers and Entrepreneurs: find a toolkit for transforming Bamboo into valuable and long-lasting products. The toolkit can be deployed in an affordable and modular fashion, based on geolocation of bamboo plantations.
- Carbon Down Under Southern Illinois University, Carbondale, United States - Growing plants naturally take CO_2 out of the atmosphere. Gigatonnes of plant waste is produced annually as an agricultural byproduct. Instead of allowing this waste to rot and return to the atmosphere as CO_2, this proposal aims to convert it into a concentrated tea-like solution and sequester it deep underground. The process that does this uses only water, oxygen, and heat to break down the biomass into water soluble products that can easily be injected deep underground where the carbon will be consumed by subsurface microbes and locked away where it can do no more harm to climate.
- CyanoCapture, University of Oxford, United Kingdom - CyanoCapture is an award-winning startup providing large-scale, affordable carbon capture to polluting industries.

Using the power of modern biotechnology, the team at Oxford University are creating genetically modified microalgae that have been shown to rapidly absorb CO_2continuously and convert this into biomass and oils. CO_2leaving power stations and factories is funnelled directly into CyanoCapture installations, where the gas is bubbled through an extensive network of large raceway ponds containing densely packed GM cyanobacteria. Each 650m x 800m CyanoCapture site is estimated to capture 100,000 tonnes CO_2/year.

- E-quester, University of Toronto, Canada - The E-quester team has developed a novel carbon dioxide direct air capture (DAC) system which is 16% more energy efficient than current commercial systems. This system captures CO_2 from the atmosphere by blowing air through a capture solution. Then, the $CO_2$is released from the capture solution through a pH-swing which allows pure gaseous CO_2 to exit the system and the capture solution to be regenerated in the team innovative Hybrid Electrochemical Regeneration System. This process is entirely electricity driven and can be combined with renewable electricity for minimum carbon emission. The captured CO_2 can then be permanently stored.
- Holocene Climate, Stanford University, United States - Holocene designs and builds chemical plants that remove carbon dioxide from the atmosphere using a novel low-temperature aqueous solvent, with the purpose of storing the CO_2 underground permanently through mineralization.
- KFC, Hohai University, Tianjin University, Shanghai Ocean University, Chinese Academy of Fishery Sciences, China – This project aims to combine deep-water mooring and anchor technology with seaweed aquaculture beds. Mooring and anchor technology has been widely used in oil and gas mining platforms, ocean drilling, and so on. In this way, it’s possible to extend seaweed pastures to deeper and further seas and carry out large-scale planting; by using biological carbon sequestration-the mechanism of seaweed carbon sequestration- carbon removal can be achieved. Seaweed has an efficient carbon fixation capacity, and the economic value of seaweed additional products is high.
- Mississippi State Energy Club-BECReative Energy, Mississippi State University United States - BECReative Energy's goal is to produce renewable energy by utilizing nature's ability to capture and fix CO_2, reducing its atmospheric content. By means of

the gasification of biomass to produce energy while capturing carbon is a solution with potential for exponential growth.

- Monash Carbon Capture and Conversion (BioTech), Monash University, Australia - The amalgamation of independent biological systems that combine to provide efficient and effective carbon removal. With a focus on the development of sustainable and durable solutions to carbon capture, utilisation and storage, Monash Carbon Capture and Conversion presents a solution that facilitates the collaboration of forests and microalgae to generate beneficial organic matter in the form of biochar and engineered timber. Working out of a single facility, the solution centres on the minimisation of waste generation and overall carbon footprint through the use of waste products and renewable energy sources.
- SASIITB, Indian Institute of Technology, Bombay India - The concept used in the study combines Bioenergy with Carbon Capture and Sequestration technology with mineralization for capture and permanent sequestration of the CO_2. The process allows for capture of CO_2 from the flue gas emitted by biomass based industries and the mineralization of the waste(s) generated from the same industry by reacting the waste with the CO_2 rich solvent, while also simultaneously regenerating the solvent, so that the permanent sequestration of CO_2due to the formation of stable mineral carbonates is achieved.
- Skyrenu Technologies, Universite De Sherbrooke and Inrs-Eau Terre Environnement Research Centre, Canada – The idea is about integrated capture and sequestration system comprising a novel modular direct-air capture device whose high-concentration gaseous CO_2 output is used for the on-site carbonation of mine waste, thereby eliminating the need to transport CO_2or mineral feedstock over long distances. Firstly, these systems will be installed at abandoned asbestos mine sites in the province of Quebec in Canada, where 2 Gt of existing mine tailings offer a CO_2sequestration potential of about 700 Mt CO_2, and where the process will be powered by the 100% renewable Hydro-Quebec grid.
- Sydney Sustainable Carbon, University of Sydney Australia – The proposal involves Direct Air Capture of CO_2 (DAC), by means of an adsorbent based on a nanomaterial whose properties can be finely tuned and which can be manufactured at low cost, coupled with deep underground permanent storage. Each DAC module will capture two tonnes of CO_2/year, be solar powered and deployed in their millions. This solution is

hugely scalable with Australia's vast area of non-arable land, high solar intensity and estimated underground storage of over 400 billion tonnes of CO_2, 800 times Australia's yearly emissions.

- Takachar (Safi Organics), University of British Columbia, North-eastern University, IISC Bangalore, Canada, Kenya, United States - The MIT-developed technology enables rapid and profitable scaling of soil carbon sequestration via decentralized, cost-competitive, biochar-based fertilizers improving farmers' yields by 27%. This is done through small-scale, low-cost, portable systems that can latch onto the back of tractors and utilize locally available crop residues/labor, thereby eliminating the biochar distribution costs. The product has improved the net income of ~1,000 farmers in pilot by up to 50%.
- UW-Madison Civil and Environmental Engineering University of Wisconsin, Madison, United States – Use of industrial waste materials to directly capture CO_2 from the atmosphere, which is then stored as a stable mineral; this occurs at ambient conditions and doesn't need any heat input or pressurization, thereby reducing costs and emissions. To safely and permanently sequestering CO_2, the processed waste materials can be further utilized for construction, providing additional economic and environmental benefits.

1.3 CCS and CCU systems

For the reasons already mentioned in paragraph §1.1, reducing greenhouse gas emissions is no longer an option, but a duty. Since the main molecule responsible for greenhouse effect is carbon dioxide, in recent years, research has been focused on how to practically reduce its emissions. Indeed, after capturing CO_2, regardless of the employed technology to do it, it must not be released back to the atmosphere. Accordingly, several options came out concerning the application of CO_2, such as carbon capture and storage systems (CCS) or carbon capture and utilization systems (CCU). In the former case, once carbon dioxide has been captured, it has to be transported to the storage site, for example through a pipeline. Some geological sites have been proposed to this aim, such as ocean depth or depleted basin of abandoned oilfields, given that they possess suitable characteristics for the storage, like porosity and permeability for easy injection of huge volumes, but also the presence of rocky walls for the segregation of carbon

dioxide and prevention of any potential leakages (Wilberforce *et al*., 2019). However, despite geological sequestration and sea disposal, no one can really ensure that leakages would never occur. In addition, this technology requires facing high operating and capital costs without any profit covering them. That is why carbon capture and utilization (CCU) systems have gained a higher attention. As a matter of fact, CO_2 can be used for different applications rather than being stocked. For instance, it can react with quicklime to obtain the calcium carbonate that can be employed in construction materials, or it can be used to synthetize CO_2-based polymers, or for biomass production. Of course, further investigations must be done to verify whether it is possible to scale up such technologies at industrial scale (Lee *et al*., 2020).

1.4 Microalgal CO_2 biological sequestration

As stated in paragraph §1.3, the utilization of captured carbon dioxide would avoid its storage burden. In this regard, a CCU system based on microalgal CO_2 sequestration is a biological process through which the CO_2 captured by any of the afore mentioned technologies is transformed into biomass by microalgae. The biomass that is obtained can be further treated to produce biofuels, cosmetics, building materials or fertilizers (Nguyen *et al*., 2022). In the next paragraphs, microalgal biomass production and the variables that affect it are discussed in detail.

1.4.1 *Cultivation systems*

Microalgae are able to perform photosynthesis by absorbing light and feeding on carbon dioxide, for biomass production (Daneshvar *et al*., 2021). Their capability to capture CO_2 is much greater than the one of terrestrial plants. Microalgae can be cultivated in seawater or in wastewater any time of the year. So far, typical systems employed for this purpose are raceway ponds and closed photobioreactors (PBRs) (Nguyen *et al*., 2022). Raceway ponds are usually made of cement or PVC, they are characterized by a circular shape and by the presence of baffles, so that nutrients mixing is provided to achieve uniform algal growth (Handler et al., 2012). A typical raceway pond is represented in figure 1.5 (Chiaramonti *et al.*, 2012).

Figure 1.5. *Raceway pond, Florence, Italy (Chiaramonti et al., 2012)*

Banerjee and Ramaswamy (2017) carried out a study to assess economic aspects about culturing microalgae in open raceway ponds, and they concluded that even though these systems are the cheapest devices for cultivation, microalgae productivity results to be low. In addition, since they are placed outdoor, such productivity may vary depending on location and climate factors, but also on seasonality. Besides, feeding nutrients to cultures on a large scale perspective still needs to be further investigated (Banerjee and Ramaswamy, 2017). Other problems are related to water losses and contamination by bacteria, moreover light supply would be effective only on the upper layers of ponds (Nguyen *et al*., 2022).

On the other hand, photobioreactors are more promising devices, as they are closed, so that no significant water losses nor contamination would occur. They allow for a better space utilization than open ponds, meaning that a higher biomass productivity can be achieved, together with the possibility of keeping the culture under more stable conditions. PBRs can be designed in many different ways, but their disadvantage is the biofouling issue, which would reduce light supply effectiveness. Anyway, such problem can be overcome by proper design features (Nguyen *et al*., 2022). Clearly, the main drawback of closed PBRs is related to the high capital costs.

1.4.2 Light supply

Light is fundamental for microalgae growth, and the way it is supplied to the culture affects their growth and biomass productivity. Light can be provided by sun or artificially by lamps. However, sunlight is effective only if it is abundant, but it might be not convenient, since it strongly depends on daytime, on the season, weather conditions and also on the location where the culture is placed. Instead artificial lamps can provide continuous and controlled illumination (for example by Light Emitting Diodes, LED), resulting in more controlled conditions and better biomass productivity (Blanken *et al*., 2013), but of course they have a weight on operating costs. The photons from blue to red wavelengths that can be captured by chlorophyll molecules in microalgae depend on the cellular architecture, pigment composition, and chloroplast arrangement. In literature there is evidence that microalgae prefer to grow under either blue (with wavelength of 420–470 nm) or red (with wavelength of 660 nm) light (Schulze *et al*., 2014). Indeed, in the work by Borella *et al*. (2021), it is demonstrated how to reduce energy losses and to increase the photosynthetic efficiency by using tailored LEDs rather than the white ones; this study highlighted the possibility of spreading out artificial light for microalgae cultures, and even if it implies further costs, they could be covered thanks to an enhanced biomass productivity.

1.4.3 Nutrients and culture medium

As reported in the review written by Daneshvar *et al*. (2021), microalgae are cultivated in solutions that are called culture media, which contain all the suitable nutrients for their growth. Nutrients can be classified into macronutrients, micronutrients and trace elements. Such distinction is made considering species amount that is required for microalgal growth. Macronutrients are essentially carbon, nitrogen, and phosphorous, that are need in higher amount. Sulphur, Cobalt, zinc, manganese, potassium and barium are the micronutrients, which are required in a lower amount. There are different recipes for culture media formulation, depending on the type of culture to be grown, so they can be case-specific. Non-specific media are used too and the advantage of the latter ones is that they can host several types of microalgae cultivations (or consortia). A lot of research is available on the possible media formulations and tests. Since microalgae can grow in wastewater, the latter one has been tested, and it was found

that not only it contains some of the nutrients, but being enriched with phosphorous and nitrogen, it becomes suitable culture medium (Daneshvar *et al*., 2021). According to the reference biomass formula $C_{106}H_{263}O_{110}N_{16}P$, 358 mg L^{-1} of carbon, 63 mg L^{-1} of nitrogen and 9 mg L^{-1} of phosphorous are the concentrations required to obtain 1 kg of microalgal biomass (Salama *et al*., 2017). What needs to be always checked is the amount of carbon, nitrogen and phosphorous in the medium, since they are the main nutrients, so that no limitations in microalgal growth would occur. Some other conditions have to be considered, like pH and temperature. Concerning pH, it usually ranges between 5 and 10, depending on the microalgal species, but the optimal growth is generally achieved around a pH of 8. For temperature, the general most suitable value is between 20°C and 36°C. Anyway, there are some species that may survive at largely basic or acid pH, or even at high temperatures around 50°C (Daneshvar *et al*., 2021).

1.4.4 CO_2 supply

As already stated above, carbon dioxide is one of the essential nutrients for microalgal growth, and there are several ways through which it can be supplied to the culture. If the carbon dioxide source is air, or flue gas or compressed CO_2, it can be injected in the culture medium by spargers, that can be placed at the bottom of the photobioreactor. It should be specified that the concentration of the dissolved CO_2 in equilibrium with the atmospheric air is strongly limiting for microalgal growth. Therefore, enriched streams with at least 2% vv CO_2 should be employed. In any case, the main problem concerns the low mass transfer rate of carbon dioxide through the medium, that eventually ends up in a lower carbon supply for microalgae, and therefore into low capture rates (Nguyen *et al*., 2022). In literature, there are several studies concerning carbon dioxide supply by direct injection of air and flue gas. For instance, in the work done by Centeno Da Rosa *et al*., 2011, *Chlorella vulgaris* and *Spirulina* microalgae strains have been tested both in a photobioreactor and in an open raceway pond. Air with variable CO_2 concentration, namely at 6%, 12% and 18% in volume, was injected directly at the bottom of both systems, where cultures were grown batch-wise for 20 days. Both microalgae species kept on growing event at 18%vv of carbon dioxide concentration, so they both resulted to be suitable for CO_2 sequestration at industrial level, but *Spirulina* performed better, since it did not even enter the cellular decline phase up to the 20th day, while *Chlorella* approached the cellular death

at the 11th day (Centeno Da Rosa *et al*., 2011). In another case study, experiments were carried out by Chiu *et al*. (2011): specifically, the first test was run in the laboratory, while the other one in a coal-fired power plant, but in both cases a photobioreactor was employed. For the indoor experience, MTF-7 and WT *Chlorella* strains were tested. A flue gas stream was continuously fed at the bottom of the bioreactor, and as a result the MTF-7 strain showed higher growth and biomass production rates than the WT one, but it also survived up to a temperature of 40°C. Indeed, MTF-7 strain was used for the outdoor experience, that was carried out in a similar way to the first one, but injecting the flue gas from the power plant in two different ways (by continuously feeding the bioreactor for 9 hours, and by doing it in 30 minutes intervals every hour). In both cases, after the flue gas load, air was injected keeping its inlet and outlet compositions under control, in order to check microalgae capture capability. In the case of intermittent flue gas supply, microalgae carbon capture efficiency was about 63% and it kept around this value over all the experiment, while in the continuous case it dropped from 95% to 50%. At the end of this experience, it was concluded that even though flue gas can be an effective carbon source for microalgae, it contains compounds like NO_x and SO_x that are toxic for the culture. In addition, it is known that flue gas is acid, so pH control can be tricky. In fact, it was proposed to set up a system with intermittent flue gas injection, not only for the results obtained, but also because it would act like a pH controller (Chiu *et al*., 2011). Another way of supplying CO_2 to microalgae culture is in the form of bicarbonates: the dissolved inorganic carbon in the medium is due to the presence of CO_2, HCO_3^- and CO_3^{2-}, whose concentrations depend on pH and temperature of the environment. CO_2 can be used directly for photosynthesis, while bicarbonates are generally converted into carbon dioxide first and then used by microalgae, although some species are also able to use the bicarbonates ions too. In such situation, pH ranges around 8, which is the optimal value for the growth, but it must be kept under control, since high alkalinity may be toxic for microalgae (Nguyen *et al*., 2022). A case study concerning carbon dioxide supply as bicarbonates will be presented in the subsequent paragraph.

1.4.5 Harvest procedure and microalgae utilization

Microalgae dimensions are in the order of about 100 μm and they are diluted in the culture medium with typical concentrations in the order of a few g L^{-1}, which is why their harvest is

quite challenging, since a liquid-solid separation has to be carried out avoiding the damage of biomass Several techniques can be used to accomplish this task, such as centrifugation, membrane filtration, flocculation, sedimentation or flotation. Centrifugation drawbacks are expensive equipment employment and high energy consumption. Membrane separation issues are related to organic matter disposal that causes fouling and calls for membrane cleaning or replacement over time. Flocculation is a technique based on three steps that are charge neutralization, bridging and sweeping effect by using flocculant agents, like polymers with tuned properties, and even though the energy demand is minimal, biomass could be polluted by the presence of such chemical agents. Sedimentation requires very long time to harvest microalgae and it is the least efficient technique among the ones discussed. Flotation consists in using air or gas bubbles to bring microalgal cells on the water surface, and it is characterized by a short operation time and low costs. Except membrane separation, all of these are well established technologies, but they can be further improved to overcome the afore mentioned problems related to microalgal harvesting procedure (Nguyen *et al*., 2022). The microalgal biomass can be employed for several applications. Concerning the agricultural field, after the harvesting step, algal biomass can be further processed by pyrolysis, torrefaction or hydrothermal carbonization, in order to change its chemical and physical properties irreversibly, so that algal biochar is obtained. The latter one can be used as land biofertilizer, because it improves soil properties, like nutrients retention, thus it is a promising application to make agriculture more sustainable (Mona *et al*., 2021). Other potential products that can be obtained from microalgal biomass can be biofuels or cosmetic components, but further studies are needed in these fields (Nguyen *et al*., 2022).

1.5 A hybrid process integrating CO_2 absorption and biological sequestration

Considering the limitations of conventional chemical carbon capture, i.e. a high thermal energy duty for solvent regeneration, and of biological carbon capture, i.e. low gas-liquid mass transfer, the possibility of setting up a hybrid process integrating carbon dioxide absorption by means of carbonates and biological sequestration by microalgae can be envisaged. This possibility is described in the review by Song *et al*., 2019, and will be summarized in the next paragraphs.

1.5.1 Process layout conceptualization

The first proposal is about absorbing CO_2 by means of carbonates or amine-based solvents; afterwards, the carbon dioxide-rich solution is sent to the photobioreactor. The process is shown in figure 1.6.

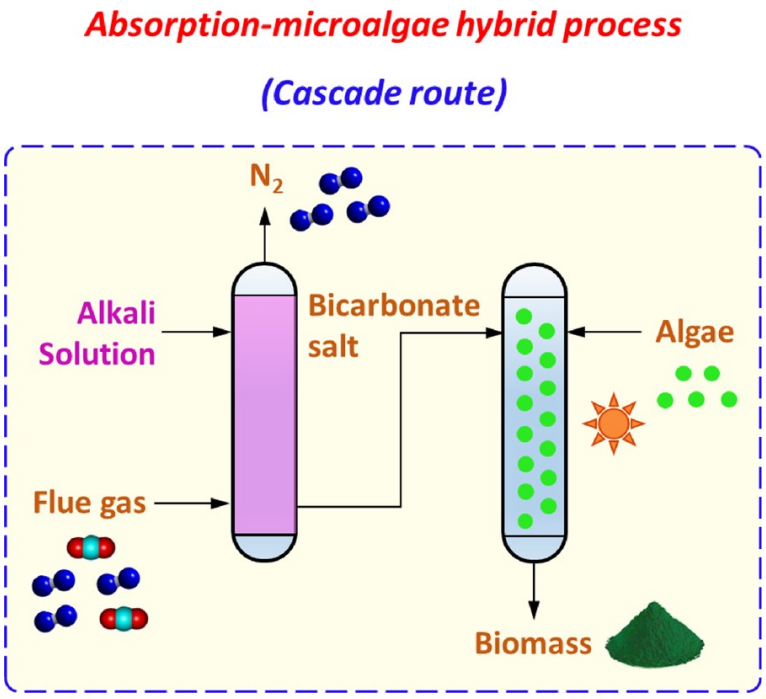

Figure 1.6. *Hybrid process-cascade route (Song et al., 2019)*

According to this idea, the direct contact between the lean carbonates solution and microalgae is avoided, which would be toxic for the microorganisms. Besides, after carbon dioxide sequestration by microalgae, carbonates would potentially be totally regenerated and they could be recycled to the absorption column (Song *et al*., 2019).

A second proposal is to carry out the overall process within the same unit, as shown in figure 1.7.

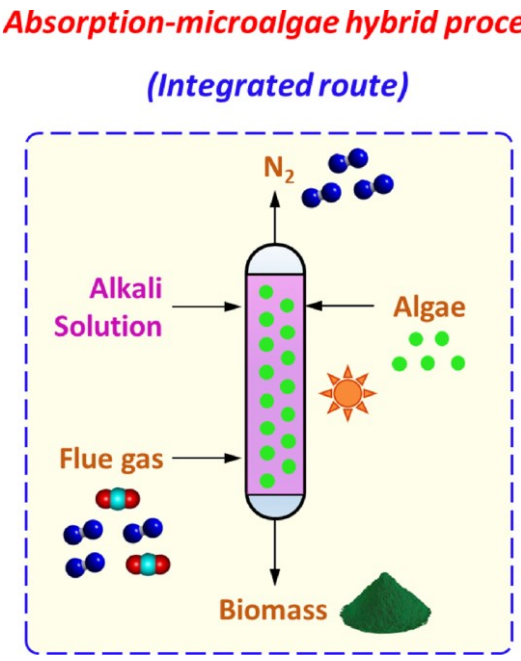

Figure 1.7. *Hybrid process-integrated route (Song et al., 2019)*

Concerning this second configuration, there are several issues related for example to pH: at the top of the column the alkali solution would increase pH too much, while at the bottom flue gas would make pH drop to too low values, both of which would be toxic for the culture. For this reason, the authors suggested to cultivate microalgae batch or semi-batch wise, so that nutrients supply can be modulated and controlled in an easier way (Song *et al*., 2019). Since a continuous process is required on industrial scale, this layout does not seem to be feasible.

Going back to the first proposal, in order to avoid the possibility of too high alkalinity for the culture that eventually may occur, in figure 1.8 two ideas are proposed.

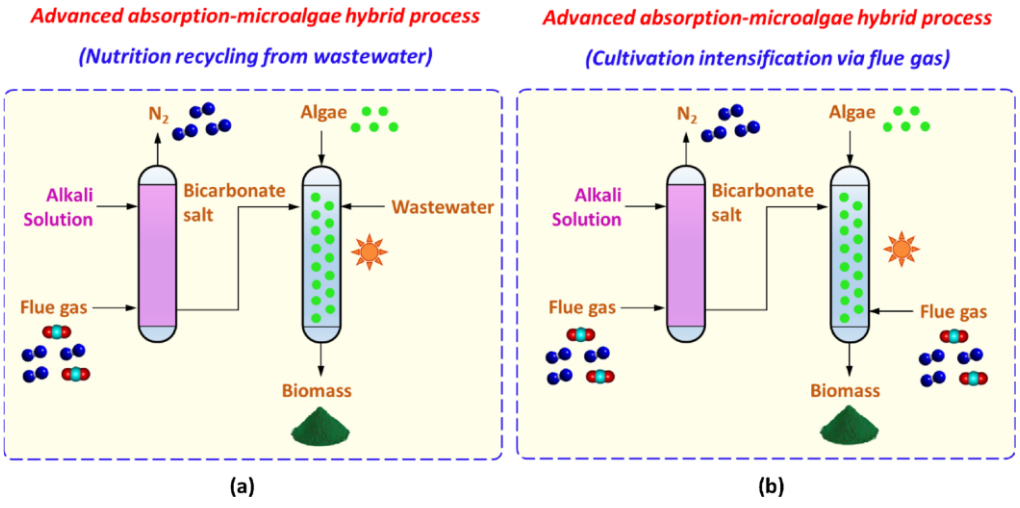

Figure 1.8. *Hybrid process-pH under control (Song et al., 2019)*

In configuration (a) wastewater is used as a source of nutrients to balance pH and keep it at optimal value, while in configuration (b) flue gas is used to achieve the same task. Both wastewater and flue gas are acid and contribute to nutrients supply to the culture, since they contain nitrogen, phosphorous and carbon of course. In this way, the problem of arising pH could be overcome and an additional nutrients source would be available for microalgae (Song *et al*., 2019).

A similar concept was also investigated by Gris *et al*., 2014, whose idea is reported in figure 1.9.

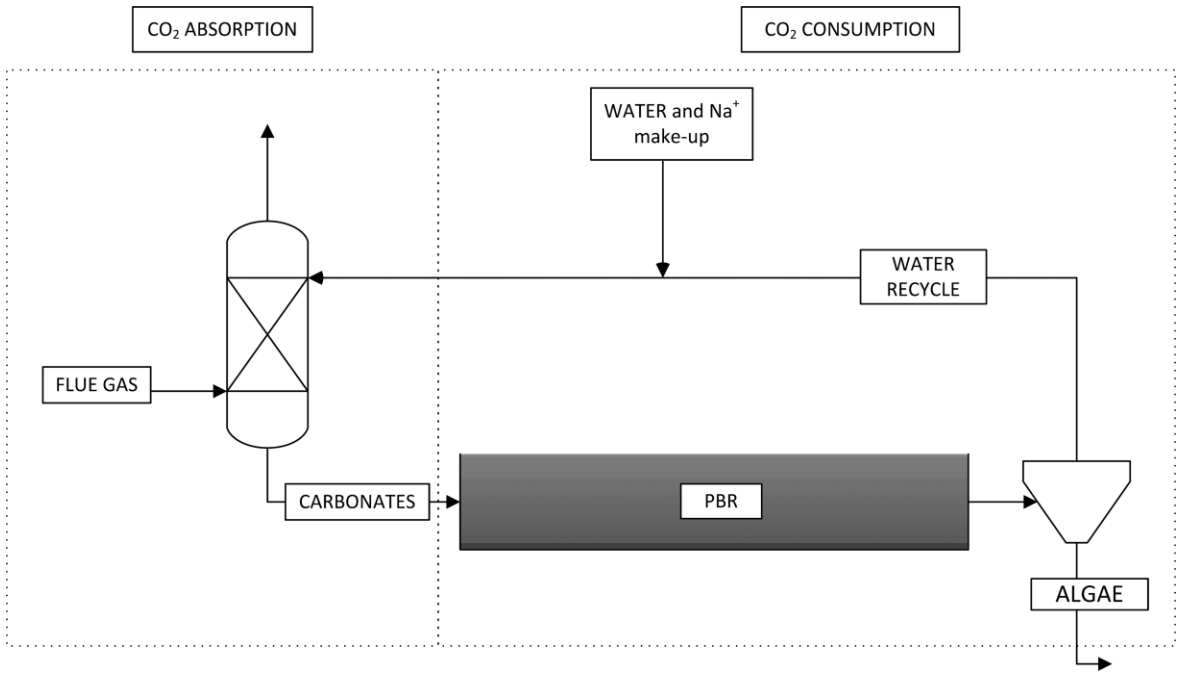

Figure 1.9. *CO_2 capturing from flue gas using carbonates (Gris et al., 2014)*

According to this idea, CO_2 is captured from flue gases by absorption in a solution of sodium carbonate, and fed to the PBR as soluble carbonates, which are then exploited by microalgae as the carbon source to produce biomass. The lean carbonate solution is recirculated back to the absorption section, where a fresh makeup is needed, since part of aqueous solution is lost in the wet biomass. An additional advantage of this approach is the possibility of using the heat released in the absorption step to control the PBR temperature during cold seasons at middle latitudes (Gris *et al*., 2014). From the experiments, that were carried out both in batch and in continuous modes, it was observed that *Chlorella protothecoides* preferably exploits the CO_2 made available in the liquid phase by the shift of carbonate equilibrium, with a consequent pH

increase leading to the inhibition of algal growth at values higher than about 9. Since the chemical control of the pH implies the addition of chemicals like HCl, that would accumulate in the system, a carbonate solution is used in the proposed process, where its flow rate and concentration are adjusted so that the CO_2 uptake by the microalgae is performed within the pH range of viability of algal cells. Experiments demonstrated that *Chlorella protothecoides* is not able to use the bicarbonate ion itself with high efficiency, but a significant growth can be achieved by selecting pH values properly. From the experiments, the best pH value to provide the sufficient carbon concentration as CO_2 resulted to be 7.5. In order to avoid a pH increase up to values for which microalgal growth would be inhibited, it is fundamental to select the recirculating flow rates and carbonates concentration suitably (Gris *et al*., 2014)

It should be mentioned that, while this integrated process looks certainly interesting as a concept, its feasibility on a large scale needs to be verified. Mostly, the efficacy of the biological carbon sequestration and solvent regeneration step strongly depends on the capability of microalgae to grow exploiting a liquid bicarbonate-rich stream as carbon source (i.e., to the possibility of controlling the pH to suitable values).

In the review written by Zhu *et al*., 2022, the bicarbonate-based carbon supply to microalgal cultivation is highlighted. BICCAPS would bring some advantages, like avoiding intensive energy use for carbonate regeneration as well as it would imply lower costs for carbon dioxide compression, transportation and temporary storage. Firstly, microalgal strains with high pH and bicarbonate concentration tolerance must be chosen, indeed *Spirulina sp.* has showed to be the most promising candidate to manage such conditions. The carbon utilization efficiency of *Spirulina sp.* is around 104±2.6%, using 8.4 g L^{-1} of $NaHCO_3$ in the culture, according to one of the experiments reported in this review. Bicarbonate is a low cost approach for carbon supply to the culture, but it really becomes economically feasible only if bicarbonate recycle is possible. For this purpose, some experiments were performed using CO_2 from air for the bicarbonate-based medium regeneration, which does not require carbon dioxide transportation from the emission site and it does not involve the presence of toxic species as flue gas. Anyway, using CO_2 from air has some limitations due to its poor mass transfer rate from the air to the culture medium, but by adjusting the concentration of bicarbonate and carbonate to have high alkalinity, CO_2 can be efficiently captured from air and it can be made available for microalgae photosynthesis, when light is available, achieving a biomass productivity of 1 g L^{-1} per day. An air compression and pumping device driven by renewable energy like wave energy is proposed

as a promising method to implement the process, but further research is required of course, as well as the economic feasibility should be evaluated. Nevertheless, the PBR design is crucial in order to reduce costs and enhance microalgal growth (Zhu *et al*., 2022).

1.5.2 Laboratory tests on batch and semi-continuous cultivations

In literature, several laboratory tests related to biological sequestration of carbon dioxide are present, but only a few concern carbon supply in bicarbonates form. Chi *et al*., 2013 focused on the possibility of setting up a Bicarbonate-based Integrated Carbon Capture and Algae Production System (BICCAPS); they prepared several cultures of the cyanobacterium *Euhalothece*, which showed the capability of using bicarbonates as inorganic carbon supply for the photosynthetic process. Cultures were set up batch-wise in T-flasks, which are the simplest type of photobioreactors. Firstly, they retrieved a correlation between $NaHCO_3$ concentration and pH, by employing a 1M $NaHCO_3$ aqueous solution that was mixed to the culture medium, determining a pH value ranging around 8. To reach an initial pH of 9.50 in the culture, solutions of 0.375 M NaOH and of 0.688 M of Na_2CO_3 were supplied, and then CO_2 was bubbled into this medium to keep pH under control. During this process, samples were taken at different pH levels, in order to measure all the involved species concentrations and the real pKa values of $NaHCO_3$ were determined at concentrations 1.0 and 0.5 M. For the true experiments, solutions at 1 M and 0.5 M of $NaHCO_3$ were used as a source of inorganic carbon, 0.465 g L^{-1} biomass were produced within 5 days which resulted to be an acceptable value, and neither CO_2 bubbling nor NaCl were necessary. It can be predicted that scaling-up this practice will be much easier than the photobioreactor with a complex CO_2 bubbling system, which would be more expensive. Chi *et al*., 2013 concluded that a biomass productivity of 1.21 g L^{-1} d^{-1} was achieved in the culture at the expenses of 0.256 M inorganic carbon that was consumed. Thus, the idea of BICCAPS as a closed-loop CO_2 utilization process seems to be feasible (Chi *et al*., 2013). The experiments conducted by da Rosa *et al*., 2015 concerned *Spirulina* semi-continuous cultivation with nutrients recycle and CO_2 supply by feeding it as a gas. They used Zarrouk culture medium without sodium bicarbonate, indeed they replaced this inorganic carbon source with CO_2 feed at a daily specific flow rate of 0.12 mL_{CO2} mL^{-1}_{medium} d^{-1}, for 1 min h^{-1} during the light period. They made this test both with and without the addition of MEA to the culture medium as nutrients were recycled and they confirmed that thanks to the presence of the

chemical solvent, *Spirulina* carbon capture capability was enhanced. Anyway, with or without MEA, it was observed an important biomass deposition on the inner walls of the bioreactor occurred, which caused a lower light exposure and the chance for parasitic microorganisms to develop inside the culture. It was concluded that *Spirulina* could perform well in bioprocesses like bioethanol production, since the obtained biomass had a high carbohydrates content, mainly due to MEA addition during the experience (da Rosa *et al*., 2015).

1.5.3 Laboratory tests on continuous cultivations

Könst *et al*., 2017 demonstrated the feasibility of TNO's (The Netherlands Organization for applied scientific research) idea of integrating carbon dioxide absorption by either amines or carbonates with biological sequestration, that is shown in figure 1.10.

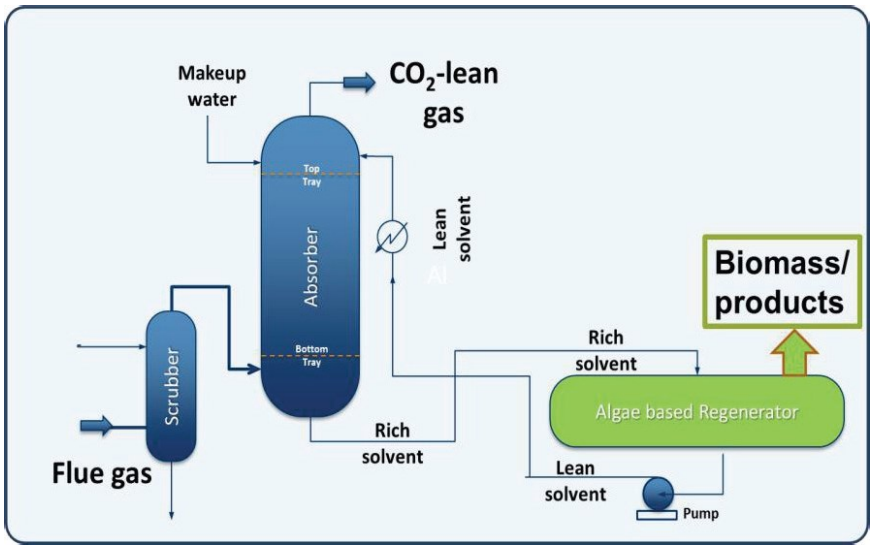

Figure 1.10. *Integrated process concept (Könst et al., 2017)*

In order to prove that this practice can be implemented, *Chlorella sp.* was cultured batch-wise for 7 days, after which continuous cultivation was carried out by feeding 0.1 M potassium carbonate as absorption liquid continuously, which was mixed with CO_2, while continuously harvesting bioreactor content at the same rate. After two weeks of continuous growth with fresh make-up of carbonate based absorption liquid, the recycle of the regenerated carbonate solution was implemented, so that it could be reloaded with CO_2 and fed again to the culture. Accordingly, a closed-loop system was established that was successfully operated for more than three weeks. In this way, it was shown that the carbonate solution is regenerated and feeding

CO_2 that is captured in bicarbonates form is possible. Könst *et al*., 2017 repeated the same procedure, but loading the carbonate absorbent with carbon dioxide from flue gas, coming from a power plant: they contacted flue gas and the solution in a chimney, and fed the culture with 4 consecutive loads, all of them prepared with the same flue gas; the culture achieved an almost constant flowrate, meaning that this process could really be scaled-up at industrial level (Könst *et al*., 2017).

1.6 Aim of the thesis

In the framework of the discussion reported above, this thesis is focused on verifying large-scale feasibility of a hybrid chemical and biological process for CO_2-fixation, combining carbon dioxide absorption by means of a carbonate-based solvent with microalgal sequestration, so that CO_2 would be fed to the culture in bicarbonates form. Even though this concept has been proposed by a few works in the literature, some of which have been described in this chapter, so far all tests are still at laboratory scale and they mainly concern batch or semi-batch cultures. The purpose is to implement a rigorous simulation of such a closed-loop continuous system, using Aspen Plus® process simulator to solve material and energy balances, to check whether it can be scaled-up at industrial level.

The feasibility of the hybrid process will be investigated in relation to different case studies, namely capturing CO_2 from a natural gas power plant, from a steam methane reforming plant for hydrogen production, and from the flue gases produced by steelmaking or cement industry.

Chapter 2 - Models, methods and reactions

This chapter focuses on thermodynamic model choice and on the description of all the components that are involved in the process. Afterwards, the reactions that occur in the system are discussed. Finally, the overall process flowsheet is shown and explained. In order to set up and simulate the process, Aspen Plus® simulator is used.

2.1 Components and thermodynamic model

The first step to accomplish inside Aspen Plus® environment is to define the species that are present in the system, hence within the Properties section, the chemical components are searched and added to the list. Here, there is the possibility to distinguish among conventional and non-conventional components, to recognize species that are not present within the simulator database, and to define microalgae in the system. In addition, all the components that follow Henry's law in vapour-liquid equilibrium behaviour have to be defined as Henry's components. To be more precise, table 2.1 reports all the listed compounds.

Species	Conventional	Henry's Component
CO_2	Yes	Yes
CO	Yes	Yes
H_2	Yes	Yes
CH_4	Yes	Yes
H_2O	Yes	No
N_2	Yes	Yes
Na_2CO_3	Yes	No
Microalgae	No	No

Table 2.1. *Chemical species in the system*

Once all the components are defined, the next task is to choose the proper thermodynamic model. It is well known that the Non-Random Two-Liquid (NRTL) model is able to describe vapour-liquid equilibria and liquid-liquid equilibria of strongly non-ideal solutions, and to

handle various combinations of polar and non-polar components (Renon and Prausnitz, 1968, Bertucco and Barbera, 2020), therefore for the current system, where aqueous solutions are present, the most appropriate model is Electrolyte-NRTL. According to it Redlich-Kwong equation of state is used to compute all the vapour phase properties, while Henry's law is employed to model the solubility of gaseous species, instead electrolytes effects are accounted by Debye-Huckel term (Aspen Plus V12.1 help, Bertucco and Barbera, 2020). Dealing with aqueous solutions, the formation of electrolytes must be accounted for, so going back to the components list, by means of the Elec-Wizard tool and adopting the true component approach, the equilibrium reactions of components dissociations are generated and they can be found within the Global Chemistry section.

2.2 Absorption column reactions

What goes on within the column is that the carbon dioxide that is present in the gaseous feed stream is chemically absorbed by using an aqueous solution of sodium carbonate as solvent. As stated in the previous paragraph, in order to consider the chemical reactions taking place inside the column, the Elec-Wizard tool has been used. In this way, also Henry's components have been selected, together with the reference species. By the way, a distinction between main reactions and salts dissociations must be highlighted.

2.2.1 Equilibria

The three main reactions occurring in the column are described by equations 2.1, 2.2 and 2.3.

$$H_2O + HCO_3^- \leftrightarrow CO_3^{2-} + H_3O^+ \quad (2.1)$$

$$2H_2O + CO_2 \leftrightarrow HCO_3^- + H_3O^+ \quad (2.2)$$

$$2H_2O \leftrightarrow OH^- + H_3O^+ \quad (2.3)$$

As already explained in Chapter 1, subparagraph §1.2.2.2 when describing CO_2 chemical absorption steps using carbonate solutions, once the sodium carbonate is turned into the bicarbonate form, the reactions featured from equation 2.1 up to 2.3 take place. Equation 2.1 represents the hydration of bicarbonate ion, which originated from sodium bicarbonate

dissociation. Equation 2.2 stands for dissolved CO_2 hydration. Eventually, equation 2.3 is related to water equilibrium dissociation. The controlling step is the hydration of dissolved CO_2, since its mass transfer is very slow, as it is reported in the review written by Borhani *et al*., 2015, concerning the case of CO_2 chemical absorption using a potassium carbonate solution.

2.2.2 Salts formation

The afore mentioned equilibria are followed by other reactions, specifically those that are described from equation 2.4 up to 2.13.

$$WEGSC_S \leftrightarrow CO_3^{2-} + 3\,HCO_3^- + 5\,Na^+ \quad (2.4)$$

$$TRONA_S \leftrightarrow CO_3^{2-} + HCO_3^- + 2\,H_2O + 3\,Na^+ \quad (2.5)$$

$$SALT4 \leftrightarrow CO_3^{2-} + 2\,Na^+ + 10H_2O \quad (2.6)$$

$$SALT3 \leftrightarrow CO_3^{2-} + 2\,Na^+ + 7H_2O \quad (2.7)$$

$$SALT2 \leftrightarrow H_2O + CO_3^{2-} + 2\,Na^+ \quad (2.8)$$

$$SALT1 \leftrightarrow CO_3^{2-} + 2\,Na^+ \quad (2.9)$$

$$NaOH{:}\,(s) \leftrightarrow H_2O + OH^- + Na^+ \quad (2.10)$$

$$NaOH(s) \leftrightarrow OH^- + Na^+ \quad (2.11)$$

$$SODIUS_S \leftrightarrow HCO_3^- + Na^+ \quad (2.12)$$

$$Na_2CO_3 \leftrightarrow CO_3^{2-} + 2Na^+ \quad (2.13)$$

All these reactions are related to the formation of hydrated-sodium carbonate salts and sodium hydroxide, except from the last one, which is simply the dissociation of sodium carbonate. When selecting the Elec-Wizard tool, then inevitably such reactions are accounted for in the simulation environment, but in order to avoid the possibility of salts precipitation when simulating the process, they are neglected from the system. In this way, also calculations are simplified, as it is going to be described in chapter 3.

Overall, the complete components list is shown in table 2.2.

Component	Conventional	Henry
CO_2	Yes	Yes
CO	Yes	Yes
H_2	Yes	Yes
CH_4	Yes	Yes
H_2O	Yes	No
N_2	Yes	Yes
Na_2CO_3	Yes	No
H_3O^+	Yes	No
OH^-	Yes	No
HCO_3^-	Yes	No
CO_3^{2-}	Yes	No
Microalgae	No	No

Table 2.2. *Complete components list*

2.3 Biomass production reaction

The liquid exiting the column is led to a photobioreactor, where the microalgal culture grows: in this way, carbon dioxide is fed to microalgae mainly in bicarbonate form. CO_2 fixation takes place by means of photosynthesis reaction, through which biomass and oxygen are produced. In order to consider this reaction in the simulation environment, a Fortran® subroutine is employed, since microalgae are non-conventional components. This algorithm contains a validated suitable kinetic model and the vector of stoichiometric coefficients, so that the reaction rate can be computed.

2.3.1 Reaction stoichiometry

First of all, stoichiometric coefficients have to be evaluated. Neglecting nutrients like nitrogen (N) and phosphorous (P), microalgae constituents are carbon (C), hydrogen (H) and oxygen (O), so starting from a weight composition that is 50% C, 7% H, and 43% O, a system of four

equations can be solved in order to obtain the microalgal molecular weight and the molar fractions of all the constituents.

$$\begin{cases} x_C = w_C \left(\frac{MW_a}{MW_C}\right) & (2.14) \\ x_H = w_H \left(\frac{MW_a}{MW_H}\right) & (2.15) \\ x_O = w_O \left(\frac{MW_a}{MW_O}\right) & (2.16) \\ x_C + x_H + x_O = 1 & (2.17) \end{cases}$$

Equations from 2.14 up to 2.16 are needed to convert constituents mass fractions into molar fractions. Indeed, w_i are the mass fractions, x_i are the molar ones, while MW_i are the elements molecular weight and MW_a is the microalgal molecular weight. The latter one is the fourth unknown to be computed. Equation 2.17 is the identity, to check that the sum of all molar fractions is equal to one. The results are reported by equations 2.18 up to 2.21.

$$\begin{cases} x_C = 0.301 & (2.18) \\ x_H = 0.505 & (2.19) \\ x_O = 0.194 & (2.20) \\ MW_a = 7.225 \frac{kg}{kmol} & (2.21) \end{cases}$$

Thus, microalgae composition is obtained and the formula on which the reaction stoichiometry is built is $\mathbf{C_{0.301}H_{0.505}O_{0.194}}$. Eventually, the biomass production reaction is represented by:

$$0.2525H_2O + 0.301HCO_3^- \leftrightarrow C_{0.301}H_{0.505}O_{0.194} + 0.33025O_2 + 0.301OH^- \quad (2.22)$$

In this case, carbon dioxide is not present among reactants, since inorganic carbon is fed to the culture as bicarbonates. In the Fortran® subroutine, the vector of stoichiometric coefficients is built, filling it with the values reported above for the species that are involved in the reaction, while for all the others the stoichiometric coefficient is equal to zero. A key aspect is that such vector must respect the order according to which the components are listed in Aspen Plus® simulator, otherwise results would not be correct.

2.3.2 Kinetic model

The kinetic model that is adopted is the one proposed by Borella *et al*., 2021, who studied the light effect on microalgal performance by cultivating *A. Maxima* using red and blue light emitting diodes (LED) with increasing light intensity. According to this model, the direct reaction rate can be expressed as:

$$R_d = \mu_{\max} C_{x,out} f_T f_{Iav} \tag{2.23}$$

In equation 2.23, μ_{max} is the maximum specific growth rate that is expressed in d^{-1}, $C_{x,out}$ is the biomass concentration exiting the reactor that is expressed in g L^{-1}, and then there are a temperature and a light functions (Borella *et al*., 2021). Specifically, the temperature function is expressed as in the article written by Bernard and Rémond, 2012.

$$f_T = \frac{(T-T_{\max})(T-T_{\min})^2}{(T_{opt}-T_{min})\left((T_{opt}-T_{min})(T-T_{opt})-(T_{opt}-T_{max})(T_{opt}+T_{min}-2T)\right)} \tag{2.24}$$

In equation 2.24, T is the process temperature that is 30°C, T_{opt} is the optimal temperature which is equal to 28.98°C, while T_{min} and T_{max} are the two liming temperatures since below the minimum temperature and above the maximum one it is assumed that no biomass growth takes place (Bernard and Rémond, 2012). For the current study that concerns *A. Platensis*, the values of T_{min}, and T_{max} are 6.57°C and 47.21°C respectively (Pastore *et al*., 2022).

The other term that appears in the direct reaction rate is the light function, that is expressed as in the article by Pastore *et al*., 2022.

$$f_{I_{av}} = \frac{I_{av}}{I_{av}+k_I\left(\frac{I_{av}}{I_{opt}}-1\right)^2} \tag{2.25}$$

Equation 2.25 takes into account the dependence of biomass growth on light intensity. Particularly, I_{av} is the average incident radiation inside the reactor, expressed in µmol m^{-2} s^{-1}, which is a function of the reactor depth h [m]. I_{av} is computed according to a Lambert-Beer law, as it is reported below (Borella *et al*., 2021).

$$I_{av} = I_0\left(\frac{1-e^{-k_a C_{x,out} h}}{k_a C_{x,out} h}\right) \tag{2.26}$$

In equation 2.26, k_a is the average biomass light absorption coefficient expressed in $m^2\ g^{-1}$, I_0 is the incident light intensity expressed in μmol $m^{-2}\ s^{-1}$, h is the reactor depth expressed in m, and $C_{x,out}$ is the outlet biomass concentration expressed in g m^{-3} (Borella *et al*., 2021).

The inverse reaction rate is calculated as in the article by Borella *et al*., 2021.

$$R_i = \mu_e C_{x,out} \tag{2.27}$$

In equation 2.27, the parameter μ_e appears, which is the negative term of the overall biomass growth rate, since it accounts for cell respiration and maintenance. It is computed as a function of light, following a Monod-like function as in the article by Borella *et al*., 2021.

$$\mu_e = \mu_{emax}\left(\frac{I_0}{I_0 + K_{im}}\right) \tag{2.28}$$

The parameter μ_e is expressed in d^{-1}, as well as μ_{emax}, which is the maintenance parameter. The value that is used for μ_{emax} is 10.51 d^{-1} (Borella *et al*., 2021). The last parameter is K_{im}, which is the half saturation constant and its value is 1224 μmol $m^{-2}\ s^{-1}$, that is specific for *A. Platensis* (Pastore et al., 2022).

Eventually, the overall biomass growth rate is calculated as shown in equation 2.29 (Pastore *et al*., 2022)

$$R_{tot} = R_d - R_i \tag{2.29}$$

The actual kinetic model should include a carbon source function, which accounts for microalgae nutrition, but parameter values are not available yet. Thus, no limitations for carbon availability has been assumed in the kinetic model development.

All the kinetic parameters are summed up in table 2.3 and they are referred to *Arthrospira Platensis*, when red and blue light is used as energy source (Pastore *et al*., 2022).

Parameter name	Parameter symbol	Units of measure	Value
Average biomass absorption coefficient	k_a	$m^2\ kg^{-1}$	36.2
Optimal radiation	I_{opt}	$\mu mol\ m^{-2}\ s^{-1}$	482.9
Half saturation constant	K_{im}	$\mu mol\ m^{-2}\ s^{-1}$	1224
Maintenance parameter	μ_{emax}	d^{-1}	10.51
Light half saturation constant	K_I	$\mu mol\ m^{-2}\ s^{-1}$	192.1
Optimal temperature	T_{opt}	°C	28.98
Minimum temperature	T_{min}	°C	6.57
Maximum temperature	T_{max}	°C	47.21
Temperature function	f_T or $\varphi(T)$	/	0.997

Table 2.3. *Kinetic parameters for RB light (Pastore et al., 2022).*

2.3.3 Evaluation of μ_{max} and experimental data simulation

The previous paragraph focused on the kinetic model structure, referring to some parameters values. But concerning about the parameter μ_{max}, experimental data obtained with bicarbonate as carbon source (Colta, 2023) are simulated in order to find the most suitable value that would be able to reproduce them. What is actually found when experimental conditions are simulated is not the maximum specific growth rate, but it is the product between this parameter and the carbon source function. Such product can be called μ_{app}, and it includes both the maximum specific growth rate and the carbon source function.

$$\mu_{app} = \mu_{max} f_C \tag{2.30}$$

In the next subparagraphs, the description of all experimental conditions and their simulations follows. All experimental data are obtained using white light lamps with an incident radiation equal to 100 μmol m^{-2} s^{-1} and a reactor depth equal to 0.04 m. Parameters for white light are summed up in table 2.4.

Parameter	Value	Units of measure
k_a	36.2	m^2 Kg^{-1}
I_{opt}	458.9	μmol m^{-2} s^{-1}
K_{im}	1224	μmol m^{-2} s^{-1}
μ_{emax}	10.51	d^{-1}
K_I	207.1	μmol m^{-2} s^{-1}
T_{opt}	28.98	°C
T_{min}	6.57	°C
T_{max}	47.21	°C
φ(T)	0.997	/

Table 2.4. *Kinetic parameters for white light (Pastore et al., 2022).*

2.3.3.1 Fixed residence time and inlet concentration

The first dataset is referred to the following conditions: a stream made of an aqueous solution of sodium bicarbonate $NaHCO_3$, is fed to the *A. Platensis* culture, which is kept in a continuous stirred tank reactor (CSTR). The reactor works at steady state and all the conditions are summed up in table 2.5 (Colta, 2023).

Temperature	30°C
Pressure	1 atm
Reactor volume	350 mL
Residence time	1.2 d
Total flow rate	0.292 L d^{-1}
Inlet concentration of $NaHCO_3$	30 g L^{-1}

Table 2.5. *Experimental conditions with fixed residence time and inlet concentration (Colta, 2023).*

The outlet concentration of the produced biomass is measured, keeping the same residence time, thus the same total flow rate, as well as the same inlet salt concentration, but considering three different inlet conditions:

- The system is supplied with air;
- The system is supplied with air containing 5% vv of CO_2;
- No gas supply to the system.

The gas flow rate is equal to 1L h^{-1} for both of the first two cases. All the experimental values are reported in table 2.6 (Colta,2023).

	$C_{x,exp}$ [g L^{-1}]	Std dev.	pH	Std dev.	CO_3^{2-} [g L^{-1}]	Std dev.	HCO_3^- [g L^{-1}]	Std dev.
No air	0.354	0.06	9.188	0.04	0.91	0.14	2.83	0.24
Air	0.353	0.04	9.19	0.08	0.78	0.04	2.22	0.24
Air+CO_2	0.445	0.04	9.07	0.10	0.88	0,27	2.82	0.16

Table 2.6. *Experimental data with fixed τ and inlet salt concentration (Colta,2023).*

Figures 2.1, 2.2 and 2.3 show the process flowsheet diagrams for the three conditions that have been simulated.

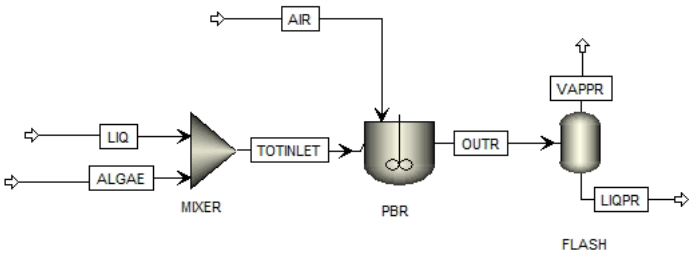

Figure 2.1. *Process flowsheet with air insufflation.*

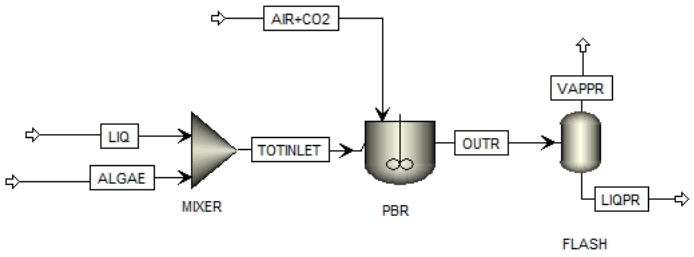

Figure 2.2. *Process flowsheet with air and CO_2 insufflation.*

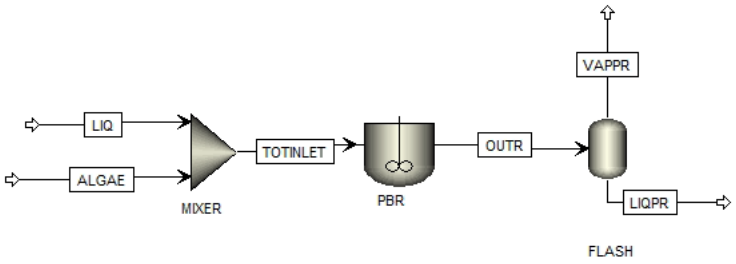

Figure 2.3. *Process flowsheet without gas insufflation.*

In order to simulate such conditions in Aspen Plus® suite, a RStoich CSTR reactor type is employed. For the inlet aqueous stream, water is defined as the solvent, and the total flow rate, whose value is given among experimental data, is considered to be the solvent flow rate. In addition to sodium bicarbonate, other salts were fed to the culture, since Zarrouk's medium is used, but for simulation purposes, only K_2HPO_4, $NaNO_3$ and NaCl are added to the inlet solution, considering concentrations of 61 mg L^{-1}, 1500 mg L^{-1}, and 20,000 mg L^{-1} respectively. The Elec Wizard tool is used, in order to account for all the ions in the liquid solution.

Note that the Fortran® subroutine was adjusted properly, namely the value of the parameter μ_{app} is set to be lower than the one proposed by Pastore *et al.*, 2022, which is 8.66 d^{-1}. The decision to reduce the maximum specific growth rate value is justified by the fact that, when simulating the experimental conditions, the calculated biomass outlet concentration resulted to

be higher than the experimental one. The reason why there is such a difference is that within the expression of the direct biomass production reaction rate the carbon source function should be present, and its value should be lower than one. Since this function is missing, a way to account for it is to reduce the value of μ_{app}. A fundamental concept is that, to be able to reproduce experimental data as accurately as possible, the reactor volume proper value is found to be the one providing the same residence time as the experimental one. Indeed, the laboratory reactor volume is referred to the volume of the liquid inside the tank, so in the simulation environment it is not possible to insert the same value, since it is required to set the total volume when defining reactor specifications. Moreover, an additional stream of microalgae is present at the reactor inlet, otherwise convergence is not achieved. Its flow rate is basically negligible if compared to the other streams, since it is equal to $9e^{-12}$ kg h^{-1}, but its presence helps the simulator to find convergence. The simulation was carried out, reproducing the three cases with the same inlet salt concentration and residence time, and the results obtained are reported in table 2.7.

	$C_{x,sim}$ [g L^{-1}]	pH	CO_3^{2-} [g L^{-1}]	HCO_3^- [g L^{-1}]	μ_{app} [d^{-1}]
No air	0.3541	8.45	1.03	19.71	4.55
Air	0.3529	9.05	3.26	15.25	4.60
Air+CO_2	0.4322	8.53	1.20	19.41	4.81

Table 2.7. *Calculated data with fixed τ and inlet salt concentration.*

Figure 2.4 shows the comparison between experimental and calculated values.

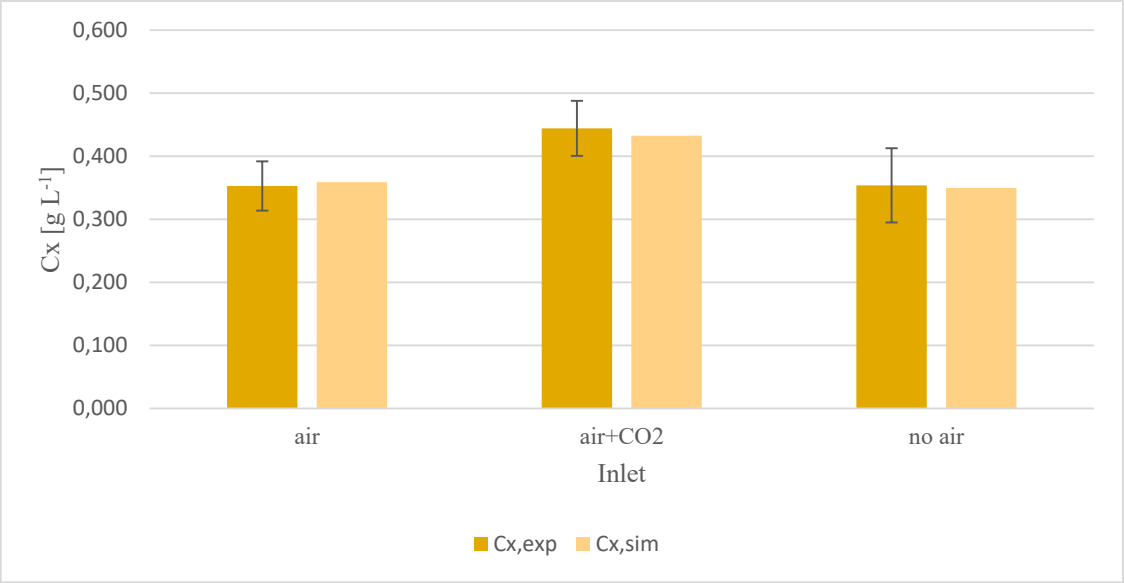

Figure 2.4. *Biomass outlet concentrations comparison.*

As it can be observed from figure 2.4, the selection of suitable value for μ_{app} allows to obtain basically the same biomass outlet concentration as the one measured experimentally. For each case, its value is searched by a try-and-error procedure, adjusting the reactor volume accordingly.

Figure 2.5 shows how μ_{app} changes with respect to the inlet conditions.

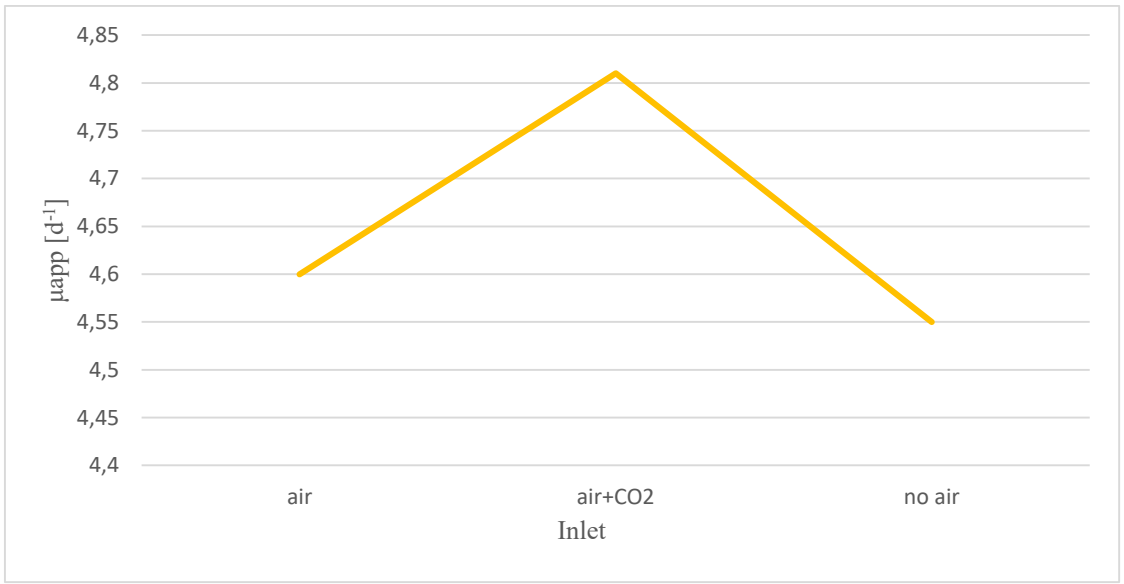

Figure 2.5. *μ_{app} [d^{-1}] vs inlet conditions.*

Eventually, figure 2.6 shows a comparison between experimental and simulated carbonates and bicarbonates outlet concentrations, but also outlet pH.

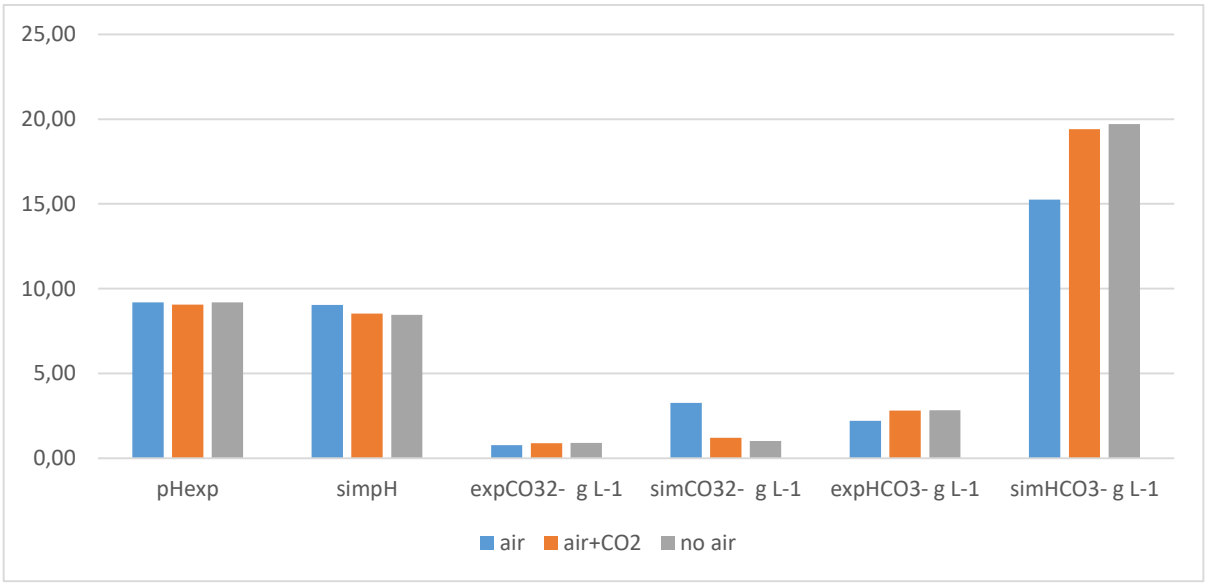

Figure 2.6. *Outlet pH, carbonates and bicarbonates concentrations [g L^{-1}] vs inlet conditions.*

It can be concluded that biomass outlet concentration and pH values that are reproduced by process simulations are basically the same as the experimental ones, while ions outlet concentrations are quite different.

2.3.3.2 Varying the residence time

Other laboratory tests are carried out by feeding the aqueous solution of sodium bicarbonate $NaHCO_3$, again with a concentration of 30 g L^{-1} of sodium bicarbonate, to a CSTR. By varying the flowrate, three different residence times were used. Temperature, pressure and volume are the same as the previous case. A stream of air containing 5% vv of CO_2 was fed to the reactor too. Outlet biomass concentration measurements are summed up in table 2.8.

Total flowrate [L d^{-1}]	**τ [d]**	**$C_{x,exp}$ [g L^{-1}]**	**Standard deviation**
0.292	1.2	0.433	0.042
0.175	2	0.663	0.09
0.117	3	0.873	0.097

Table 2.8. *Experimental data with variable residence time, with air+5%vv CO_2.*

In order to simulate these conditions, as described in the previous subparagraph, μ_{app} was varied, until an outlet biomass concentration close enough to the experimental one was obtained. The reactor volume was changed accordingly, in order to obtain the corresponding residence time. Results are shown in table 2.9.

τ [d]	**$C_{x,sim}$ [g L^{-1}]**	**μ_{app} [d^{-1}]**
1.2	0.4327	4.81
2	0.667	4.4
3	0.873	4.3

Table 2.9. *Simulated data with variable residence time, with air+5%vv CO_2.*

The comparison between experimental and simulated data is shown in figure 2.7.

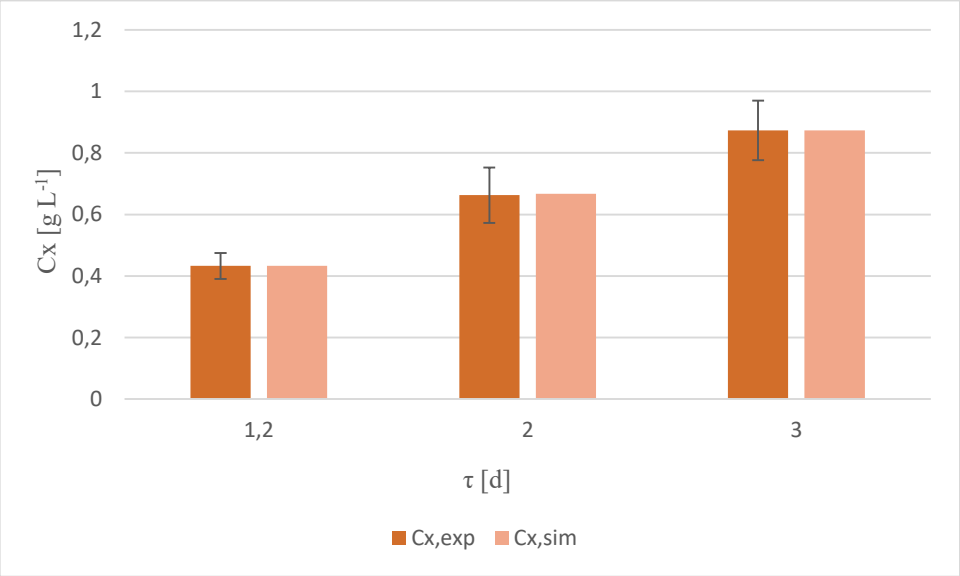

Figure 2.7. *Simulated data vs experimental data with variable residence time, with air+5%vv CO_2.*

Also in this case, data could be reproduced using a suitable value for μ_{app} for each condition. Figure 2.8 features how this parameter varies depending on the residence time.

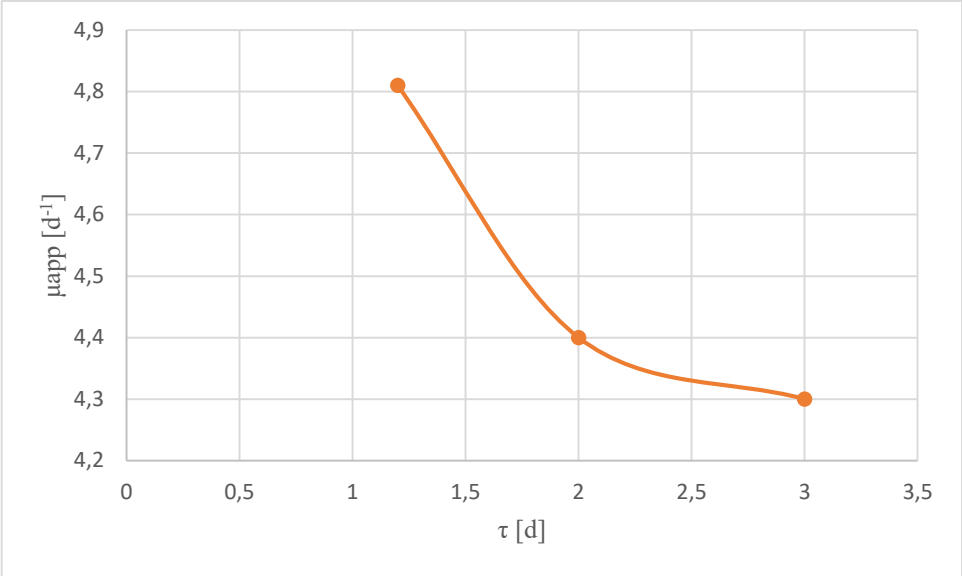

Figure 2.8. *μ_{app} [d^{-1}] vs τ [d].*

Observing this plot, the lower the residence time, the higher is the value of μ_{app}. Actually, it does not change that much, and it is similar to the value for the previous set of experiments.

2.3.3.3 Varying inlet concentration

The last dataset is referred to variable inlet concentration of $NaHCO_3$ to the reactor. The residence time is kept constant and equal to 1.2 d, all the reactor conditions are the same as those aforementioned. Also in this case, a stream of air containing 5%vv of CO_2 is fed to the reactor. Table 2.10 gathers all the experimental data.

$C_{NaHCO3,in}$ [g L^{-1}]	$C_{x,exp}$ [g L^{-1}]	Standard deviation
6	0.249	0.01
15	0.38	0.06
30	0.433	0.04
45	0.588	0.16
60	0.534	0.08

Table 2.10. *Experimental data with variable inlet concentration and with air+5%vv CO_2.*

Simulations results are reported in table 2.11.

$C_{NaHCO3,in}$ [g L^{-1}]	μ_{app} [d^{-1}]	$C_{x,sim}$ [g L^{-1}]
6	4.3	0.245
15	4.7	0.39
30	4.81	0.4327
45	5.3	0.597
60	5.1	0.533

Table 2.11. *Simulated data with variable inlet concentration and with air+5%vv CO_2.*

In order to compare experimental and simulated data, a histogram is built again, as it is shown in figure 2.9.

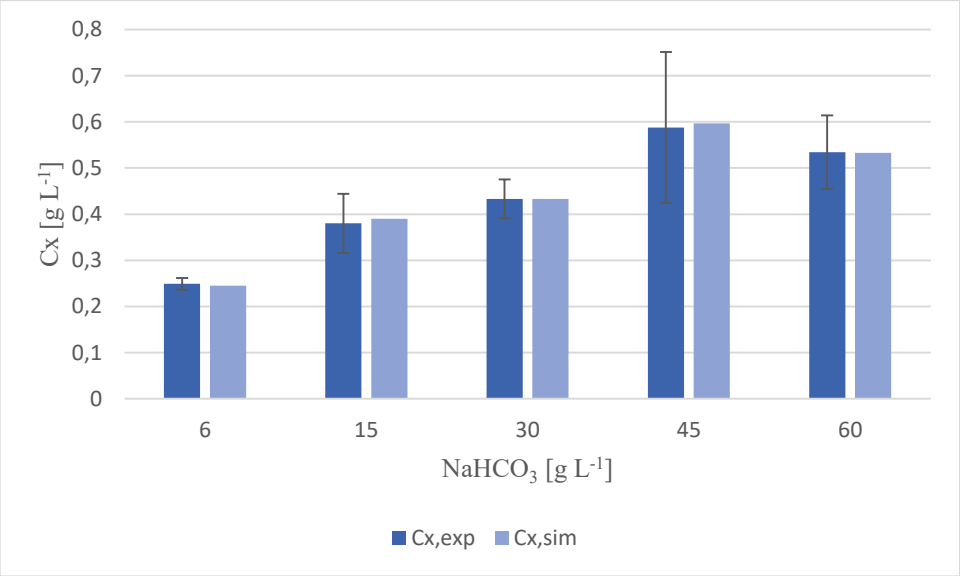

Figure 2.9. *Simulated vs experimental data with variable $NaHCO_3$ inlet concentration, with air+5%vv CO_2.*

Also for these conditions, it is possible to reproduce experimental data in a quite accurate way, since results are once again within the standard deviation range. To see how μ_{app} value changes with respect to $NaHCO_3$ inlet concentration, figure 2.10 can be observed.

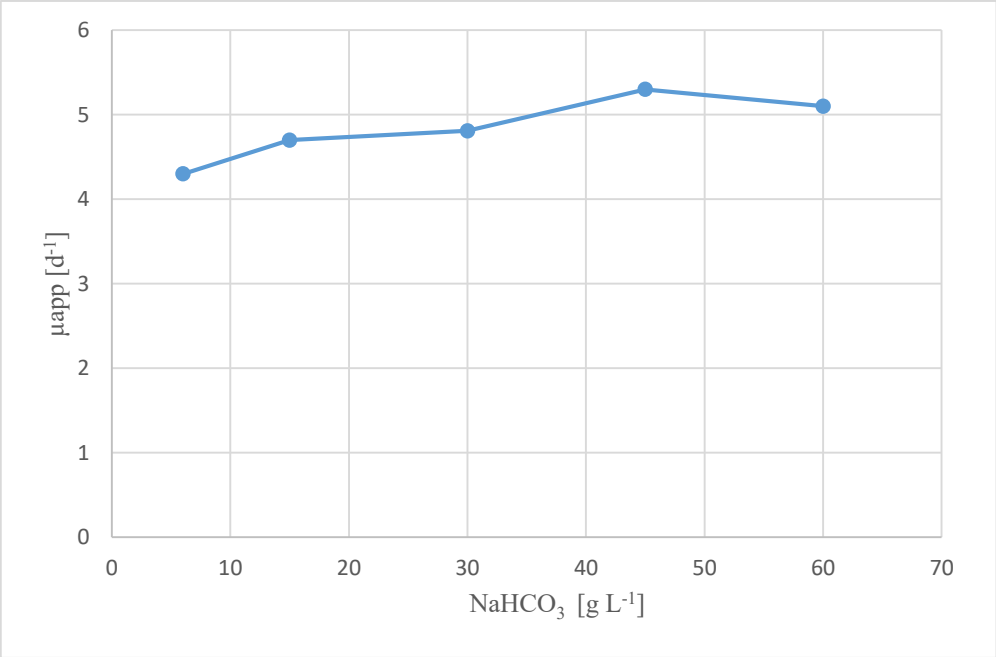

Figure 2.10. *μ_{app} [d^{-1}] vs $NaHCO_3$ [g L^{-1}] inlet concentration.*

As for the case with variable residence time, here it can be noticed that μ_{app} value needs to be changed depending on sodium bicarbonate inlet concentration. The values are quite close to each other, but they increase up to $NaHCO_3$ concentration of 45 g L^{-1}, while in correspondence of the highest concentration, a smaller μ_{app} is required to achieve that given biomass production. This could be due to the fact that microalgae are not able to feed on carbon via bicarbonates in an effective way, when their concentration is too high, and this translates into a lower biomass production. Indeed, the experimental value of the biomass concentration corresponding to 60 g L^{-1} of sodium bicarbonate is lower than the one corresponding to 45 g L^{-1}, and in order to reproduce this biomass concentration, μ_{app} has to be reduced.

From these results, it can be concluded that there is a dependence of the parameter μ_{app} on the inlet bicarbonate concentration, but it is worth noting that its values range between 4.3 and 5.3, which is an extremely small variation interval. In addition, the dataset referring to variable residence times is the most complete one (Elena Barbera, personal communication), hence for the purpose of this work, carbon concentration in the stream entering the reactor is computed for both experimental conditions and simulated ones, in order to check whether the average of the values of μ_{app} used for simulating the aforementioned dataset, can be employed to simulate the integrated process. This computation is explained in the next paragraph, while the average value of μ_{app} is computed according to equation 2.31.

$$\mu_{app} = \frac{\mu_{app,\tau_1} + \mu_{app,\tau_2} + \mu_{app,\tau_3}}{3} = 4.50\ d^{-1} \quad (2.31)$$

2.4 Process layout

The complete process flowsheet diagram is shown in figure 2.11.

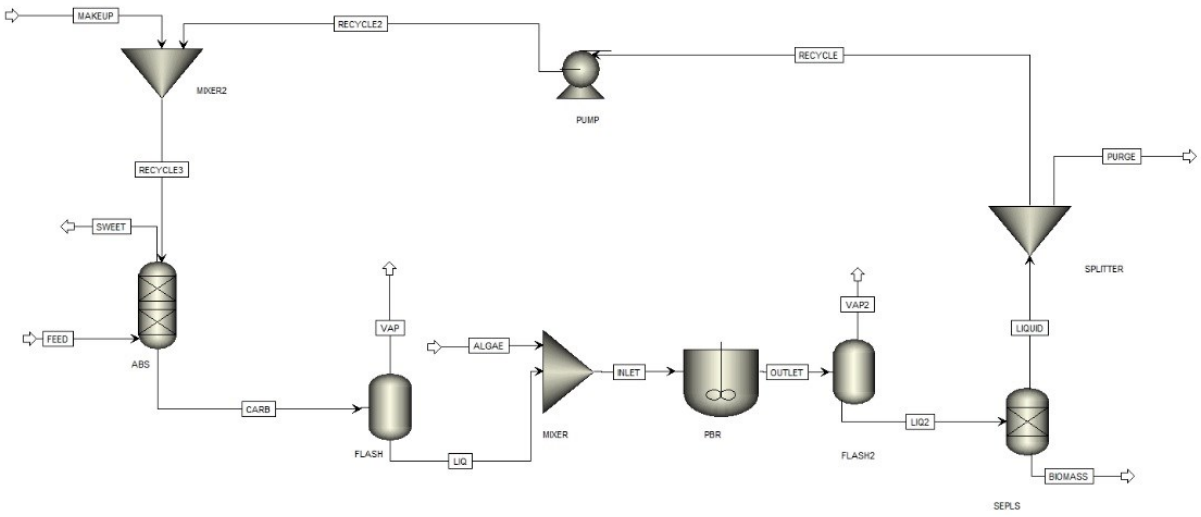

Figure 2.11. *Complete process flowsheet diagram.*

This integrated process consists in a first section, where CO_2 is chemically absorbed in a packed column operating at a pressure of 2.5 bar, by means of an aqueous solution of sodium carbonate. The liquid exiting the column goes through a flash drum where pressure is lowered to 1 atm, so that the volatile components exit from the top, while the liquid stream is withdrawn from the bottom. Before entering the photobioreactor, that is initially modelled as a CSTR, the bicarbonates solution is mixed with a microalgae stream, whose flow rate is so low, namely equal to $9e^{-8}$ kg h^{-1}, which is not present in the system. This is done because without this additional microalgae stream, convergence cannot be achieved. The kinetic model parameters that are used for the process simulation are those referred to red and blue light, that are summarized in table 2.3, while the incident radiation I_0 is equal to 420 μmol m^{-1} s^{-1} and the reactor depth is assumed to be 0.05 m (Elena Barbera, personal communication) Afterwards, the stream exiting the mixer enters the reactor, where the biomass production reaction takes place. As for the simulation of the laboratory data, this reaction is accounted for by means of the Fortran® subroutine, where a value of 4.50 d^{-1} is used for μ_{app}. This value was chosen

because, considering the experimental dataset with different residence times, the concentration of carbon entering the photobioreactor is represented by equation 2.32.

$$[C]_{in} = \frac{[NaHCO_3]_{in}}{MW_{NaHCO_3}}(MW_C) = \frac{30\frac{g}{L}}{84\frac{g}{mol}}\left(12\frac{g}{mol}\right) = 4.28571\frac{g}{L} \quad (2.32)$$

In order to check whether an average value of μ_{app} among the three cases can be used, the same type of evaluation in terms of carbon concentration entering the reactor is made for the process.

$$[C]_{in,1} = \frac{[CO_2]_{in}}{MW_{CO_2}}(MW_C) = \frac{0.00626111\frac{g}{L}}{44\frac{g}{mol}}\left(12\frac{g}{mol}\right) = 0.001708\frac{g}{L} \quad (2.33)$$

$$[C]_{in,3} = \frac{[HCO_3^-]_{in}}{MW_{HCO_3^-}}(MW_C) = \frac{13.4359\frac{g}{L}}{61\frac{g}{mol}}\left(12\frac{g}{mol}\right) = 2.643\frac{g}{L} \quad (2.34)$$

$$[C]_{in,4} = \frac{[CO_3^{2-}]_{in}}{MW_{CO_3^{2-}}}(MW_C) = \frac{7.74093\frac{g}{L}}{60\frac{g}{mol}}\left(12\frac{g}{mol}\right) = 1.548\frac{g}{L} \quad (2.35)$$

$$[C]_{in,tot} = \sum_{i=1}^{4}[C]_{in,i} = 4.193\frac{g}{L} \quad (2.36)$$

From equation 2.32 up to 2.35, all the dissolved inorganic carbon sources are taken into account, so that the total carbon concentration entering the reactor can be computed, as it is featured in equation 2.36, so by summing up all contributions. Since this value is very close to the experimental inlet carbon concentration, the decision to use the average value of μ_{app} among those used for each of three cases, was taken.

The liquid exiting the reactor goes through another flash drum, which has the purpose to take out all volatile components that are not dissolved in the liquid. Then the liquid stream enters a solid-liquid separator, where biomass is separated at the bottom concentrated at 20% by mass with a water content equal to 80%, according to the performance of a good biomass lamella clarifier and thickner (Alberto Bertucco, personal communication). Instead, the recovered solution is led to a splitter, where there is a purge stream coming out, and the recycle stream. This one is firstly pressurized up to 2.5 bar, since this is the operating pressure of the absorber. Then, it is mixed with the aqueous solution of sodium carbonate, and the resulting stream enters the top of the column.

The design choices concerning all the operating units involved in this hybrid process are discussed in the next chapter.

Chapter 3 - Results and Discussions

This chapter aims to report all the results obtained from the simulations of a base case. Firstly, several options are presented, which focus on the comparison between natural light and LED light employment for the microalgal culture. In this perspective, four industrial fields are considered. Then, a description of the design choices follows, concerning the absorption column and the photobioreactor. Eventually, the final process flow diagram is presented and simulated, together with complete process information.

3.1 Photobioreactor surface and volume evaluation

It is well known that microalgae need light in order to grow. Light can be supplied to the culture either by exposing it to sunlight or artificially. The two options have been evaluated by collecting irradiance data and calculating the volume and the surface required for the microalgal culture. In order to carry out the computations, four case studies have been selected as far as the CO_2 source is concerned: a gas-fired power plant, cement industry, steel and iron mill, and a steam methane reforming plant. Since these are the most polluting industrial sectors, data concerning their flue gas streams have been selected and used for the assessment of the reactor dimensions. First of all, natural light information was retrieved from the web site JRC Photovoltaic Geographical Information System (PVGIS) - European Commission (europa.eu). Here, the town of Gela (Caltanissetta, Italy) was selected as the geographical location for which irradiance values on an hourly basis was taken, in order to cover a whole day. This procedure was followed for every month of the year. Then, using Excel® software, an integral mean of the hourly irradiance values was computed, in order to obtain the irradiance average value for a day referred to a given month. Having the irradiance on a daily basis for each month, hence expressed in MJ m^{-2} d^{-1}, computations concerning natural light are possible. On the other hand, when considering artificial light, irradiance values are taken from Borella *et al*., 2021, where the optimal microalgal growth conditions are searched by using different red and blue LED light intensities, which are expressed in μmol (of photons) m^{-2} s^{-1}.

3.1.1 Gas-fired power plant

The first case study is the one related to a gas-fired power plant. The flue gas composition was taken from Barbera *et al*., 2022, and it is reported in table 3.1.

Parameter	Value
Flue gas flow rate [kg s^{-1}]	897.4
Temperature [°C]	143
Pressure [bar]	1
CO_2 molar fraction [%]	4.04
N_2 molar fraction [%]	74.32
O_2 molar fraction [%]	12.09
H_2O molar fraction [%]	8.67
Ar molar fraction [%]	0.88

Table 3.1. *Flue gas stream characteristics (Barbera et al., 2022).*

The average molecular weight of the mixture is computed as:

$$MW_{av} = \sum_{i=1}^{5} x_i MW_i \tag{3.1}$$

In equation 3.1, x_i are the components molar fractions and MW_i are their molecular weights. The mixture molecular weight results to be 28.369 kg $kmol^{-1}$, and it is used to obtain carbon dioxide molar flow rate, which is equal to 1278 mol s^{-1}. Assuming that 90% of this flow rate is captured by absorption, and that is fed to a microalgal culture, then the produced biomass flow rate can be calculated.

$$\dot{m}_{biomass} = \frac{0.9\dot{m}_{CO_2}}{1.83\left(\frac{kg_{CO_2}}{kg_{algae}}\right)} = 872128\frac{ton}{d} \tag{3.2}$$

In equation 3.2, the term 1.83 kg_{CO2} kg_{algae}^{-1} is the stoichiometric ratio meaning that one kilogram of biomass is able to capture 1.83 kg of carbon dioxide (Aghaalipour *et al.*, 2020). Since the daily irradiance value is available for every month, it is possible to compute the areal productivity, which is better expressed as ton ha^{-1} d^{-1}(Borella *et al.*, 2021). The areal productivity represents the produced biomass per unit of surface and in this case, it is computed as the irradiance divided by the biomass lower heating value, times the photosynthetic efficiency.

$$Areal_{prod} = \frac{Irr}{LHV} photosyn_{eff} \tag{3.3}$$

For biomass, the value of LHV is assumed to be 18 MJ kg^{-1} (Zaimes and Khanna, 2013), while three different photosynthetic efficiencies have been considered, namely 2%, 4%, and 6%. Carrying out this step for every month, considering the three photosynthetic efficiencies, the next task is to multiply the areal productivity by 31, which is the number of days in a month, so that this quantity results to be expressed as ton ha^{-1}. Figures 3.1, 3.2, and 3.3 show the areal productivity variation along a year, expressed as ton ha^{-1}, considering each of the three photosynthetic efficiencies.

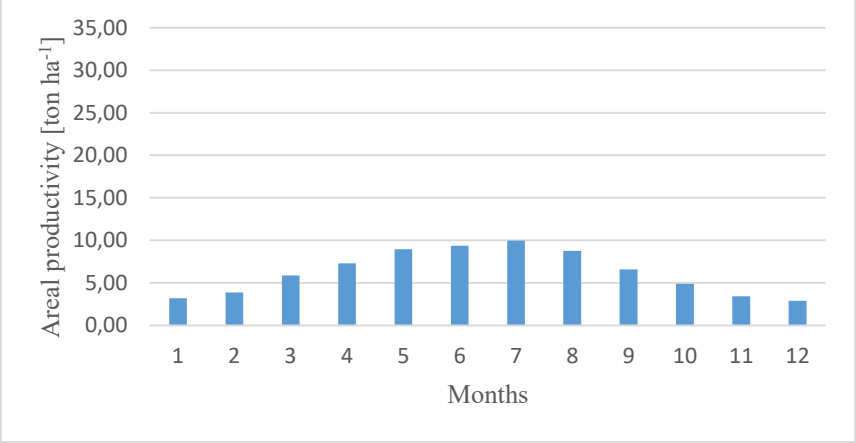

Figure 3.1. *Areal productivity [ton ha^{-1}] along a year, with photosynthetic efficiency of 2%.*

Figure 3.2. *Areal productivity [ton ha^{-1}] along a year, with photosynthetic efficiency of 4%.*

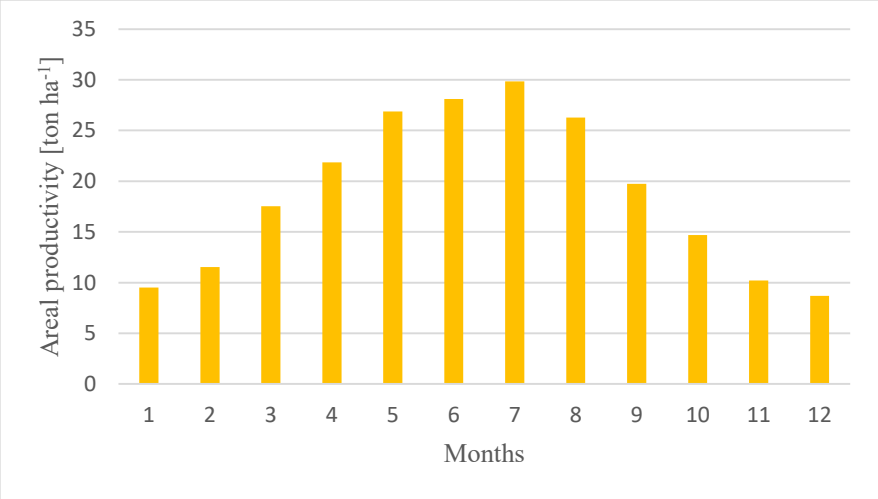

Figure 3.3. *Areal productivity [ton ha^{-1}] along a year, with photosynthetic efficiency of 6%.*

As expected, the higher areal productivities are obtained in summer. The next task is to evaluate the area that is required for microalgae cultivation.

$$Area_{required} = \frac{\dot{m}_{biomass}}{Areal_{prod}} \tag{3.4}$$

In equation 3.4, the numerator term is the yearly biomass production, expressed in ton y^{-1}.

Results are listed in table 3.2.

Photosyn eff [%]	Areal prod [ton ha^{-1} y^{-1}]	Area [ha]
2	74.9	11634
4	149.9	5817
6	224.9	3878

Table 3.2. *Required surface for the culture, using natural light.*

Results confirm what was stated in chapter 1, namely it is not convenient to use natural light, not only for seasonality and for light-dark periods during a day, but also because a huge surface would be required.

Instead, when artificial light is used, the procedure for computing the irradiated area is different. The produced biomass mass flow rate is the same as before, but the areal productivity values are taken from Borella *et al*., 2021, as well as the irradiance values and the LED efficiencies (referred to red and blue LED lamps). Table 3.3 shows the results.

$Areal_{prod}$ [g m^{-2} d^{-1}]	$Areal_{prod}$ [ton ha^{-1} y^{-1}]	$Area_{required}$ [ha]	Irradiance [kW ha^{-1}]	LED efficiency	Power required [kW]
22.4	81.76	10670	134.4	0.791	1,812,434
28	102.2	8533.5	201.6	0.789	2,180,434
31	113.2	7707.7	268.8	0.787	2,632,572
39	142.4	6126.6	336	0.785	2,622,360
48.5	177.03	4926.6	672	0.775	4,271,822

Table 3.3. *Area and power that are required, using artificial light (Areal productivities, irradiances and LED efficiencies by Borella et al., 2021).*

Note that the irradiance values have been converted from μmol m^{-2} s^{-1} into kW ha^{-1} (Borella *et al*., 2021). The required area has been computed as reported in equation 3.4, while the required power has been obtained from:

$$Power_{required} = \frac{(Irradiance)(Area_{required})}{LED\ efficiency} \quad (3.5)$$

Even using artificial light, the surface would be enormous.

Another evaluation has been done for the reactor volume. Assuming as a reference a volumetric productivity of 0.8 g L^{-1}, that is 0.1825 ton m^{-3} y^{-1} (Alberto Bertucco, personal communication), and dividing the produced biomass flow rate by this value, a volume of 4,779,000 m^3 would be needed. So, it was concluded that the idea of using the flue gas from a gas-fired power plant is not feasible to set up the hybrid process for CO_2 capture and fixation.

3.1.2 Cement production plant

Another industrial sector that has been investigated is the one of cement production. Specifically, the flue gas stream data are those of a cement plan placed in Québec, Canada, and they are reported in a paper by Nwaoha *et al*., 2018. These data are summarised in table 3.4.

Parameter	Value
Temperature [°C]	105
Pressure [kPa]	101.5
Flue gas flow rate [m^3 s^{-1}]	115
N_2 [vv%]	65.31
CO_2 [vv%]	11.5
O_2 [vv%]	10
H_2O [vv%]	13.17
NO_x [ppm]	198
SO_2 [ppm]	170

Table 3.4. *Cement production flue gas data (Nwaoha et al., 2018).*

The calculation procedure is exactly the same as the one described in § 3.1.1. Accordingly, CO_2 flow rate to be fed to the culture is equal to 1,624,000 kg d^{-1}. Considering that its 90% is captured, then the produced biomass mass flow rate is equal to 291,500 ton y^{-1}. Also the areal productivity calculation procedure is the same as the afore mentioned one, so the results obtained for the case where natural light is used are reported in table 3.5.

Photosyn eff [%]	**Areal prod [ton ha^{-1} y^{-1}]**	**Area [ha]**
2	74.97	3888.2
4	149.9	1944
6	224.9	1296

Table 3.5. *Required surface for the culture, using natural light.*

Similar computations were carried out for LED light, for which areal productivity, irradiance and LED efficiencies have been taken from Borella *et al*., 2021. Results are listed in table 3.6.

$Areal_{prod}$ [g m^{-2} d^{-1}]	$Areal_{prod}$ [ton ha^{-1} y^{-1}]	$Area_{required}$ [ha]	Irradiance [kW ha^{-1}]	LED efficiency	Power required [kW]
22.4	81.76	3565.1	134.4	0.791	605,750
28	102.2	2852.1	201.6	0.789	728,741
31	113.2	2576.1	268.8	0.787	879,854
39	142.4	2047.6	336	0.785	876,441
48.5	177.025	1646.5	672	0.775	1,427,722

Table 3.6. *Area and power that are required, using artificial light (Areal productivities, irradiances and LED efficiencies by Borella et al., 2021).*

Also in this case, results suggest that the integrated process is not feasible, since too wide areas are required, for both natural and LED light. Considering the same volumetric productivity as in subparagraph §3.1.1, the required volume for the reactor would be equal to 1,597,000 m^3.

3.1.3 Steel mill

The iron and steel production plant that has been considered is the one cited by Rigamonti and Brivio, 2022. The emitted CO_2 molar flow rate is equal to 2.26 kmol s^{-1}. Assuming that the 90% of it is captured, the produced biomass mass flow rate amounts to 1,542,266 ton y^{-1}, which has been obtained as already explained in §3.1.1. The afore mentioned calculation procedure has been followed, so that results for natural light and artificial light are obtained and reported in tables 3.7 and 3.8 respectively.

Photosyn eff [%]	**Areal prod [ton ha^{-1} y^{-1}]**	**Area [ha]**
2	74.97	20,572.87
4	149.93	10,286.36
6	224.90	6857.592

Table 3.7. *Required surface for the culture, using natural light.*

$Areal_{prod}$ [g m^{-2} d^{-1}]	$Areal_{prod}$ [ton ha^{-1} y^{-1}]	$Area_{required}$ [ha]	Irradiance [kW ha^{-1}]	LED efficiency	Power required [kW]
22.4	81.76	18,863	134.4	0.791	3,205,100
28	102.2	15,091	201.6	0.789	3,855,865
31	113.2	13,630.3	268.8	0.787	4,655,423
39	142.4	10,834	336	0.785	4,637,365
48.5	177.025	8,712	672	0.775	7,554,263

Table 3.8. *Area and power that are required, using artificial light (Areal productivities, irradiances and LED efficiencies by Borella et al., 2021).*

Considering the same volumetric productivity as in §3.1.1, the required volume for the reactor would be equal to 8,450,770 m^3. Again, the area required for the reactor is too high, for both natural and artificial light, as well as the required volume.

3.1.4 Steam methane reforming plant

The last case study refers to a steam methane reforming plant. Calculations have been carried out for both steam methane reforming (SMR) flue gas stream and pressure-swing absorption (PSA) tail gas. Figure 3.4 shows the process block flow diagram, which is referred to SMR plant that produces 150000 $Nm^3\ h^{-1}$ of hydrogen.

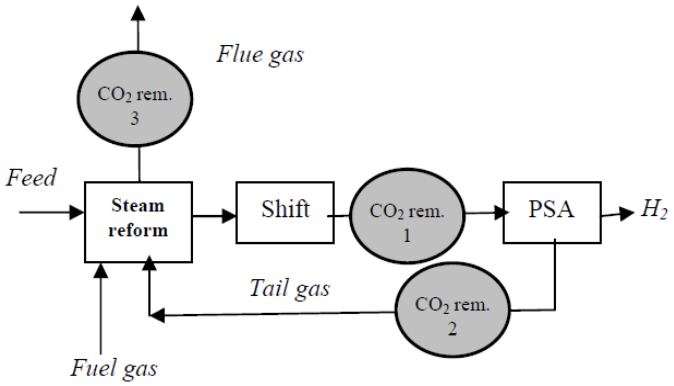

Figure 3.4. *SMR block flow diagram (Collodi and Wheeler, 2010).*

The required information has been taken from the internal report by Collodi and Wheeler, 2010, and it is listed in table 3.9.

Stream	CO_2 concentration [mol%]	CO_2 flow rate [kmol h^{-1}]
PSA tail gas	45.1	1000
SR flue gas	19.0	1850

Table 3.9. *SR and PSA flue gas composition (Collodi and Wheeler,2010).*

The usual procedure has been implemented and the results referred to natural light are reported in tables 3.10 and 3.11.

Photosyn eff [%]	Areal prod [ton ha^{-1} y^{-1}]	Area [ha]
2	74.9	2529
4	149.9	1264
6	224.9	842.8

Table 3.10. *Required surface for the culture, using natural light, for PSA tail gas.*

Photosyn eff [%]	Areal prod [ton ha^{-1} y^{-1}]	Area [ha]
2	74.9	4678
4	149.9	2340
6	224.9	1559

Table 3.11. *Required surface for the culture, using natural light, for SR flue gas.*

The same holds for computations concerning artificial light, whose results are shown in tables 3.12 and 3.13.

$Areal_{prod}$ [g m^{-2} d^{-1}]	$Areal_{prod}$ [ton ha^{-1} y^{-1}]	$Area_{required}$ [ha]	Irradiance [kW ha^{-1}]	LED efficiency	Power required [kW]
22.4	81.76	2318.50	134.4	0.791	393,940.02
28	102.2	1854.80	201.6	0.789	473,926.32
31	113.15	1675.30	268.8	0.787	572,200.43
39	142.35	1331.65	336	0.785	569,980.96
48.5	177.025	1070.81	672	0.775	928,498.42

Table 3.12. *Area and power that are required, using artificial light for PSA tail gas (Areal productivities, irradiances and LED efficiencies by Borella et al., 2021).*

$Areal_{prod}$ [g m^{-2} d^{-1}]	$Areal_{prod}$ [ton ha^{-1} y^{-1}]	$Area_{required}$ [ha]	Irradiance [kW ha^{-1}]	LED efficiency	Power required [kW]
22,4	81.76	4289.227	134.4	0.791	1,4524,654.03
28	102.2	3431.382	201.6	0.789	1,747,3766.29
31	113.15	3099.313	268.8	0.787	2,109,7153.75
39	142.35	2463.556	336	0.785	2,101,5321.74
48.5	177.025	1981.004	672	0.775	3,423,3938.14

Table 3.13. *Area and power that are required, using artificial light, for SR flue gas (Areal productivities, irradiances and LED efficiencies by Borella et al., 2021).*

Eventually, also the required volume has been computed, using the same volumetric productivity as in the previous case studies. When artificial light is used, the reactor volume would be 1038688.52 m^3 for PSA tail gas, while it would be equal to 1,922,000 m^3 for SR flue gas.

Steam methane reforming plant results are slightly better than the other cases, since a lower value for the reactor area would be required. But it is not enough, because its values are still high. Therefore, it has been decided to reduce by one order of magnitude the CO_2 flow rate in PSA tail gas and to carry out these evaluations once again. Results are shown in tables 3.14 and 3.15.

Photosyn eff [%]	**Areal prod [ton ha^{-1} y^{-1}]**	**Area [ha]**
2	74.9	253
4	149.9	126
6	224.9	84.3

Table 3.14. *Required surface for the culture, using natural light, for PSA tail gas with reduced flow rate.*

$Areal_{prod}$ [g m^{-2} d^{-1}]	$Areal_{prod}$ [ton ha^{-1} y^{-1}]	$Area_{required}$ [ha]	Irradiance [kW ha^{-1}]	LED efficiency	Power required [kW]
22.4	81.76	231.85	134.4	0.791	39,394.00
28	102.2	185.48	201.6	0.789	47,392.63
31	113.15	167.53	268.8	0.787	57,220.04
39	142.35	133.17	336	0.785	56,998.10
48.5	177.025	107.08	672	0.775	92,849.84

Table 3.15. *Area and power that are required, using artificial light, for PSA tail gas with reduced flow rate (Areal productivities, irradiances and LED efficiencies by Borella et al., 2021).*

Finally, the required volume for the reactor, considering a volumetric productivity of 0.292 ton m^{-3} y^{-1}, is equal to 64,918.03 m^3.

It can be concluded that the latest results are better, since there are orders of magnitude of difference, if compared to the other cases. It was concluded that the PSA tail gas stream with reduced CO_2 flow rate is the basis to start the simulation of the integrated process, in order to assess its actual feasibility.

3.2 Absorption column

The first operation unit in the process flowsheet (see figure 2.11) is the absorption column. In this paragraph, simulations set up is explained, up to the column design choices.

3.2.1 Equilibrium simulation

After defining the system components in the Properties section of Aspen Plus®, following the procedure that is described in chapter 2, the simulation environment has been used in order to simulate the column at equilibrium conditions. For the gas feed, a PSA tail gas from a steam methane reforming plant has been used. Since from the internal report by Collodi and Wheeler, 2010, only CO_2 flow rate is known, the stream composition, total flow rate, and conditions have been taken from the article written by Katebah *et al*., 2022, which are reported in table 3.16.

Component	Molar fraction
CO_2	0.641
CO	0.01
CH_4	0.1
H_2	0.242
N_2	0.002
H_2O	0.005

Table 3.16. *Molar composition of the gas feed to the column (Katebah et al., 2022).*

The total feed flow rate is equal to 166.896 kg h^{-1} and its pressure is 2.5 bar, and this information is referred to PSA unit tail gas of methane-steam reforming plant (Katebah *et al*., 2022), while temperature is simply assumed to be 30°C. Once the gas feed stream has been defined, the focus is on the solvent stream. To begin the equilibrium simulation, an aqueous solution has been used with the following characteristics: 10% wt of Na_2CO_3, 77°C, 2.5 bar, and a total flow rate equal to 100 kmol h^{-1}. The salt concentration and the temperature have been chosen, considering data reported by Knuutila *et al*., 2010, where several experiments are described, aiming to assess the best conditions for CO_2 chemical absorption, using hot potassium carbonate or sodium carbonate aqueous solutions. Indeed, in this article, several salts concentrations and different temperatures are investigated, among which those that used to start simulating the system. Afterwards, in Aspen Plus® main flowsheet, the column block has been defined using Radfrac column typology. Inside block specifications, the equilibrium calculation type is selected, and as a first guess, 100 equilibrium stages are set up. The gas stream was imposed to enter at the bottom stage, while the solvent one at the top stage. The column pressure is set equal to 2.5 bar, as well as the one of the solvent stream. There are two product streams: a gas one exiting from the top, and a liquid stream going out from the bottom. The latter one is the rich water solution, that is going to be the reactor feed.

In the reaction section, the equilibria that have been defined inside the Chemistry folder, are inserted, so that block reactions are specified, also because they are recalled within the block itself, since the starting and the ending stages where they take place have to be specified.

Running the simulation, no convergence was found, even if the number of equilibrium stages has been changed, namely it has been reduced. Therefore, it was decided to change the block typology, by selecting a flash tank. In this way, the separation feasibility could be checked. Figure 3.5 shows the process flowsheet when the flash tank is used, instead of the column.

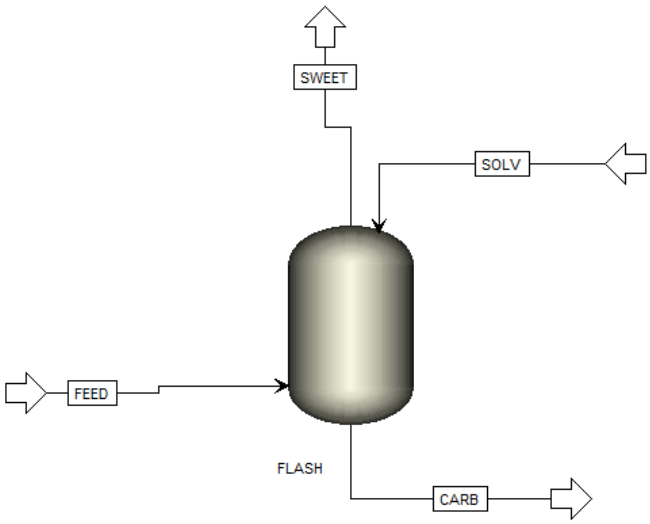

Figure 3.5. *Equilibrium simulation using a flash tank.*

Convergence was reached and the outlet liquid is characterized by pH equal to 9.32, which is in agreement with the usual pH values for microalgal cultures, since they range between 5 and 10 (Daneshvar *et al*., 2021). Subsequently, the flash tank was substituted by a Radfrac column again, with a number of equilibrium stages equal to 10. The new process flowsheet is shown in figure 3.6.

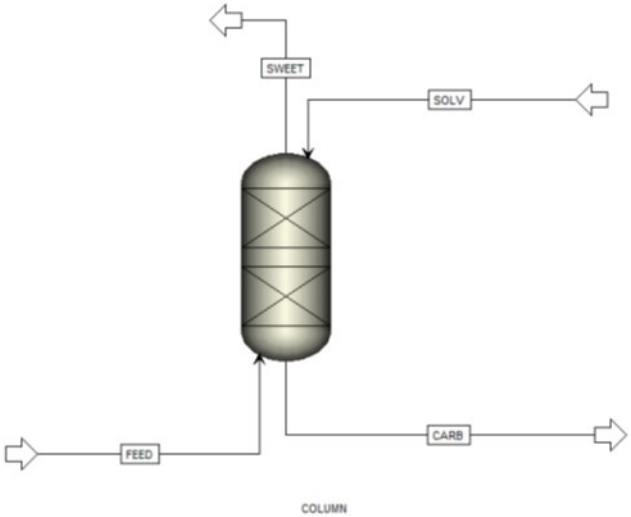

Figure 3.6. *Equilibrium simulation using a Radfrac column.*

Aiming to achieve convergence, some modifications have been applied. Namely, keeping the same gas feed composition, the flow rate was changed: instead of 5 kmol h^{-1} (Katebah *et al.*, 2022), its value was computed using CO_2 flow rate taken from the article by Collodi and Wheeler, 2010. It was reduced by one order of magnitude, and then the total molar flow rate of the gas feed was computed according to equation 3.4.

$$Feed_{flowrate} = \frac{\dot{n}_{CO_2}}{y_{CO_2}} = \frac{100\frac{kmol}{h}}{0.641} = 156\frac{kmol}{h} \tag{3.4}$$

This value has been used for all the simulations conducted in the thesis. Instead, all molar fractions and the pressure are kept the same (Katebah *et al.*, 2022). In this way, convergence was achieved, with CO_2 capture below 2% and pH below the value of 8. Then, some changes have been applied to the solvent stream, by increasing the flow rate up to 200 kmol h^{-1}.

In addition, on the website https://fr.wikipedia.org/wiki/Fichier:Solubilite_Na2CO3.png, the solubility curve of sodium carbonate in water is available, and it is reported in figure 3.7.

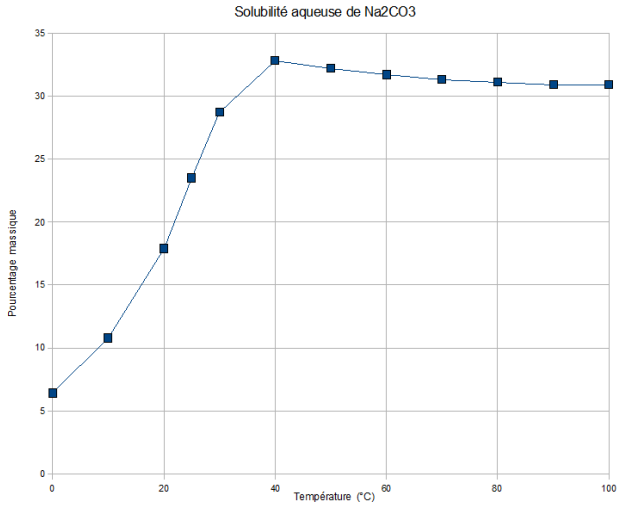

Figure 3.7. *Na_2CO_3 solubility in water (https://fr.wikipedia.org/wiki/Fichier:Solubilite_Na2CO3.png).*

This plot shows the limiting sodium carbonate concentrations in water depending on temperature, beyond which, precipitation occurs. So, its concentration in the solvent stream has been changed, namely the value of 32% wt was chosen, while temperature is kept equal to 77°C. Running the simulation, pH value reached 8.63, but CO_2 capture was as low as 4.7%.

Anyway, this equilibrium simulation is just a starting point, since real results are obtained using the rate-based approach.

3.2.2 Rate-based approach

Inside Radfrac block specifications section, the calculation type is changed from equilibrium to rate-based, so that non-equilibrium separation can simulated by the software. Still within the block section, Column Internals subdivision is fulfilled with column design specifications. Specifically, the rating mode is selected, as well as the packing type. For the latter one, Sulzer "Structured Packings Energy-efficient, innovative & profitable" manual is examined, to choose the best packing type. For this application, Sulzer Mellapak structured packing is selected. Its features are (Sulzer "Structured Packings Energy-efficient, innovative & profitable" manual, structured_packings.pdf (sulzer.com)):

Pressure drop per theoretical stage 0.3-1.0 mbar;

Pressure drop at 70 80% flooding about 2 mbar m^{-1};

Minimum liquid load approx. 0.2 m^3 m^{-2} h^{-1};

Maximum liquid load up to more than 200 m^3 $^{m-}$2 h^{-1} (typical in desorption columns).

This packing type is usually employed in CO_2 absorbers. The size is selected as 250X, since it allows for lower pressure drops per unit of packing height, with respect to 250Y size. The corrugation angle is imposed to be equal to 60°, so that the contact between the two phases is enhanced, with respect to the case where the default value of 45° is used. Inside the rate-based modelling folder, mass transfer conditions are defined. Namely, the reaction condition factor is set equal to 0.9, to state that reactions occur in the liquid film, while the film discretization ratio is imposed equal to 5, so that being greater than 1, thinner film regions are considered in proximity of the interface between vapour and liquid. The column height has been varied in the range between 5-20 m, while the diameter is made range between 0.8-2 m. Also the number of equilibrium stages is made vary from 10 to 30. It is worth noting that "equilibrium stages" is not in conflict with "non-equilibrium calculations". Indeed, in Aspen Plus®, one equilibrium stage results in a mass transfer integration step. These three choices are meant to help reaching

convergence. Another key aspect is that the gas feed molar composition has been changed, since the previous one contained a very high CO_2 concentration. The new composition is retrieved from the paper by Pellegrini et al., 2020, where carbon dioxide removal from PSA tail gas is studied. This information is reported in table 3.17.

Component	Molar fraction
CO_2	0.5095
CO	0.1454
CH_4	0.0945
H_2	0.2369
N_2	0.0075
H_2O	0.0062

Table 3.17. *Molar composition of the gas feed to the column (Pellegrini et al., 2020).*

The temperature of this stream is equal to 28°C (Pellegrini *et al*., 2020), while pressure is kept equal to 2.5 bar (Katebah *et al*., 2022). The total molar flow rate is the one computed using equation 3.4. The final convergence is reached, using an aqueous solution of sodium carbonate concentrated at 14% wt, entering the column with a temperature of 35°C, and the column final characteristics are listed in table 3.18.

Parameter	Value
Height [m]	5
Diameter [m]	0.9
Equilibrium stages	20

Table 3.18. *Column features.*

Under these conditions, the liquid exiting the column has a pH equal to 9.019, while carbon dioxide capture is equal to 99.999%. The rich solution is fed to a flash tank, in order to flash out the vapour phase, and the liquid stream exiting this unit is characterized by a pH equal to

9.43, and contains the 95.6% of CO_2 that was in the column liquid outlet. The flash is operated at atmospheric pressure and at 30°C. The process flowsheet up to this point is shown in figure 3.8.

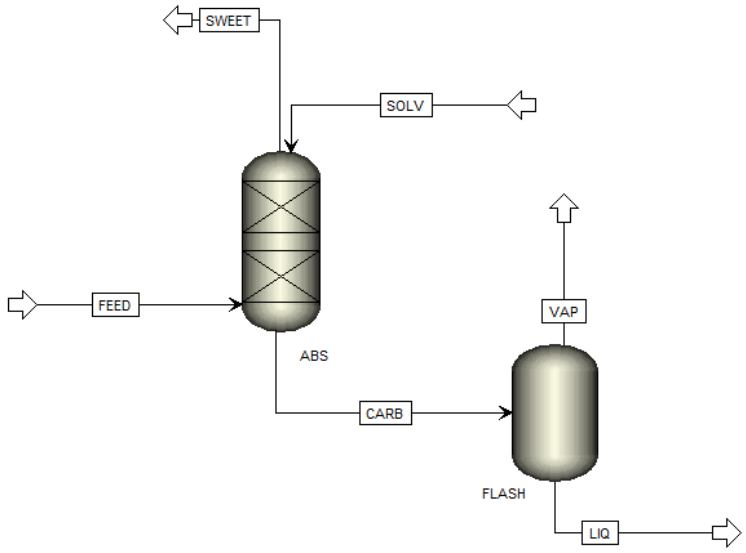

Figure 3.8. *Rate-based simulation.*

3.2.3 Solvent composition and flow rate

Previously, the choice of working with an aqueous solution of sodium carbonate, that is concentrated at 14% wt has been mentioned, together with the temperature choice of 35°C. Looking at figure 3.7, at this temperature, the solubility of this salt in water is equal to 33% wt, but keeping its concentration this high means having precipitation issues inside the column. To avoid these problems, it is better to work below the solubility limit. Simulations have been carried out ranging between 10 and 20% wt for Na_2CO_3 concentration, and between 30 and 45°C for the solvent inlet temperature. In addition, several attempts have been made by varying the solvent flow rate and the column height too, that are described below.

3.2.3.1 Carbon dioxide capture and outlet liquid pH dependence on column height

Simulations converged with a column diameter of 0.95 m, corresponding to a flooding percentage of 87.66%, while the solvent stream has a temperature of 35°C, a sodium carbonate

concentration of 14% wt and a water flow rate of 140,000 kg h^{-1}. Figure 3.9 shows the profile of carbon dioxide capture along packing height.

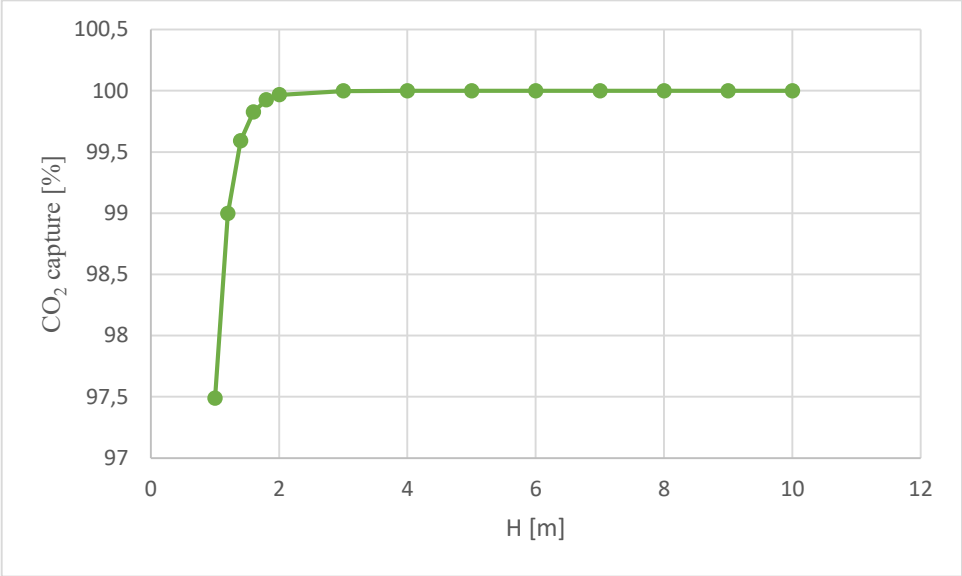

Figure 3.9. *CO_2 capture vs H.*

Changing the packing height, carbon dioxide capture is more affected than pH. Overall, the latter one changes from 9.04 down to 9.02, and from the value of 3 m on, it remains constant. CO_2 capture changes from 95.726 % corresponding to 1 m, up to 99.999% when the height is equal to 10, even if above the value of 4 m, it remains constant as well.

3.2.3.2 Carbon dioxide capture and outlet liquid pH dependence on solvent flow rate

When simulating this system, it was noticed that what makes the difference for the value of the pH in the outlet liquid is the ratio between CO_2 flow rate that is fed to the bottom, and Na_2CO_3 flow rate entering at the top of the column. This ratio cannot be below the value shown in equation 3.5, in order to ensure the desired value of pH.

$$Ratio_{pH} = \frac{\dot{m}^{in}{}_{Na_2CO_3}}{\dot{m}^{in}{}_{CO_2}} = \frac{23000\frac{kg}{h}}{4400.96\frac{kg}{h}} = 5.226 \quad (3.5)$$

The values in equation 3.5 are taken from Aspen Plus® stream results section.

According to simulation results, CO_2 percentage capture is constant at 99.99% for water flow rates from 80,000 kg h^{-1} to 200,000 kg h^{-1}, and the pH value is constant as well around the value of 9.01. Results confirm that what is fundamental is to keep the ratio between the inlet flow rates of carbon dioxide and sodium carbonate equal to a proper value.

Before starting to simulate the photobioreactor, the sodium ion concentration is checked because it is known that each microalgal species has its own alkalinity tolerance. According to Batac et al., 2020, who describe the procedure and the results obtained by feeding CO_2 in bicarbonate form to an *Arthrospira Platensis* culture, the presence of Na^+ and K^+ ions causes a decline in biomass productivity. So it is important to modulate their concentrations. For this reason, water flow rate is increased to 900,000 kg h^{-1}, while keeping Na_2CO_3 equal to 23,000 kg h^{-1} to ensure a suitable pH value, in order to have no more that 1% by mass of Na^+ ion in the liquid stream entering the reactor. Hence, the total solvent flow rate is equal to 923,000 kg h^{-1}, and the sodium carbonate concentration is 2.5% wt. In order to avoid flooding, the column diameter and height are set equal to 1.83 m (flooding percentage of 80%) and 5 m respectively. In this way, the liquid exiting the column is characterized by 1% wt of Na^+ and a pH equal to 9.3, while CO_2 capture remains 99.99%.

3.3 Photobioreactor

Once convergence is reached on the absorption column, the reactor can be introduced in the simulation environment. It was decided to model it as a continuously stirred tank reactor (CSTR), so Rstoich CSTR from the model palette in Aspen Plus® was selected. In order to achieve all the specifications, the procedure that is followed is in agreement with the one described in chapter 2.

3.3.1 Computing reactor volume and biomass production

Figure 3.10 shows the process flowsheet up to this point.

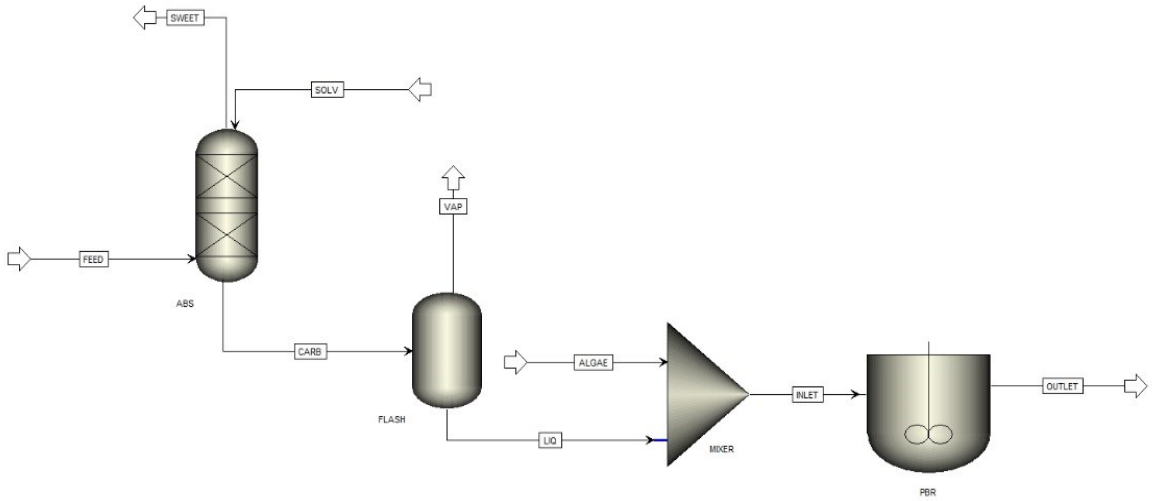

Figure 3.10. *Process flowsheet including reactor simulation.*

The liquid stream coming from the flash tank is fed to the reactor. It is mixed with an additional microalgae stream for convergence purposes, as explained in chapter 2. In fact, the latter one is equal to $9e^{-8}$ kg h^{-1}, so it is absolutely negligible if compared to the liquid flow rate coming from the absorber, since its value is in the order of 1,000,000 kg h^{-1} (see Appendix C). The Fortran® subroutine is recalled inside Aspen Plus® "Reactions" section, in order to account for the kinetics of biomass production. The reactor temperature and pressure are set to 30°C and 1 atm respectively, while the volume is set randomly. Namely, starting from the value of 40,000 m^3, following the criterion that the quantity of carbon that is fixed in the reactor must be the equal to the amount that is absorbed. This value is calculated as:

$$F_{C,CO_2}^{abs} = \frac{\dot{m}_{CO_2}^{in} - \dot{m}_{CO_2}^{out}}{MW_{CO_2}} \cdot MW_C = \frac{(4400.96 - 0{,}440096)\frac{kg}{h}}{44\frac{kg}{kmol}} \cdot 12\,\frac{kg}{kmol} = 1200\,\frac{kg}{h} \qquad (3.6)$$

Concerning the column, the amount of absorbed carbon is equal to captured CO_2 only, because carbon monoxide is not included in the equilibria that occur in the system.

The same rationale is followed for the reactor, where carbon amount calculation includes CO_2, HCO_3^- and CO_3^{2-}, which are the carbon sources participating to the equilibria.

$$F_{C,CO_2}^{PBR} = \frac{\dot{m}_{CO_2}^{in} - \dot{m}_{CO_2}^{out}}{MW_{CO_2}} \cdot MW_C \tag{3.7}$$

$$F_{C,HCO_3^-}^{PBR} = \frac{\dot{m}_{HCO_3^-}^{in} - \dot{m}_{HCO_3^-}^{out}}{MW_{HCO_3^-}} \cdot MW_C \tag{3.8}$$

$$F_{C,CO_3^{2-}}^{PBR} = \frac{\dot{m}_{CO_3^{2-}}^{in} - \dot{m}_{CO_3^{2-}}^{out}}{MW_{CO_3^{2-}}} \cdot MW_C \tag{3.9}$$

The reactor volume then is increased, until the sum of the results of F_{C,CO_2}^{PBR}, $F_{C,HCO_3^-}^{PBR}$, and $F_{C,CO_3^{2-}}^{PBR}$ is equal to 1200 kg h^{-1}. To match this condition, it was necessary to increase the solvent stream flow rate. By a try-and-error procedure, varying the solvent flow rate and the reactor volume, convergence was reached as well as the desired carbon capture inside the reactor. This result was obtained in correspondence of a solvent flow rate equal to 2,000,000 kg h^{-1} and a liquid volume inside the reactor of 137,128 m^3. The corresponding residence time is 2.912 days, while biomass production is 2400.4 kg h^{-1} and its outlet concentration is 1226.5 g m^{-3}. It is worth noting that, the system needs to be diluted, and that with a higher solvent flow rate, a biomass production matching the desired carbon capture is obtained. On the other hand, having a higher solvent flow rate to be fed to the absorber, column diameter and height must be changed, in order to meet all the column design specifications (see §3.2). Specifically, the new diameter and packing height are equal to 2.8 m (floding percentage of 78%) and 7 m respectively.

3.3.2 Solid-Liquid separator

A flash tank is added to the process flowsheet after the photobioreactor, in order to separate all the volatile species. The liquid stream, which contains biomass too, is fed to a solid liquid separator, as it is shown in figure 3.11.

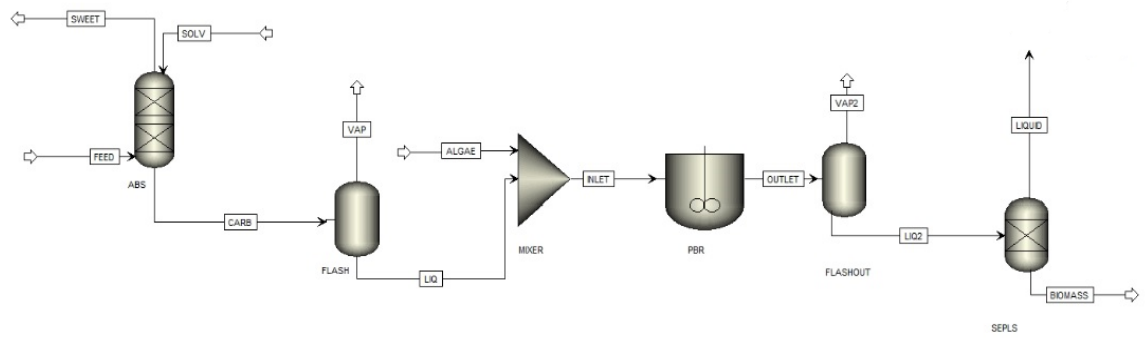

Figure 3.11. *Process flowsheet including the solid-liquid separator.*

Since all the biomass produced has to be collected in the stream exiting from the bottom of this separator, and that its mass fraction must be equal to 0.20, the split fractions are imposed for each component present in the system. For component biomass the split fraction is set equal to 1, while for the other species, this value has been calculated, as shown below.

$$Biomass\ total\ flow\ rate = \frac{\dot{m}_{biomass}^{produced}}{0.20} \tag{3.10}$$

$$Split\ fraction_{conventional\ comp} = \frac{Biomass\ total\ flow\ rate}{Liq_2} \tag{3.11}$$

Indeed, knowing biomass flow rate and mass fraction, from their ratio, the total flow rate value is obtained for stream “biomass”. Dividing the latter one by the flow rate of the stream entering the separator, the split fraction is obtained. This value must be the same for each conventional component. At present, a generic separator is used, but in the real plant, a bladed static separator should be chosen, considering that it is one of the cheapest devices for biomass separation (Alberto Bertucco, personal communication).

3.4 Complete process flow diagram and results of the base case

Here, the complete process layout, some considerations about the purge percentage, the fresh make-up, and some worth noting aspects concerning the photobioreactor depth are presented.

3.4.1 Final process flow diagram

The base case has been simulated considering that red and blue light is used (parameters for the kinetic model are reported in table 2.3), with an incident radiation of 420 μmol m^2 s^{-1}, and a reactor depth of 0.05 m. Figure 3.12 shows the final process layout.

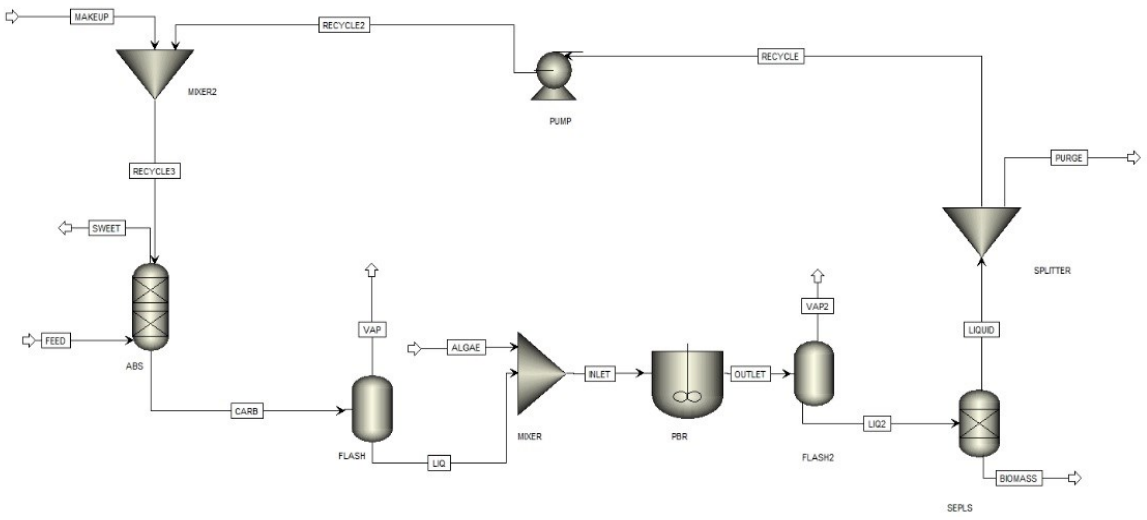

Figure 3.12. *Complete process flow diagram.*

The liquid exiting from the separator is led to a split section. Here, a part is purged put, while the rest is recycled back to the absorber. Before reaching the column though, a pump ensures to reach the absorption pressure of 2.5 bar. The pump efficiency is assumed equal to 90%. Once pressure is restored, the recycle stream is mixed with some fresh make-up, and the resulting stream is fed to the top of the column. The fresh make-up is needed because of the losses occurring along the process (stream tables are reported in Appendix C).

3.4.2 Solvent regeneration and recycle: a mass balance on carbon

The liquid stream coming from the solid-liquid separator has to be recycled back to the absorber, but before another separation step is needed, in order to restore the solvent characteristics. A splitter is used to model this step. Different purge percentages have been simulated and the corresponding fresh make-up has been computed accordingly. From figure 3.13 up to 3.16, the carbon flow rates are reported as a function of purge fraction.

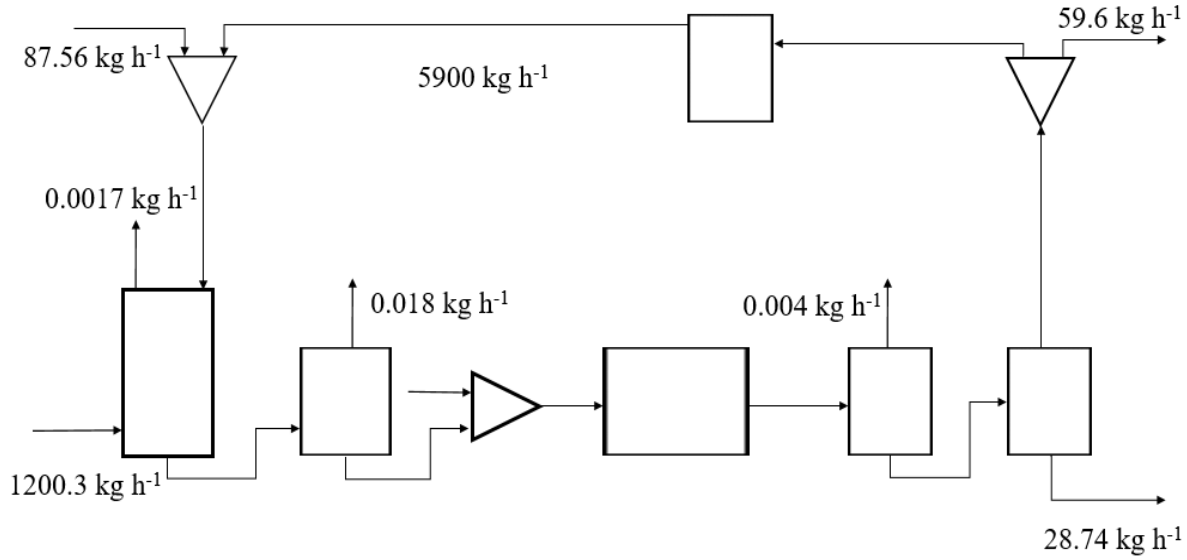

Figure 3.13. *Block flow diagram with 1% of purge.*

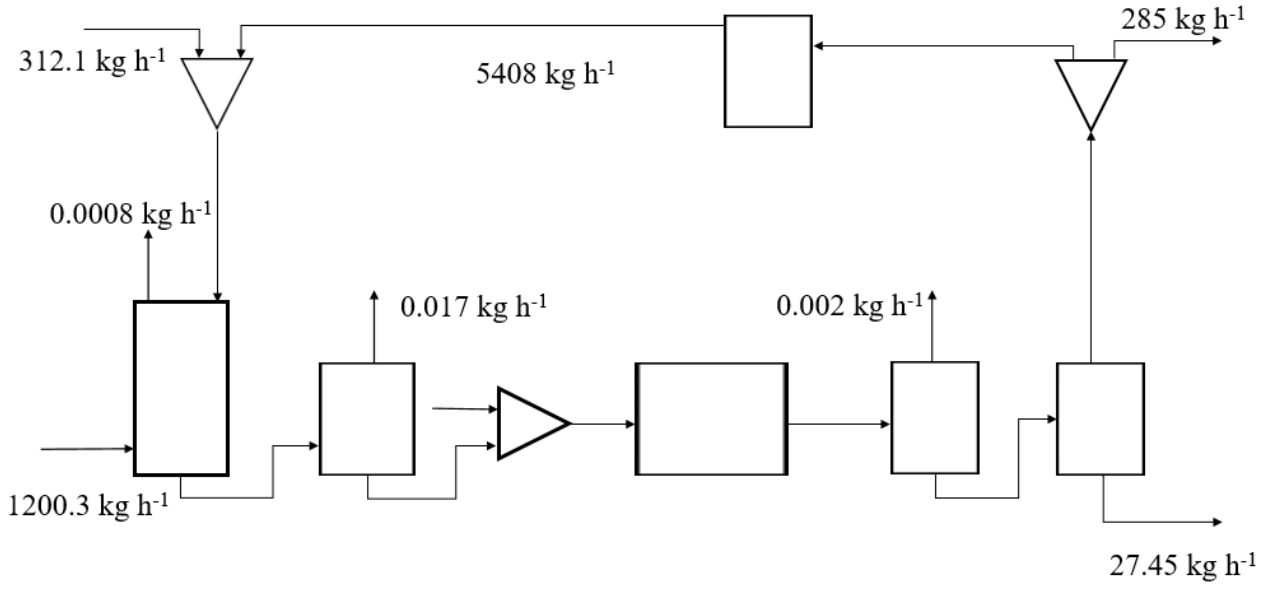

Figure 3.14. *Block flow diagram with 5% of purge.*

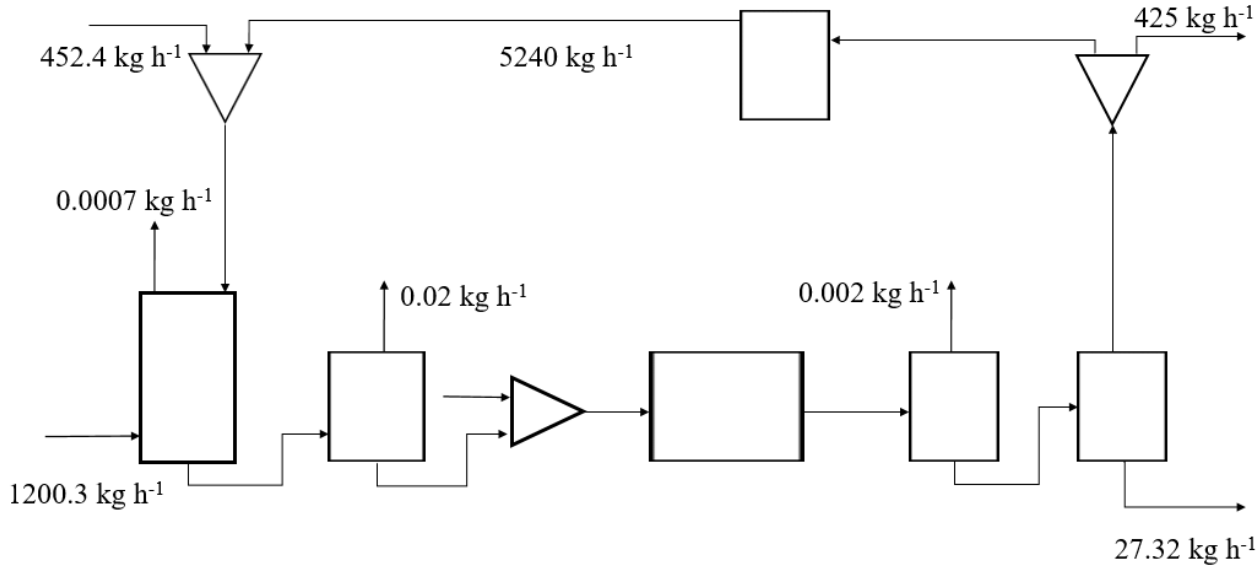

Figure 3.15. *Block flow diagram with 7.5% of purge.*

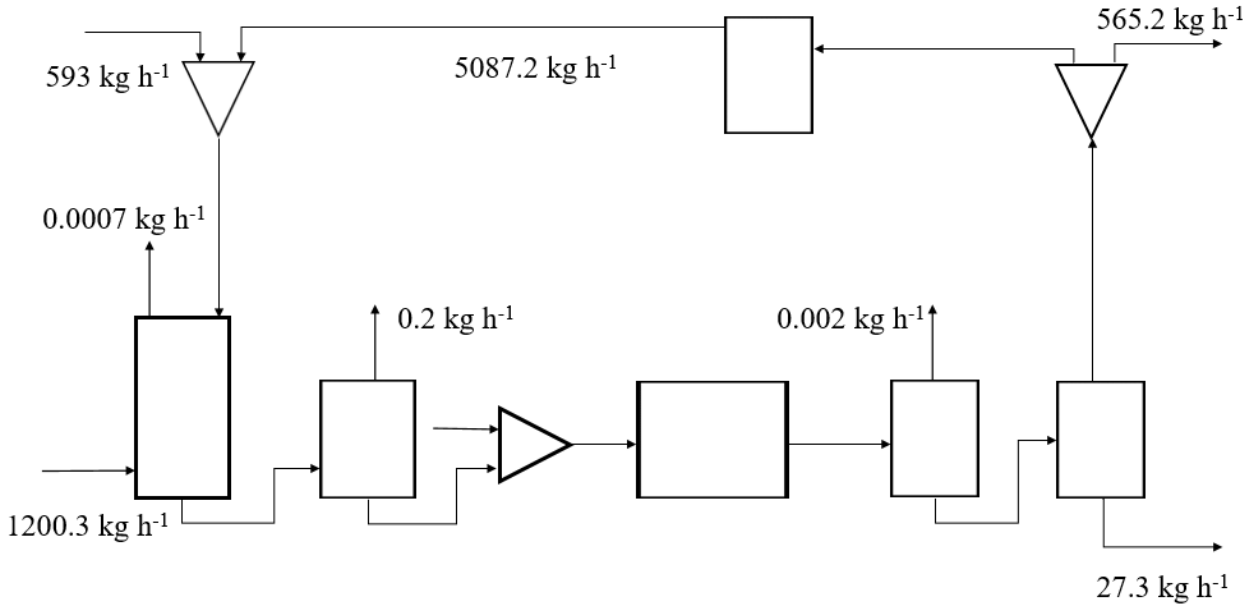

Figure 3.16. *Block flow diagram with 10% of purge.*

Note that along the process, some losses inevitably occur. When biomass is separated, it is unavoidable that a part of carbonate and bicarbonate ions are drown in the stream exiting the bottom of the solid-liquid separator. In addition to this, a purge stream is necessary, considering

that even if not present in this simulation, microalgae nutrients must be recycled. Since there is a purge stream, a solvent make-up is required, in order to obtain the composition needed to achieve the desired CO_2 separation. Obviously, changing the flow rate that is purged put, the fresh make-up flow rate varies accordingly, as figure 3.17 shows.

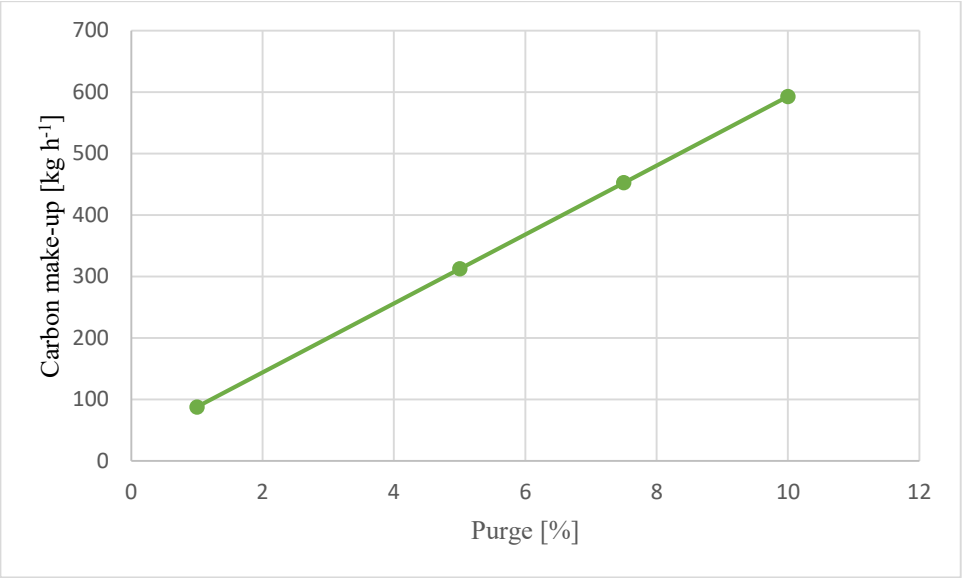

Figure 3.17. *Carbon make-up trend varying purge percentage.*

For each of the four cases considered, the make-up flow rate is computed by subtracting the recycle stream flow rate from the original solvent flow rate. The lower the purge, the lower the fresh make-up, hence a lower economical effort is required to make the process work properly. The drawback is that microalgae produce exopolysaccharides, which constitute the extra-cellular polymeric substance (Colta, 2023). For this reason, the purge percentage cannot be lower than 5% (Colta, 2023), otherwise such natural polymers may accumulate in the system, causing several issues. That is why, even though convergence is reached in any of the four cases showed above, purge percentage was kept equal to 10%.

3.4.3 Compensation point and reactor depth effect

Up to this point, simulations have been carried out considering a reactor depth of 5 cm and an incident radiation equal to 420 μmol m^{-2} s^{-1}. However, it is necessary to recall that microalgae

metabolism includes both growth and respiration phenomena. The compensation point is defined when light intensity is such that the growth rate is equal to the respiration rate (Shi *et al*., 2022). Indeed, the expression for the biomass production reaction rate is composed by two terms, a positive and a negative one. The first one is referred to microalgal growth, while the second one accounts for maintenance. In order to compute the radiation in correspondence of which compensation point occurs, the net biomass production rate is set equal to zero, as it is reported in equation 3.12.

$$\mu_{app}\varphi(T)\frac{I(comp)}{I(comp)+K_I\left(\frac{I(comp)}{I_{opt}}-1\right)^2}-\mu_{emax}\left(\frac{I_0}{I_0+K_{im}}\right)=0 \tag{3.12}$$

This expression is taken from the article by Pastore *et al*., 2022, where the kinetic model adopted for the simulations in described (see chapter 2). Solving this equation, considering an incident radiation of 420 μmol m^{-2} s^{-1}, the compensation intensity results equal to 142.2 μmol m^{-2} s^{-1}. The reason why its value is high could be due to the fact that the maintenance term, namely the parameter μ_{emax} is quite relevant. Anyway, once compensation irradiance is obtained, the compensation depth must be computed. To do so, the relation between light intensity and reactor depth (Pastore *et al*., 2022) is used.

$$I(comp)=I_0\exp(-\overline{k_a}C_{x,out}h) \tag{3.13}$$

From equation 3.13, the product between the biomass outlet concentration and the reactor depth is computed.

$$C_{x,out}h=\frac{1}{\overline{k_a}}\ln\left(\frac{I(comp)}{I_0}\right) \tag{3.14}$$

Following the rationale reported in equation 3.15, the outlet biomass concentration is constant because the flow rate is constant.

$$\dot{m}_{biomass}^{produced}=2400\frac{kg}{h}=V_R\cdot P_v=V_R\cdot\frac{C_{x,out}}{\tau}=V_R\cdot\frac{C_{x,out}}{V_R}\cdot\dot{V} \tag{3.15}$$

Eventually, the reactor depth at the compensation point can be calculated, according to equation 3.16.

$$h = \frac{C_{x,out}h}{C_{x,out}} = 0.0244\ m \tag{3.16}$$

The intensity light profile along the reactor depth is shown in figure 3.18.

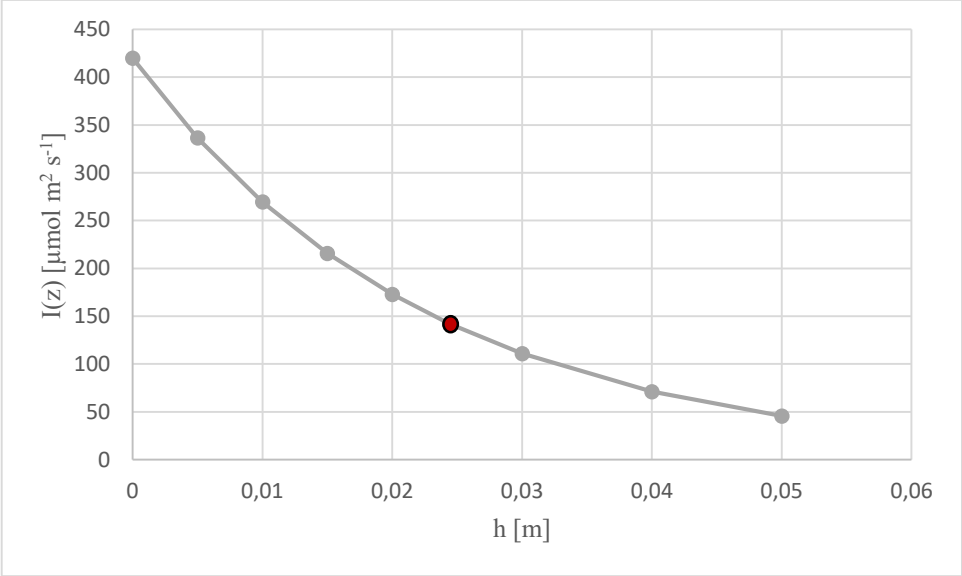

Figure 3.18. *Light profile along reactor depth.*

The reactor depth that has been used to simulate the system is greater than the compensation one. This means that there is an energy loss, because beyond the red point, maintenance is greater than the growth rate. For this reason, the simulation was repeated considering the new depth. Firstly, the new light profile is shown in figure 3.19.

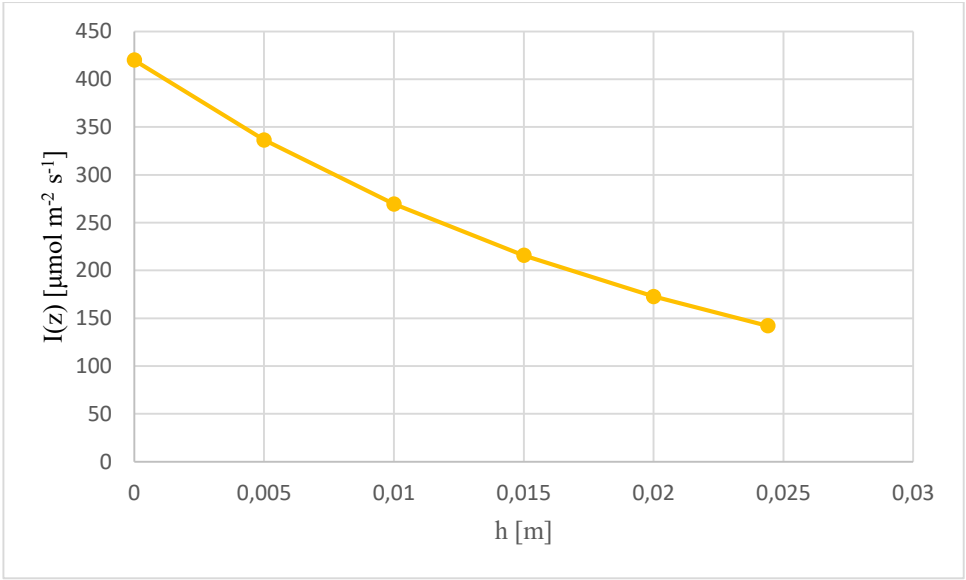

Figure 3.19. *New light profile along reactor depth.*

From figure 3.19 it is possible to see that microalgal growth is greater than maintenance over all the reactor depth, because compensation starts beyond the depth used. So there is no energy waste, because the one provided to the system is employed for growth only.

Table 3.19 compares the results obtained from the simulations.

	h = 0.05 m	**h = 0.0244 m**
V_L [m^3]	137,128	40267
τ [d]	2.912	0.855
$C_{x,out}$ [g m^{-3}]	1226.5	1226.5
$\dot{m}_{biomass}$ [kg h^{-1}]	2400.4	2400.4

Table 3.19. *Results comparison using two different reactor depths.*

It is possible to conclude that using a suitable reactor depth, namely the one where compensation occurs, the same biomass production can be achieved using a smaller volume and a shorter residence time. In addition, the outlet biomass concentration is the same. Even if reactor features have been changed, flow rates are constant and this could explain why biomass concentration remains equal to the one obtained using a bigger depth.

Chapter 4 - Photobioreactor design proposal

In this chapter calculations and simulations results are presented to discuss carbon fixation using microalgae that are grown in an open pond first. Then, a design proposal is developed for the photobioreactor, after comparing a continuously stirred tank reactor (CSTR) performance to the one of a plug flow reactor (PFR). Afterwards, the evaluation of the photosynthetic efficiency is carried out, considering different conditions, namely different incident radiations. Eventually, costs related to energy expenses for the electricity needed to use LED lamps are presented.

4.1 The Open pond option

Similarly to what has been described in chapter 3, sun light information was retrieved from the web site JRC Photovoltaic Geographical Information System (PVGIS) - European Commission (europa.eu). Selecting Sahara Desert as the geographical location, the procedure described in paragraph §3.1 was applied to obtain the results shown in table 4.1. The base of calculation is again the production of 2400 kg h^{-1} of biomass, i.e. to fix 4400 kg h^{-1} of CO_2.

Photosynthetic efficiency [%]	**Areal productivity [ton ha^{-1}]**	**Area [ha]**
1	48.49	433.6
1.5	72.88	288.5
2	97.17	216.2

Table 4.1. *Open pond area computations.*

It can be concluded that even though the open pond is built in one of the places where highest irradiance hits the Earth, the area for the plant remains huge. Besides the results reported in table 4.1, figures 4.1, 4.2 and 4.3 show the areal productivity trend along the year.

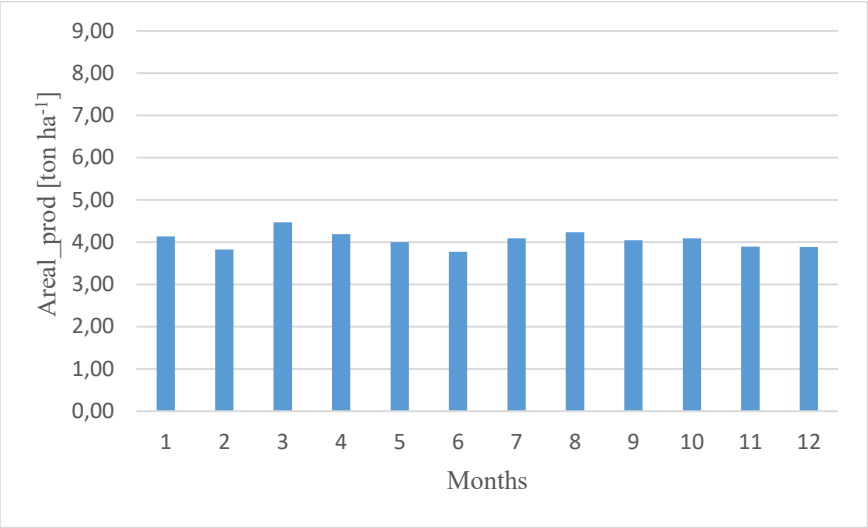

Figure 4.1. *Areal productivity trend along a year, with photosynthetic efficiency of 1%.*

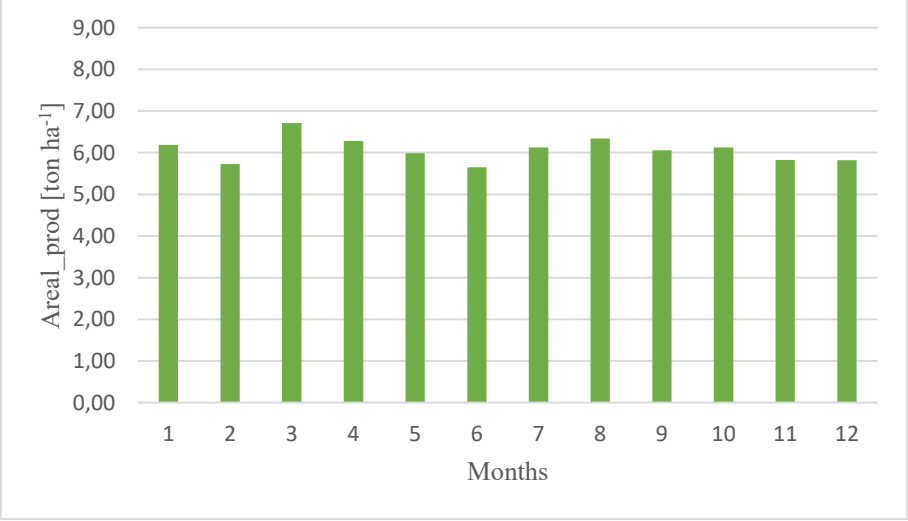

Figure 4.2. *Areal productivity trend along a year, with photosynthetic efficiency of 1.5*

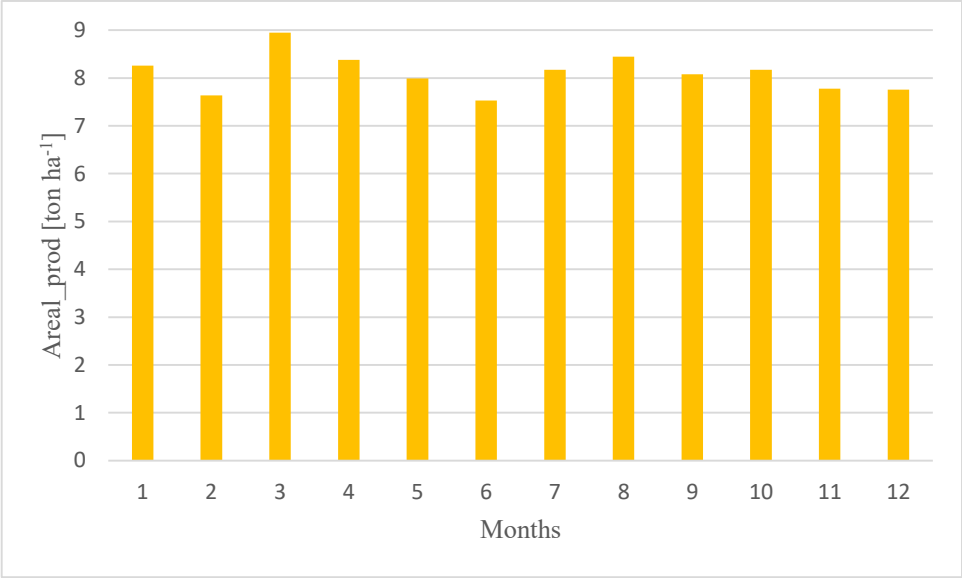

Figure 4.3. *Areal productivity trend along a year, with photosynthetic efficiency of 2%.*

As can be observed, the areal productivity trend along the months is flatter than the one considering the town of Gela, meaning that Sahara Desert is more suitable than the previous location, as far as light energy supply is concerned. All the advantages and disadvantages of using an open pond have already been described in chapter 1. Last but not least, in order to make the efficiency of sunlight exploitation to be acceptable, the pond depth should not be greater that a few centimetres, which translates in covering huge areas, as confirmed by computations. Instead, PBRs can be designed in many different ways in order to optimise space utilization, but their disadvantage is high complexity of the plant, i.e. the capital cost. Anyway, also the problem of biofouling has to be solved, maybe by means of proper design features (Nguyen *et al*., 2022). The high capital costs and the energy requirements of PBRs will be discussed at the end of this chapter.

4.2 Effect of internal mixing in microalgae cultivation

So far, all simulations were carried out with the photobioreactor modelled as a CSTR. Now, the CSTR results are compared to those obtained when a PFR model is used. In order to assess the PFR performance, the operating conditions, summarised in table 4.2, are kept equal, as well as the kinetic model parameters, to the CSTR case.

Quantity	Value
Inlet flow rate [kg h^{-1}]	$2 \cdot 10^6$
Temperature [°C]	30
Pressure [atm]	1
Incident radiation [μmol m^{-2} s^{-1}]	420

Table 4.2. *Operating conditions.*

Simulations where the reactor is modelled as a PFR were carried out in two different ways:

- feeding an additional stream of microalgae to the reactor and varying its flow rate;
- recycling the reactor outlet to its entrance and varying the recycle ratio.

In both cases, a multi-tubular reactor was used, and its volume is equal to the volume of liquid computed when modelling the reactor as a CSTR, namely 137,128 m^3. The diameter and the length of each pipe, together with the number of tubes required to ensure this value are summarised in table 4.3.

Quantity	Value
Diameter [m]	0.05
Length [m]	700
Number of tubes	99,770

Table 4.3. *Reactor specifics.*

The length of each pipe was decided considering that, in Aspen Plus® simulator, there is a limiting value for the number of pipes, which cannot exceed 99,999. About the diameter, it was set equal to the reactor depth used while simulating the base case of a CSTR, not at the compensation point.

4.2.1 Simulation with an additional microalgae feed stream

The process flow diagram is shown in figure 4.4, and it is similar to the case with a CSTR PBR.

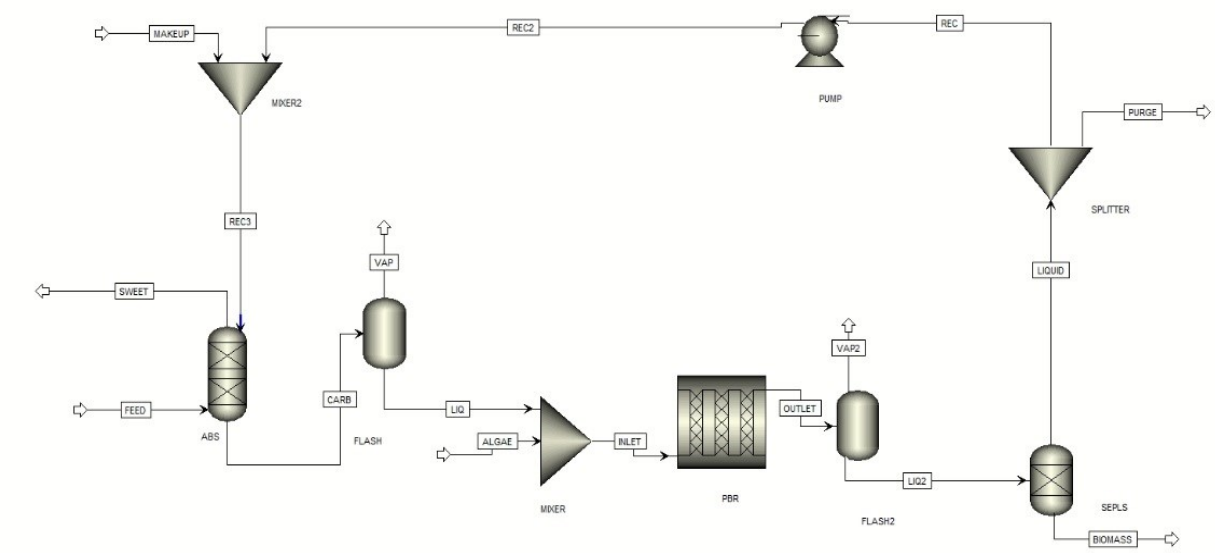

Figure 4.4. *Process layout with additional microalgae stream.*

The only difference is the value of the additional microalgae stream, which is made vary to see its effect on carbon capture, biomass production and on the residence time. Figures 4.5 and 4.6 show these trends, from which it is concluded that at least 50 kg h^{-1} of microalgae flow rate should be recycled to the PBR not to hamper its net production rate is the set value (2400 kg h^{-1}), with a corresponding residence time of about 2.9 d.

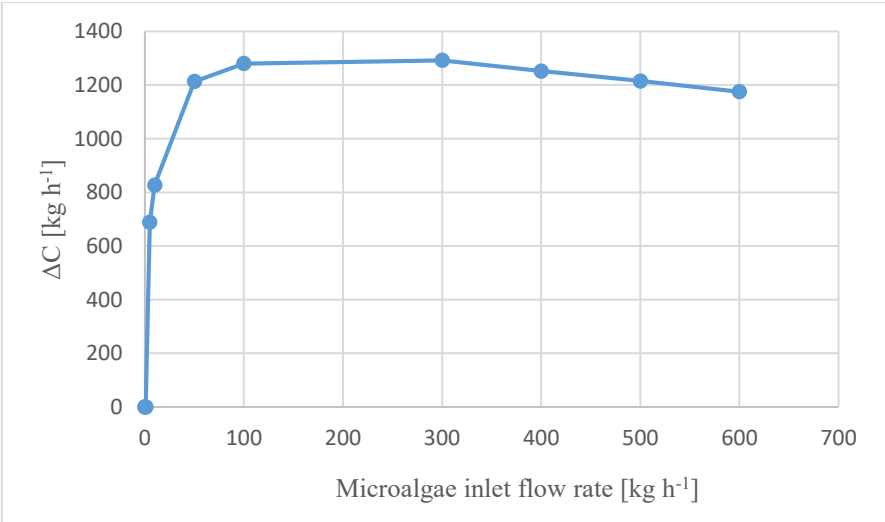

Figure 4.5. *Carbon capture vs Microalgae inlet flow rate.*

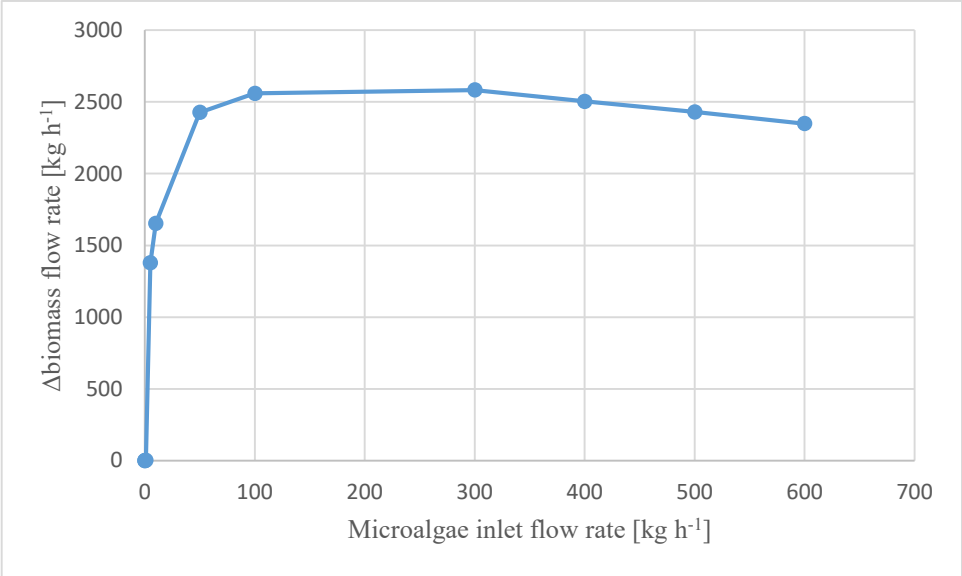

Figure 4.6. *Biomass production vs Microalgae inlet flow rate.*

From these plots, it is evident that both carbon capture and biomass production increase with increasing biomass inlet flow rate, but this effect is less pronounced above 50 kg h^{-1}. Of course, when the microalgae inlet flow rate is equal to the one used in the case of a CSTR, no biomass production occurs, in agreement with the fact that a plug flow reactor must be operated using a recycle. In fact, when the additional microalgae inlet stream is very small, if compared to the process stream flow rate, anything that enters the reactor is swept to the outlet, and no biomass production occurs. Instead, when microalgae inlet flow rate is increased, the larger it is, the higher the biomass production, because it is like having a recycle loop in the system, that allows for back-mixing inside the reactor (Paolo Canu, 2020-2021).

An interesting aspect is that the PFR shows a slight maximum in terms of biomass production, that occurs when the microalgae inlet stream has a flow rate equal to 300 kg h^{-1}: beyond this value, the trend starts to decrease, and an asymptotic value of the residence time is achieved.

4.2.2 Simulation of PFR with recycle

The process layout is shown in figure 4.7.

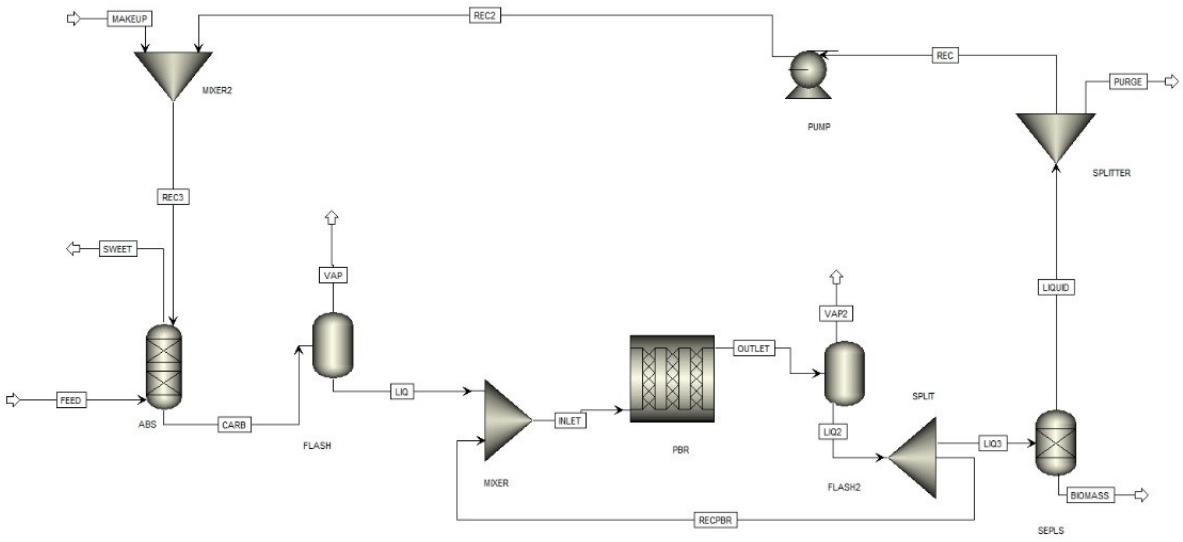

Figure 4.7. *Process layout with a recycle loop.*

In this case, the recycle ratio, that is obtained dividing the flow rate of stream called "RECPBR" by the one called "LIQ", is varied, in order to assess its effects. As before, the reactor volume was kept constant and equal to the CSTR case. Figures from 4.8 up to 4.10 show how carbon capture, the net biomass production, and the single pass residence time change with respect to the recycle ratio. The plotted data are summarised in tables 4.4 and 4.5.

Recycle ratio	**ΔC [kg h^{-1}]**
0.1	1385
0.5	1402
1	1230
5	1268
10	1236
50	1207

Table 4.4. *ΔC variation with recycle ratio.*

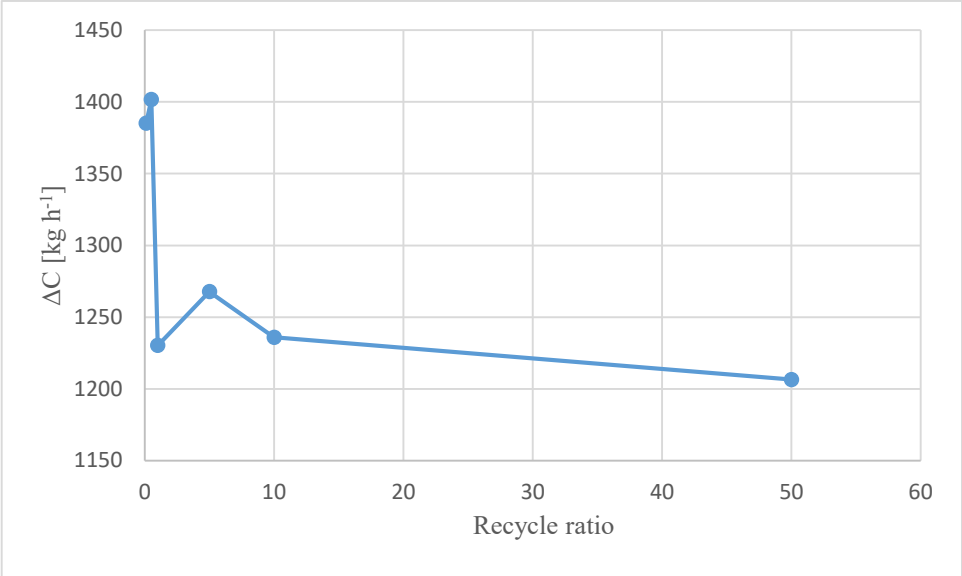

Figure 4.8. *Carbon capture vs recycle ratio.*

Recycle ratio	Net biomass production [kg h^{-1}]
0.1	2770
0.5	2803
1	2736
5	2535
10	2472
50	2409

Table 4.5. *Net biomass production variation with recycle ratio.*

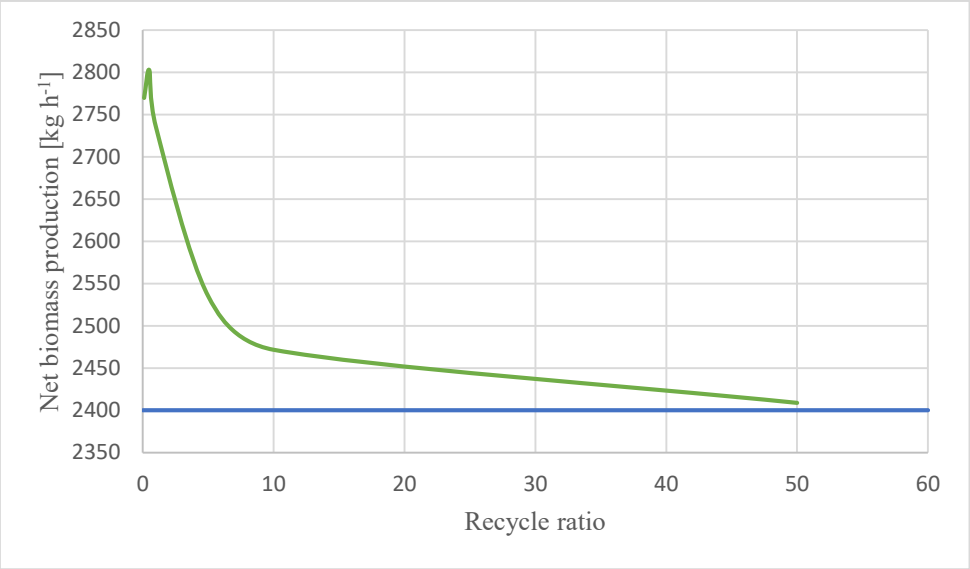

Figure 4.9. *Net biomass production vs recycle ratio.*

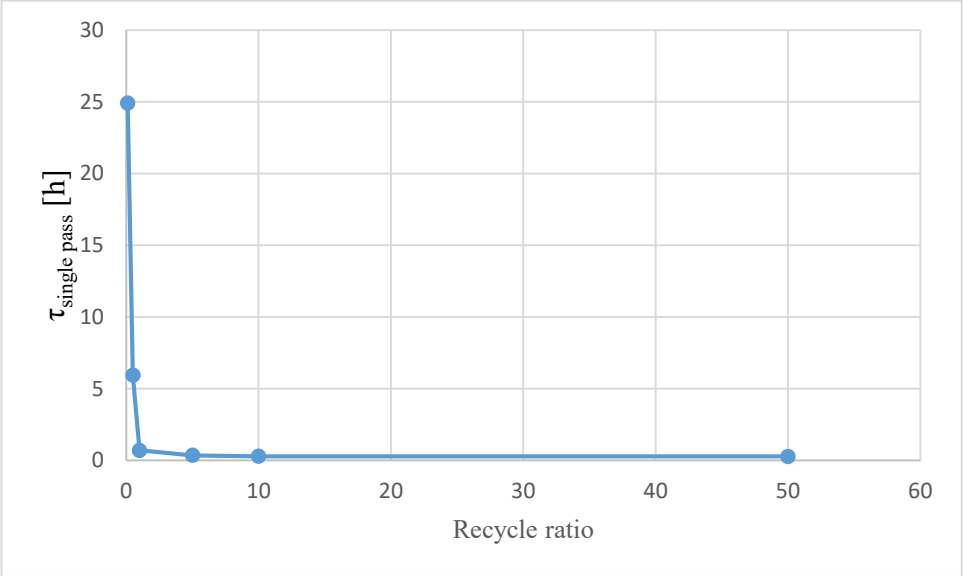

Figure 4.10. *Single pass residence time vs recycle ratio.*

It can be seen that a recycle ratio of at least 50 has to be used in order to fix the carbon flow rate absorbed in the column (1200 kg h^{-1}). The drawback is that the corresponding single pass residence time results equal to 41.2 min, while it should be around the value of 16 min to avoid oxygen inhibition and to have a suitable velocity inside the pipes, so that no sedimentation occurs (Trentin *et al.*, 2020). So the recycle ratio was further increased, and when it is imposed equal to 260, the afore mentioned value for the single pass residence time is met. In such conditions, carbon capture is slightly higher than the one occurring in the column. Higher values

of the recycle ratio are further investigated, but the single pass residence time results to be too low. As it is stated in the article by Trentin *et al*., 2020, depending on the length of the pipes, the recycle ratio changes, namely the shorter the tubes, the higher the recycle ratio. Although the length used for these simulations is equal to 700 m, high values for the recycle ratio would be needed, in order to obtain the desired carbon biological fixation and a suitable single pass residence time. Another issue is related to photo-inhibition due to the presence of oxygen (Trentin *et al*., 2020). Even though simulations are carried out using a kinetic model that does not account for it, it is known that along the reactor, as biomass is produced, oxygen concentration increases and inhibits the reaction. To avoid this issue, an optimum combination between reactor diameter, length and recycle ratio should be found, so that the whole volume can be effectively employed to host photosynthesis. Indeed, a key aspect is that a suitable biomass concentration should be provided at the reactor inlet, in order to prevent oxygen accumulation inside the pipes, hence the system needs to work under turbulent regime (Trentin *et al*., 2020).

It can be concluded that the PFR is more performing that a CSTR, even though a strong back-mixing must be provided, in order to achieve the biomass production wanted with a suitable single pass residence time. Under such conditions, it is known that a PFR approaches the behaviour of a CSTR, even if there is still a dominant direction (Paolo Canu, lecture notes). However, high recycle flow rate means larger energy duty. Also for this reason, the design proposal that is described in the following chapter, refers to the reactor modelled as a CSTR.

4.3 Reactor design proposal

This paragraph aims to describe how the photobioreactor could be laid out. This design refers to the results obtained when simulating the system using the compensation depth. The main features are reported in table 4.6.

Quantity	Value
Incident radiation	420 μmol m^{-2} s^{-1}
h (compensation)	0.0244 m
V_{liquid}	40266.7 m^3
τ	0.855 d

Table 4.6. *Simulation results at compensation point.*

It is assumed that the overall volume is divided into 250 modules, each one characterized by a side area of 4 m^2 and a volume equal to 161.1 m^3. Each module is composed by several flat PBRs, where the reaction medium is kept, which are separated from each other by LED panels. Figures 4.11 and 4.12 show the views of a module.

Figure 4.11. *Front and perspective view of a module.*

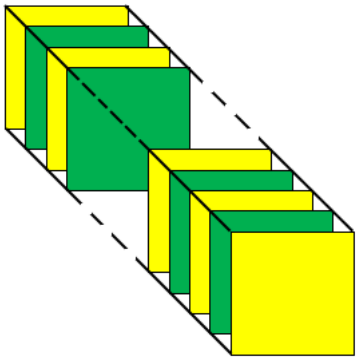

Figure 4.12. *Isometric view of a module.*

The yellow panels represent LED lamps, while the green ones the flat PBRs. The side surface of both is equal to the one of the module. Each LED is 2.5 cm thick, instead each flat PBR has a depth equal to the double of the one computed at compensation conditions, namely 0.0488 m. Except for the external ones, LED panels are double and placed side by side, as it can be seen from the perspective view in figure 4.11. All features are summed up in table 4.7.

Quantity	Value
Module, LED and flat PBR side area	4 m^2
Module length	81.47 m
LED thickness	0.025 m
Flat PBR depth	0.0488 m
Number of LED in a module	1648
Number of flat PBRs in a module	825

Table 4.7. *Module features.*

At this point, knowing the side area of a LED lamp, how many LEDs there are in a module and the number of modules, the total irradiated area can be computed, as it is reported in equation 4.1.

$$Area_{tot,irr} = Area_{LED} N_{LED} N_{modules} = 4m^2 \cdot 1648 \cdot 250 = 1.65 \cdot 10^6 m^2 \quad (4.1)$$

The modules can be contained in a shed, according to the vertical and plane view arrangements proposed in figures 4.13 and 4.14.

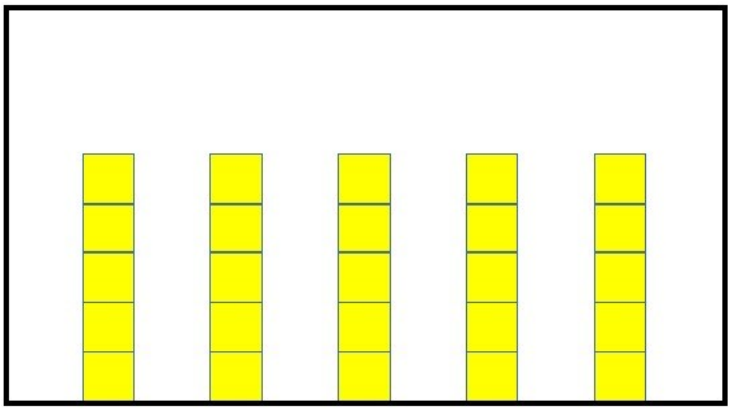

Figure 4.13. *Frontal view of a shed.*

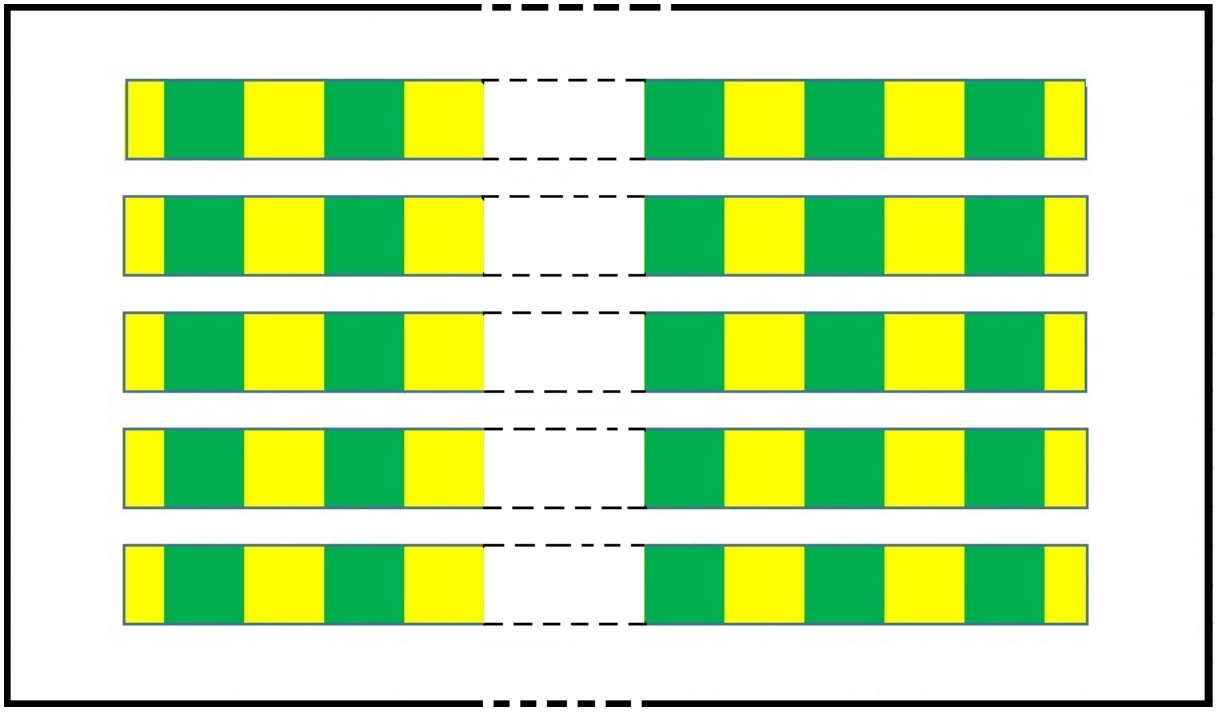

Figure 4.14. *View from the top of a shed.*

It is suggested to place 25 modules in each shed, so that the total number of sheds is equal to 10. Each shed can have an 18 m by 90 m base area, and can be 12 m high. In this way, there is 1 m of distance between one stack of modules and the other.

4.4 Incident radiation effects

Having assessed the reactor typology and proposed a design arrangement, the effects linked to different incident light intensities are studied. Specifically, keeping the same kinetic parameters, and process rationale, the incident radiation value was varied, to see how the reactor volume, the residence time and photosynthetic efficiency may change. Table 4.8 sums up the light intensity and the reactor depth at compensation point, for each case.

I_0 [µmol m^2 s^{-1}]	I(comp) [µmol m^2 s^{-1}]	h (comp) [m]
100	35.43	0.0234
200	69.09	0.0240
300	102.10	0.0243
420	142.25	0.0244

Table 4.8. *Compensation point irradiance and depth.*

Computations at compensation point are carried out following the procedure described in §3.3.3. Light profiles are shown from figures 4.15 up to 4.18.

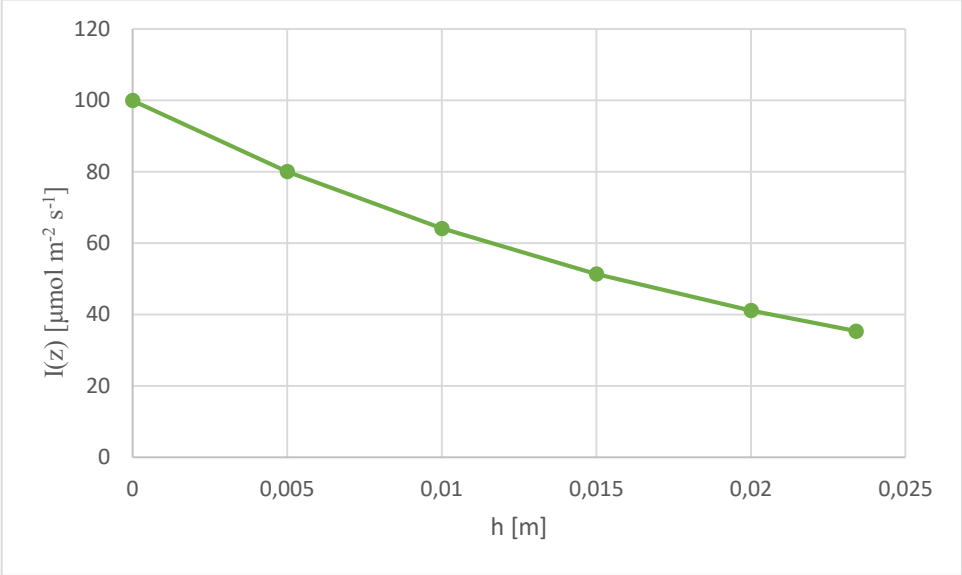

Figure 4.15. *Light profile with I_0=100 µmol m^2 s^{-1}.*

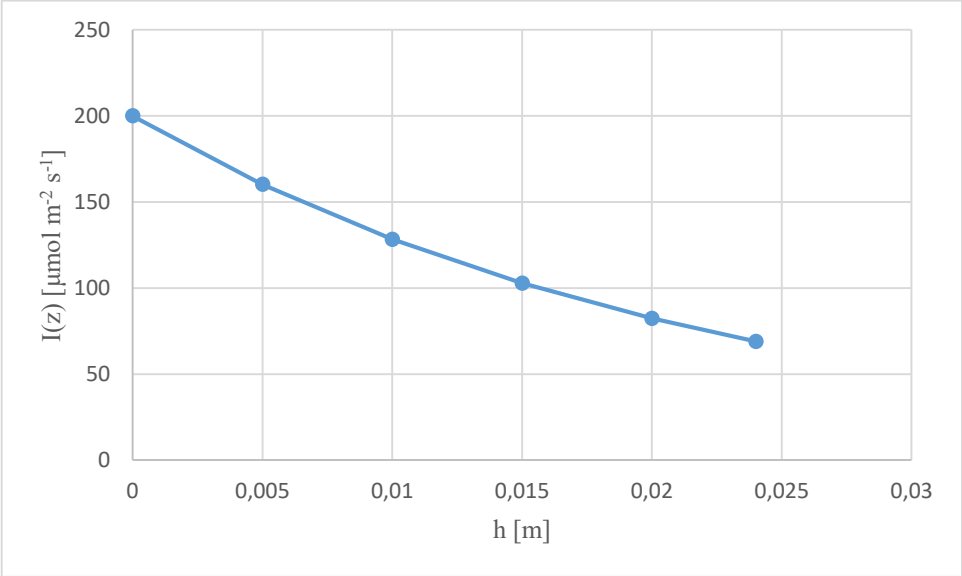

Figure 4.16. *Light profile with I_0=200 µmol m^2 s^{-1}.*

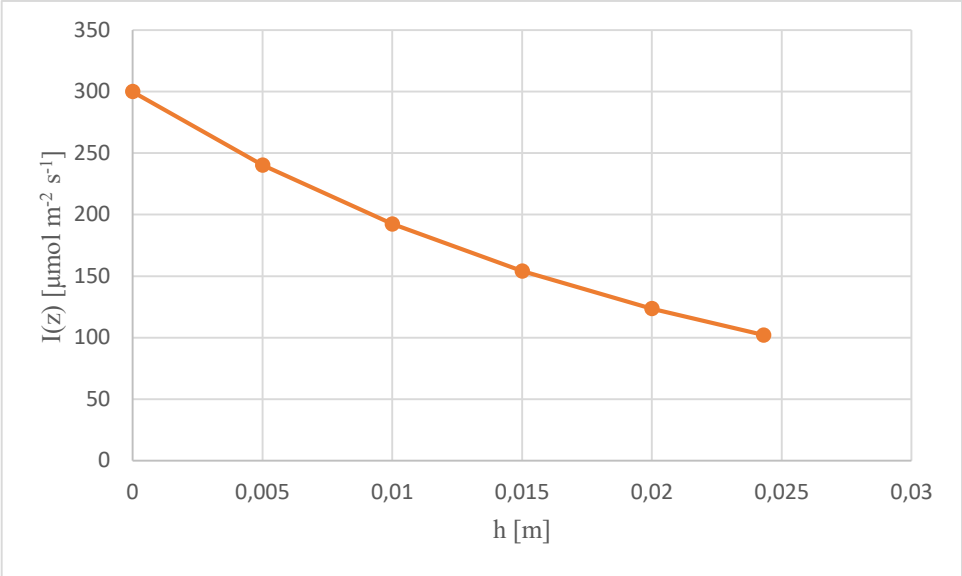

Figure 4.17. *Light profile with I_0=300 µmol m^2 s^{-1}.*

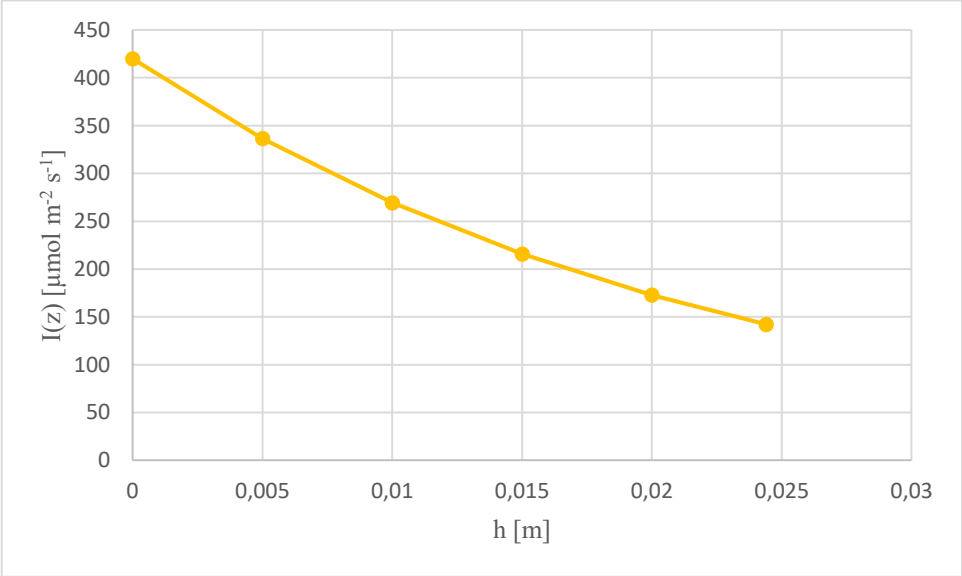

Figure 4.18. *Light profile with I_0=420 µmol m^2 s^{-1}.*

Once the compensation depth is calculated, process simulations were performed for each I_0, and the results are reported in table 4.9.

I_0 [µmol m^2 s^{-1}]	V_{liquid} [m^3]	τ [h]	Irradiated area [m^2]
100	85,851	47.75	$3.67 \cdot 10^6$
200	50,737	25.85	$2.11 \cdot 10^6$
300	41,583	21.19	$1.71 \cdot 10^6$
420	40,267	20.52	$1.65 \cdot 10^6$

Table 4.9. *Process simulations results.*

The compensation depth was computed assuming that the outlet biomass concentration (i.e. biomass production) remains the same, and indeed, this was confirmed by simulations results. This is so because the reactor volume has been modified until a biomass production of 2400 kg h^{-1} occurred. Naturally, the residence time changes from case to case. It can be observed that the lower the incident radiation, the higher its value because the volume of liquid inside the reactor is larger. As the incident radiation is increased, the volume and the residence time decrease. The total irradiated area is computed following the same procedure described in §4.3, and it is useful in order to assess photosynthetic efficiencies, which are presented and discussed in the next paragraph.

Anyway, the computations related to the compensation light intensity have been repeated using the average light intensity, instead of the incident radiation, in the maintenance term, as shown in equation 4.2.

$$\mu_{app}\varphi(T)\frac{I(comp)}{I(comp)+K_I\left(\frac{I(comp)}{I_{opt}}-1\right)^2}=\mu_{e,\max}\left(\frac{I_{av}}{I_{av}+K_{im}}\right) \tag{4.2}$$

Results are reported in table 4.10.

I_0 [µmol m^2 s^{-1}]	I_{av} [µmol m^2 s^{-1}]	I(comp) [µmol m^2 s^{-1}]	h(comp) [m]
100	62.19	22.31	0.0107
200	123.03	43.30	0.011
300	183.5	63.63	0.0111
420	256.4	87.74	0.0111

Table 4.10. *Compensation light intensities and depths update.*

As observed in chapter 3, the fact that compensation light intensity is high, is due to the maintenance term, whose value is quite high. Indeed, using a lower irradiance value in it, namely the average one, compensation light intensities result lower than the previous ones, as well as depths. Simulations should be repeated by using I_{av} instead of I_0 in the kinetic expression of the maintenance term, but it is wise to further investigate the form of the growth kinetic model before performing more rigorous simulations. In addition, a more reasonable approach would be to make the average along the reactor depth, with respect to the growth rate rather than to the light intensity, so that the punctual growth rates are calculated and averaged. This

change would result in a more realistic model, but the computational effort would be much larger. For these reasons, this part is left to a further thesis work.

4.5 Economic evaluation of energy requirements

Knowing the total irradiated area, the total energy required for the microalgal culture can be computed. This task has been accomplished, considering the different incident radiations. The procedure is reported in the equations below (Borella *et al*., 2021).

$$Incident\ light\ intensity = I_0 \cdot 0.224 \frac{J}{\mu mol} \tag{4.3}$$

$$TRP = Incident\ light\ intensity \cdot Area_{tot,irr} \tag{4.4}$$

$$LED_{electrical\ consumption} = \frac{Required\ power}{\eta_{LED}} \tag{4.5}$$

$$Photosyn.eff = \frac{Biomass\ production\ rate \cdot LHV_{biomass}}{TRP} \tag{4.6}$$

$$Photosyn.eff_{tot} = \frac{Biomass\ production\ rate \cdot LHV_{biomass}}{LED_{electrical\ consumption}} \tag{4.7}$$

$$NRP = \left(I_0 - I(comp)\right) \cdot 0.224 \left(\frac{J}{\mu mol}\right) \cdot Area_{tot,irr} \tag{4.8}$$

$$Photosyn.eff_{net} = \frac{Biomass\ production\ rate \cdot LHV_{biomass}}{NRP} \tag{4.9}$$

In equations 4.3 and 4.8, 0.224 is the factor to convert a photons flux into an energy flux, while η_{LED} is the LED lamps efficiency, assumed equal to 0.8 (Borella *et al*., 2021). TRP is the total required power, NRP is the net required power. Tables with complete calculations can be found in Appendix B. Figure 4.19 allows to compare the three photosynthetic efficiencies computed for each incident radiation.

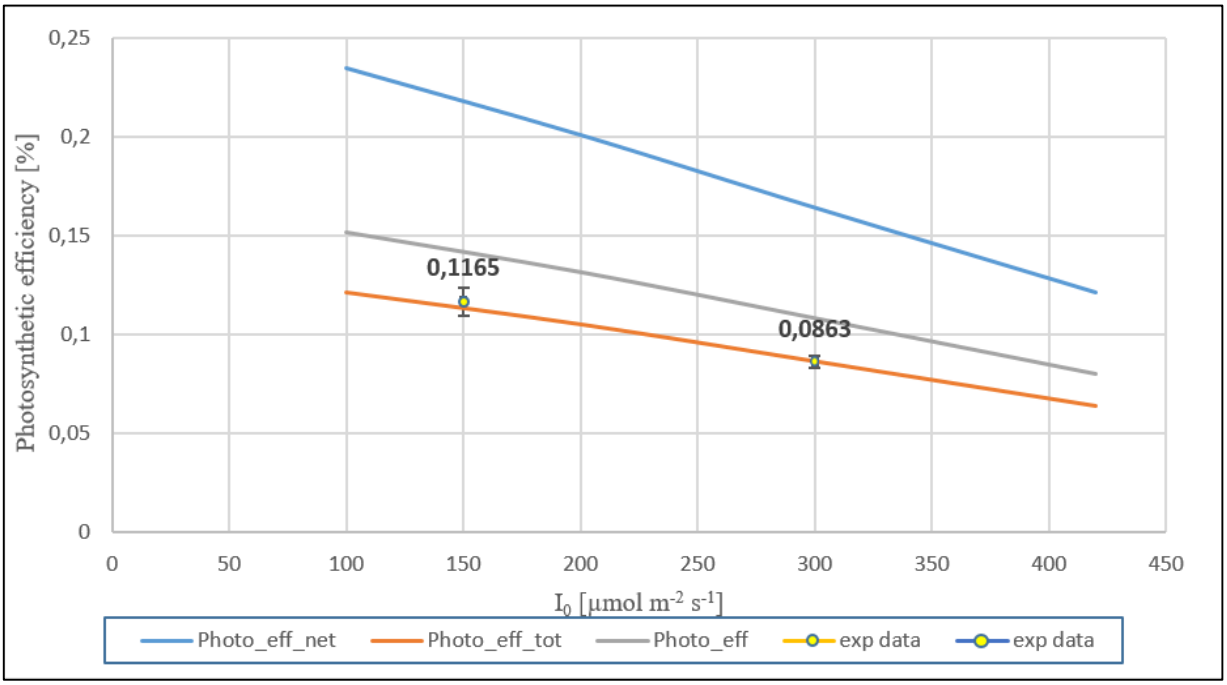

Figure 4.19. *Photosynthetic efficiencies vs I_0.*

Firstly, it is evident that the lower the incident radiation, the higher the photosynthetic efficiency achieved. The total photosynthetic efficiency trend is clearly the lowest one. Instead, the net photosynthetic efficiency is the highest one, since it has been computed considering optimistically that the power provided to the system can be totally employed for biomass production, even beyond the compensation depth, for instance, by coupling a second flat PBR, without LED panel, right after the illuminated flat PBR. Finally, the photosynthetic efficiency, that has been calculated as shown in equation 4.6, is the one based on the PAR (Photosynthetically Active Radiation) (Borella *et al*., 2021). Also two experimental values were reported in figure 4.19, which were computed as reported in equation 4.6, according to experimental data measured by Borella (personal communication). These two points overlap on the total photosynthetic efficiency, while they should be closer to the middle trend. This happened probably because the simulated photosynthetic efficiency is overestimated.

It is also noteworthy to see how the reactor volume, the volumetric productivity, the irradiated area and the required total power change as a function of the incident radiation intensity (See Appendix B for table with values). These profiles are shown from figure 4.20 to 4.24.

lues). These profiles are shown from figure 4.20 to 4.24.

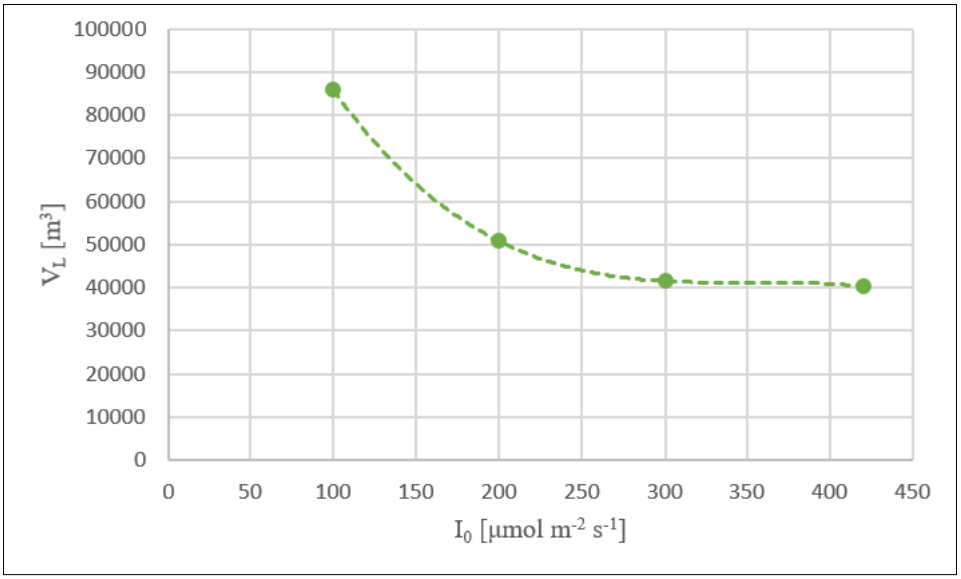

Figure 4.20. *Volume vs I_0 ($y = -0.0029x^3 + 3.0152x^2 – 1054.8x + 164047$. $R^2 = 1$).*

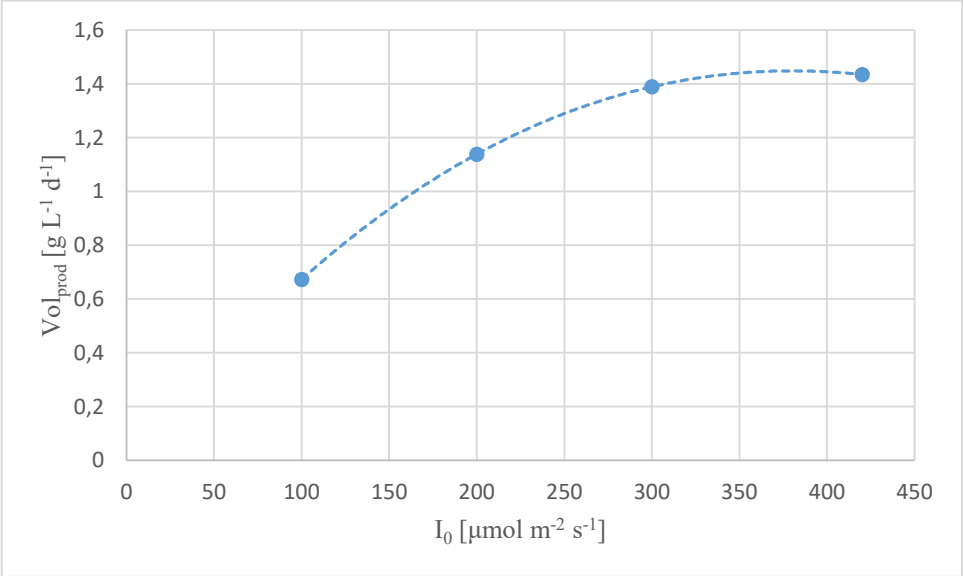

Figure 4.21. *Volumetric productivity vs I_0 ($y = 3 \cdot 10^{-9}x^3 - 1 \cdot 10^{-5}x^2 + 0.0083x – 0.0281$. $R^2 = 1$).*

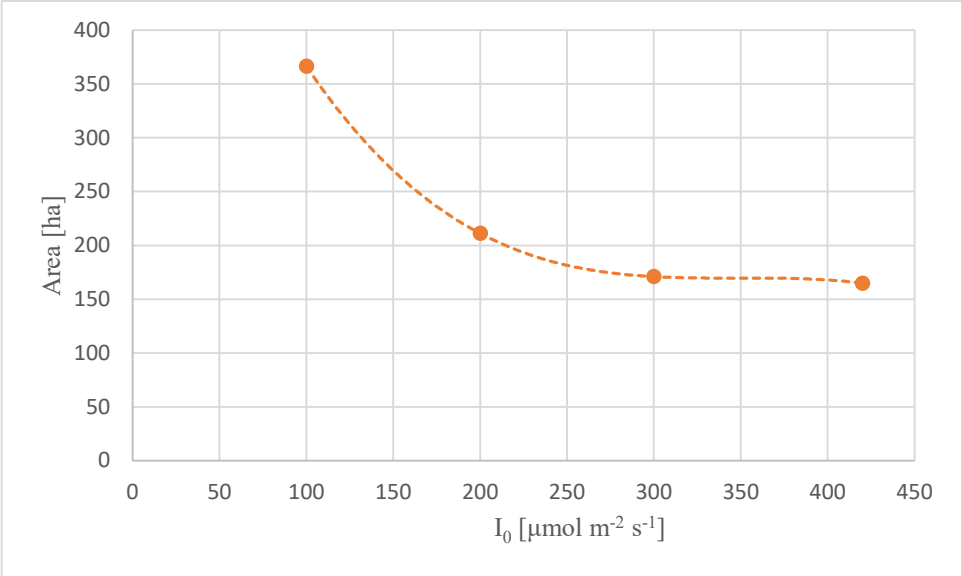

Figure 4.22. *Irradiated area vs I_0 ($y = -1 \cdot 10^{-5}x^3 + 0.0135x^2 - 4.708x + 714.81$. $R^2 = 1$).*

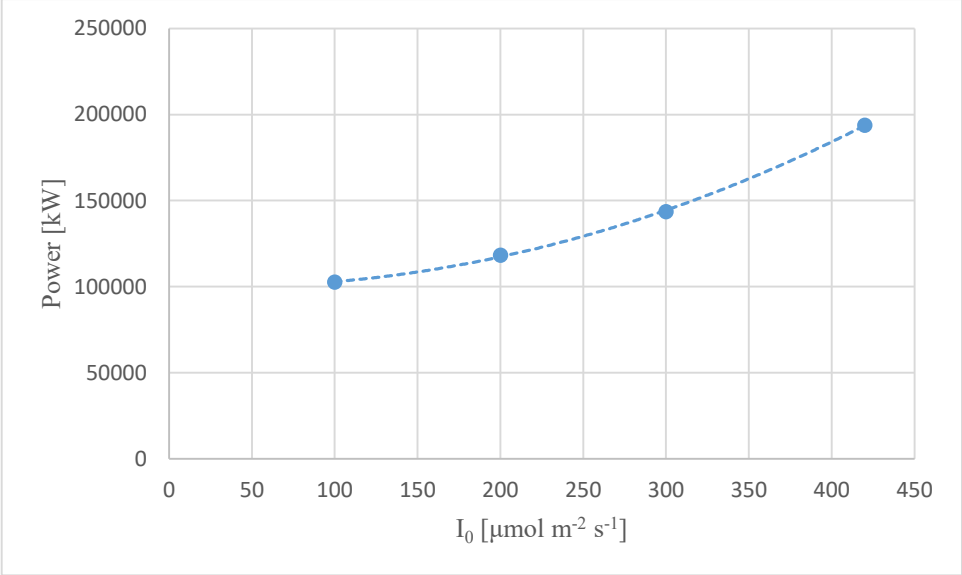

Figure 4.23. *Required power vs I_0 ($y = 0.6328x^2 - 45.708x + 101171$. $R^2 = 0{,}9996$).*

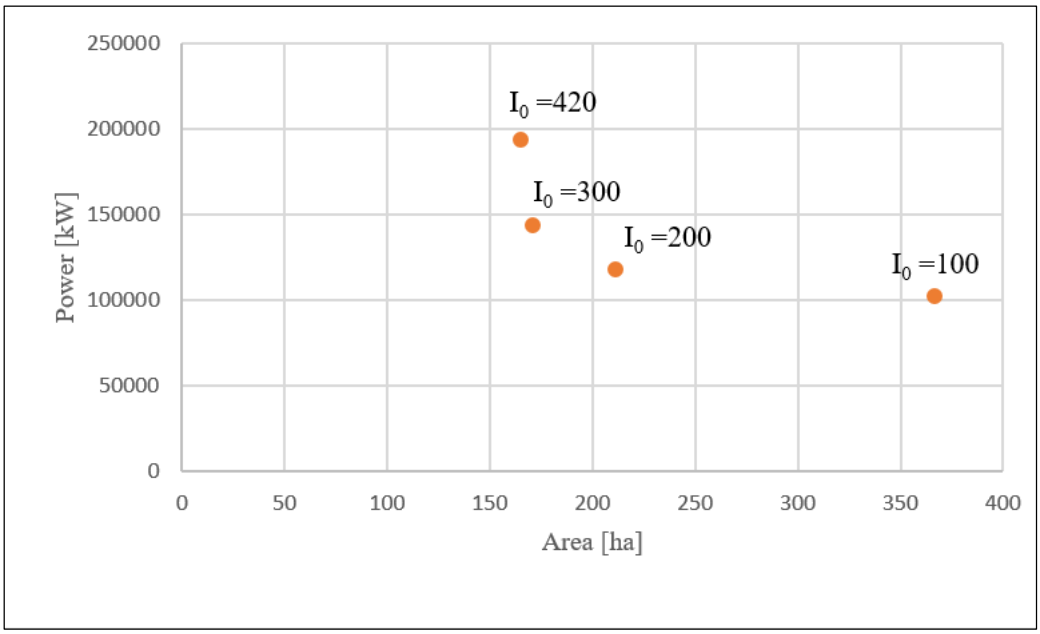

Figure 4.24. *Required power vs Area.*

From figures 4.20 and 4.21 it can be seen that the higher I_0, the lower the volume of liquid and the higher the volumetric productivity. This was expected, since a lower volume corresponds to a lower residence time, and considering that the volumetric productivity is the ratio between the outlet biomass concentration and the residence time, the conclusion is straightforward. Also the irradiated area is higher when I_0 is lower, as shown in figure 4.22. On the other hand, it must be recalled that the lower the incident radiation, the lower the power required for biomass production (see figure 4.23) and the higher the photosynthetic efficiency which is calculated. The irradiated area results wider in the case of 100 µmol m^2 s^{-1}, so one may think that the more LEDs lamps are required. This is the result from computations, but it should be mentioned that the number of lamps might not change in this case. Indeed, keeping the same area, the number of lamps with I_0= 100 µmol m^2 s^{-1} would be about one fourth of the one required if I_0 = 420 µmol m^2 s^{-1}. This is so because, LEDs would still emit 420 µmol m^2 s^{-1}, but the power distribution could be modulated, in order to ensure 100 µmol m^2 s^{-1} uniformly, over the whole area, by adopting a suitable optical system. Figure 4.24 shows how the required electrical power varies with the total irradiated area. For this profile, it was not possible to have a good fitting. This could be due to the fact that, even if the total irradiated area does not change that much when using an incident light intensity of 300 µmol m^{-2} s^{-1} instead of 420 µmol m^{-2} s^{-1}, the required power, that is linked to the value of I_0, decreases of almost 50,000 kW.

Eventually, it is interesting to discuss, at least from a qualitative point of view, how operating costs and capital costs can influence the value of the total irradiated area, and if it possible to fine an optimal value of incident light intensity.

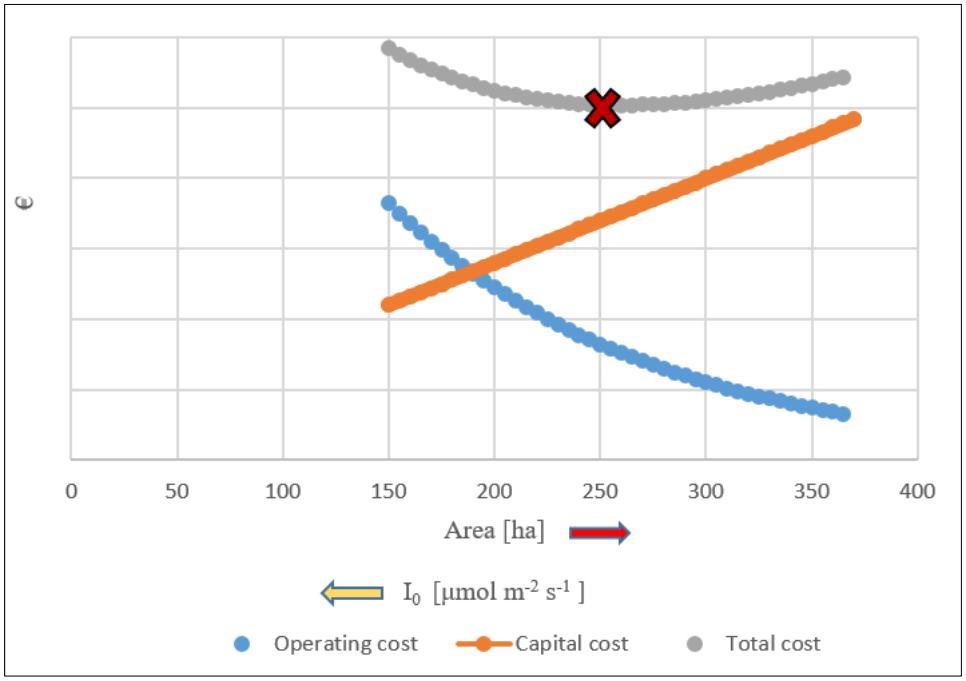

Figure 4.25. *Operating costs, capital costs and total costs vs Area.*

Figure 4.25 shows, from a qualitative point of view, how the total cost profile (grey curve) changes, depending on the total irradiated area (i.e. the incident light intensity), and resulting from the sum of operating and fixed costs. It can be observed that a minimum of the total cost curve can be found, corresponding to a precise incident radiation value. Unfortunately, the condition of optimum cannot be calculated until reliable values of both operating and equipment costs are assessed.

From an economic point of view, the operating cost related to energy supply per kg of saved CO_2 is eventually assessed. To do it, several hypothetical photosynthetic efficiencies were considered, each one smaller than the maximum theoretical value of about 30% (Borella *et al.*, 2021), which are summed up in table 4.11.

Photosyn.eff	**Power [kW]**	**Power [kWh kg_{CO2}^{-1}]**	**Power [kWh ton^{-1}_{CO2}]**
0.05	240,000	54.53	54,534
0.1	120,000	27.26	27,267
0.15	80,000	18.17	18,178
0.20	60,000	13.63	13,163
0.25	48,000	10.91	10,906

Table 4.11. *Power per saved CO_2.*

The power that is required has been computed by using the inverse formula of the one reported in equation 4.6.

$$TRP = \frac{Biomass\ production\ rate \cdot LHV_{biomass}}{Photosyn.eff} \tag{4.10}$$

The power per flow rate of CO_2 fixed (or per kg of CO_2 fixed) is computed based on its inlet flow rate to the absorber, and it is eventually expressed on the base of 1 ton of CO_2.

Assuming hypothetical different costs per kWh of electricity, the operating costs related to energy expenses for microalgae production can be obtained as summarised in table 4.12.

Photo.eff / **€ kWh^{-1}**	**5%**	**10%**	**15%**	**20%**	**25%**
	€ ton^{-1}_{CO2}	€ ton^{-1}_{CO2}	€ ton^{-1}_{CO2}	€ ton^{-1}_{CO2}	€ ton^{-1}_{CO2}
0.025	1363	682	454	341	273
0.05	2727	1363	909	682	545
0.075	4090	2045	1363	1022	818
0.1	5453	2727	1819	1363	1091

Table 4.12. *Energy operating costs.*

Analysing table 4.12, where only operating costs are evaluated, it is concluded that achieving photosynthetic efficiencies above 20% would be required, in connection with suitable renewable electricity production systems, in order to spend below 1000 € ton^{-1}_{CO2}. Note that the lowest cost per electricity (0.025 € kWh^{-1}) is in line with total production cost of electricity in the case of a wind mill field, as well as a photovoltaic panels field. Remembering that, at present, according to ETS (European Emissions Trading Scheme), the market value of 1 ton of CO_2 is almost 90€, it is still not technically clear how to increase microalgae photosynthetic efficiency up to such values, since from laboratory measurements, the value of 12% has not been exceeded (Borella *et al*., 2021). Therefore, at present, the process of sequestering carbon dioxide from tail gases of industrial productions by using microalgae does not appear economically feasible. On one hand, open ponds would require huge land area to be used, on the other hand, closed PBR energy duties result in excessive costs for electricity supply.

4.6 Final remarks and future perspectives

Nowadays, microalgae research field is strongly investigated, and there is a lot of research going on, in order to optimise several aspects of carbon biological fixation into biomass. Unfortunately, what limits the process scale-up at industrial level is the photosynthetic efficiency. This limit has not been overcome, and the only way to implement this process on a large scale, is to increase its value beyond those that have been obtained experimentally. Indeed, only with a photosynthetic efficiency of at least 20-25%, the operating cost related to the culture energy supply can be considered affordable.

With respect to that, Richard Sayre's work is quite interesting as it sets evidence to the fact that research can go over the limit concerning the photosynthetic efficiency. Specifically, the biomass yield could be increased by 40% by genetically modifying microalgae and cyanobacteria. Sayre proposed to reduce the cross section of the light-harvesting antenna complex, that is made of proteins and pigments. By tuning it properly, the value of the ratio Chlorophyll a/Chlorophyll b could be varied. Sayre and his team have found that the optimal value of this ratio is 5. In this way, through the protein NAB1, the antenna size can be controlled, and when light intensity is higher, less Chlorophyll b is produced, while the reverse occurs for lower light intensity (Sayre, 2020). In a recent review by Subramanian and Sayre (2022), several suggestions are reported, in order to improve biomass production. Firstly, the

strain selection, which should be oriented towards the most performing microalgae species. Then, stress tests like starving conditions have to be considered, to assess and classify the performances, as well as tuning their cellular structure properties. In addition to this, the recognized bottleneck is the enzyme expression during electrons transport, that inevitably limits the photosynthesis reaction rate. To overcome this issue, genetic modifications should be considered, as the one described in the article by Sayre, 2020.

In conclusion, research is still going on in microalgae field, and for sure it is a very promising field, but from a practical point of view, biomass production from carbon biological fixation is not feasible yet. Despite all efforts and studies that are in progress, with current technologies, the integrated process of carbon capture and biological fixation cannot be implemented at industrial level, as long as the value of avoiding fossil CO_2 emissions to the atmosphere remains so low.

Conclusions

The purpose of this thesis was to develop and simulate an integrated process that consists in CO_2 absorption in a packed column by means of a sodium carbonate aqueous solution, followed by its biological fixation using an *Arthrospira Platensis* culture, with recycle of the liquid solution to the absorber. Process simulations were carried out on Aspen Plus® process simulator, while a Fortran® subroutine was employed to account for biomass production reaction rate. The final goal was to assess industrial scale applicability and the economic evaluation of the energy supply to microalgae culture.

Firstly, by fitting experimental data about *Arthrospira Platensis*, a suitable value for the maximum specific growth rate parameter was found. Actually, it was found the value of the apparent specific growth rate was found, namely the product between the real parameter and the carbon function, which resulted equal to about 4.5 d^{-1}.

With reference to the most polluting industrial sectors, namely a gas-fired power plant, cement production plant, a steel mill and a stream-methane reforming plant, the open pond option was investigated, concluding that it is not viable owing to the huge surface area required. So the process was developed referring to a closed photobioreactor. Absorption column and photobioreactor design were done setting a biomass production of 2400 kg h^{-1}, which corresponds to a flow rate of 4400 kg h^{-1} of captured CO_2. It was found a CSTR reactor volume equal to 137128 m^3 and a residence time of 2.91 d, if the reactor depth is 0.05 m and if an incident light intensity of 420 μmol m^{-2} s^{-1} is used. Issues about solvent regeneration and recycle were assessed. Then, the compensation light intensity and the reactor depth have been computed and used to optimise the process, with the constraint that the same value of biomass production must be achieved. It was concluded that working at compensation point lowers the reactor volume to 40267 m^3. In addition, a comparison between CSTR and PFR with internal recycle performances was made, and results showed that the PFR ensures a productivity that is 10% larger than the one of the CSTR, by optimising the recycle ratio. Anyway, the photobioreactor design proposal was based on the assumption of a CSTR model. So, the effect of constant incident light intensity, between 100 and 420 μmol m^{-2} $h^{-1}$was investigated, in order to see how the irradiated area, the reactor volume, the required power and the photosynthetic efficiency

would change. It was concluded that the lower the incident radiation, the higher the photosynthetic efficiency and the lower the required power. The drawback is that the lower the incident radiation, the higher the total irradiated area, as well as the reactor volume. The limit that cannot be overtaken concerns the photosynthetic efficiency. Indeed, the values that have been calculated in this work do not exceed 23%. Considering the unit cost of electrical energy, it was possible to predict the cost of the energy duty to sustain the process, and the specific value to fix 1 ton of CO_2 into microalgal biomass. It was concluded that, at present, such cost is far higher than the value of the CO_2 emission avoidance, according to the ETS (European emissions Trading Scheme).

In summary, integrated CO_2 absorption and biological fixation could be scaled at industrial level, only if a way to improve microalgae photosynthetic efficiency above 25% is found.

Appendix A - Fortran subroutine

```
C$ #2 BY: PATNAIK DATE: 14-NOV-1998 INCLUDE COMMONS FOR
RADFRAC/RATEFRAC
C$ #1 BY: ANAVI DATE:  1-JUL-1994 NEW FOR USER MODELS
C
C     User Kinetics Subroutine for RCSTR
C     (USER type Reactions)
C
      SUBROUTINE bioprod   (SOUT, NSUBS,  IDXSUB, ITYPE,  NINT,
     2                      INT, NREAL,  REAL,   IDS,    NPO,
     3                      NBOPST,  NIWORK, IWORK,  NWORK,  WORK,
     4                      NC,  NR, STOIC,  RATES,  FLUXM,
     5                      FLUXS,   XCURR,  NTCAT,  RATCAT, NTSSAT,
     6                      RATSSA,  KCALL,  KFAIL,  KFLASH, NCOMP,
     7                      IDX, Y,  X,  X1, X2,
     8                      NRALL,   RATALL, NUSERV, USERV,  NINTR,
     9                      INTR,    NREALR, REALR,  NIWR,   IWR,
     *                      NWR, WR, NRL,    RATEL,  NRV,
     1                      RATEV)
C
      IMPLICIT NONE
C
C     DECLARE VARIABLES USED IN DIMENSIONING
C
      INTEGER NSUBS,  NINT,   NPO,    NIWORK, NWORK,
     +        NC, NR, NTCAT,  NTSSAT, NCOMP,
     +        NRALL,  NUSERV, NINTR,  NREALR, NIWR,
     +        NWR
C
```

```
c         include "ppexec_user.cmn"
c      EQUIVALENCE (RMISS, USER_RUMISS)
c      EQUIVALENCE (IMISS, USER_IUMISS)
#INCLUDE "dms_ncomp.cmn"
C
C.....RCSTR...
#include "rcst_rcstri.cmn"
#include "rxn_rcstrr.cmn"
         EQUIVALENCE (VOL, RCSTRR_VOLRC) ! RCSTR reactor volume
C
C.....RPLUG...
#include "rplg_rplugi.cmn"
C         include "rplg_rplugr.cmn"
C      EQUIVALENCE (XLEN, RPLUGR_UXLONG)
C      EQUIVALENCE (DIAM, RPLUGR_UDIAM)
C
C.....RBATCH...
#include "rbtc_rbati.cmn"
#include "rbtc_rbatr.cmn"
C
C.....PRES-RELIEF...
#include "prsr_presri.cmn"
#include "rbtc_presrr.cmn"
C
C.....RADFRAC/RATEFRAC
#include "rxn_disti.cmn"
#include "rxn_distr.cmn"
C
C.....REACTOR (OR PRES-RELIEF VESSEL OR STAGE) PROPERTIES...
```

```
#include "rxn_rprops.cmn"
      EQUIVALENCE (TEMP, RPROPS_UTEMP)    ! Reactor/stage temperature (K)
      EQUIVALENCE (PRES, RPROPS_UPRES)    ! Reactor/stage pressure (N/m^2)
      EQUIVALENCE (VFRAC, RPROPS_UVFRAC)  ! Molar vapor fraction in the
reactor/stage
      EQUIVALENCE (BETA, RPROPS_UBETA)    ! Liquid 1/Total liquid molar ratio in the
reactor/stage
      EQUIVALENCE (VVAP, RPROPS_UVVAP)    ! Volume occupied by the vapor phase
in the reactor (m^3)
      EQUIVALENCE (VLIQ, RPROPS_UVLIQ)    ! Volume occupied by the liquid phase in
the reactor (m^3)
      EQUIVALENCE (VLIQS, RPROPS_UVLIQS)  ! Volume occupied by the liquid and
solid phases in the reactor (m3)


#include "shs_stwork.cmn"


C.....THE PLEX
#include "dms_plex.cmn"
      REAL*8 B(1)               ! Real Plex area
      EQUIVALENCE (B(1),IB(1))
      INTEGER DMS_IFCMNC        ! Determines DMS_PLEX offsets for component data
areas
C
C     INITIALIZE RATES
C
C     DECLARE ARGUMENTS
C
      INTEGER IDXSUB(NSUBS),  ITYPE(NSUBS),   INT(NINT),
     +        IDS(2), NBOPST(6,NPO),  IWORK(NIWORK),
     +        IDX(NCOMP_NCC), INTR(NINTR),    IWR(NIWR),
     +        NREAL,  KCALL,  KFAIL,  KFLASH, NRL,
```

```
     +      NRV,   I
      REAL*8 SOUT(1), WORK(NWORK),
     +      STOIC(NC,NSUBS,NR),  RATES(1),
     +      FLUXM(1),   FLUXS(1),   RATCAT(NTCAT),
     +      RATSSA(NTSSAT),  Y(NCOMP_NCC),
     +      X(NCOMP_NCC),   X1(NCOMP_NCC),  X2(NCOMP_NCC)
      REAL*8 RATALL(NRALL),   USERV(NUSERV),
     +      REALR(NREALR),   WR(NWR),   RATEL(1),
     +      RATEV(1),   XCURR,  VOL

C     DECLARE LOCAL VARIABLES
C
      INTEGER IMISS
      REAL*8 REAL(NREAL), RMISS,  XLEN,   DIAM,   TEMP,
     +      PRES,   VFRAC,  BETA,   VVAP,   VLIQ,
     +      VLIQS,   LMW,
     +      ntotC,   nliq,   vdotliq,   tauliq,
     +      pm(NCOMP_NCC),   m(NCOMP_NC), c(NCOMP_NC),
     +      mumax,   T,  Tmin,   Topt,   Tmax,   fT, muemax, Kim,
     +      I0,  kalga,  h, Iav, ki, Iopt, fIav,
     +      Rd,  mue,   Ri, Rtot,   ni(NCOMP_NC)



! Component ID
! 1              O2
! 2              CO2
! 3              CO
! 4              CH4
! 5              H2
! 6              N2
```

```
! 7              Na2CO3
! 8              H2O
! 9              H3O+
! 10              Na+
! 11             OH-
! 12             HCO3-
! 13             CO3--
! 14  NCOMP_NCC+9+1   ALGAE

C
C     BEGIN EXECUTABLE CODE
C

! Conventional components outlet molar flow rate kmol/s  by Aspen
      ntotC = SOUT(NCOMP_NCC+1)

! Total molar liquid flow rate  kmol/s
          nliq = ntotC*(1-vfrac)

! Volumetric flow rate  [m^3/s] stwork_v1=mixture molar volume by Aspen

      vdotliq = nliq*(STWORK_VL)

! Residence time [sec]
          tauliq = VLIQ/vdotliq

! restituzione del PM della miscela
      LMW = DMS_IFCMNC('MW')        ! offset of molecular weights in the plex

      pm = B(LMW+1:LMW+NCOMP_NCC)
```

```
!         pmmix = SOUT(NCOMP_NCC+9)  ! Conventional mixture average molecular weight

! Conventional components flow rate [kg/s] in the liquid
      m = nliq*X*PM

! Biomass mass flow rate [kg/s] in the liquid
          m(NCOMP_NCC+1) = SOUT(NCOMP_NCC+9+1)

!      IF (m(ncomp_ncc+1) .EQ. 0) m(ncomp_ncc+1) = 0.015/3600
! Biomass concentration [kg/m^3]
      c = m/vdotliq
! Reaction rate computation [kg/m^3 s]
      mumax = 4.503/(3600*24)  ! s^-1

      ! Temperature factors
      T=TEMP-273.15   ! °C
      Tmin = 6.57 ! °C
      Topt = 28.98 ! °C
      Tmax = 47.21    ! °C
      fT = ((T-Tmax)*(T-Tmin)**2)/
     &     ((Topt-Tmin)*((Topt-Tmin)*(T-Topt)-
     &     (Topt-Tmax)*(Topt+Tmin-2*T)))



      ! Light factors
      I0 = 420    ! mumol/m2/s incident radiation
      kalga = 0.0362*1000    ! m2/kg average biomass absorption coefficient
      h = 0.0244   ! m
```

```
      Iav = I0*(1-exp(-(kalga*c(NCOMP_NCC+1))*h))/
     & ((kalga*c(NCOMP_NCC+1))*h)
      ki = 192.1    ! mumol/m2/s RB
      Iopt = 482.9 !for RB light
      fIav = Iav/(Iav+ki*(((Iav/Iopt)-1)**2))

      ! Direct reaction rate
      Rd = mumax*c(NCOMP_NCC+1)*fT*fIav

      muemax = 10.51/(3600*24) ! s^-1 max
      Kim = 1224 !mumol/m2/s
      mue = muemax*(I0/(I0+Kim))

      ! Inverse reaction rate
      Ri = mue*c(NCOMP_NCC+1)

      Rtot = Rd-Ri



! Stoichiometric coefficients fro biomass production reaction
      ni = (/ 0.330255,   ! O2
     &        0,      ! CO2
     &        0,      ! CO
     &        0,      ! CH4
     &        0,      ! H2
     &        0,      ! N2
     &        0,      ! Na2CO3
     &       -0.2525,   ! H2O
     &        0,   ! H3O+
     &        0,      ! Na+
```

```
     &       0.301,      ! OH-
     &      -0.301,   ! HCO3-
     &       0,       ! CO3--
     &       1 /)     ! ALGAE




      RATES(1:NCOMP_NCC) = (ni(1:NCOMP_NCC)/7.22533)*Rtot*VLIQ ! Conventional
components  (kmol/s)
      RATES(NCOMP_NCC+1) = ni(NCOMP_NCC+1)*Rtot*VLIQ       ! biomass (kg/s)
c write results in a .TXT file
     open(1,FILE='cstrbioprod.dat')


         write (1, *) tauliq/86400, "time in d"
         write (1, *) VLIQ, "volume occupied by liquid in m3"
     write (1, *) VLIQ/h, "reactor surface"
!    write (1, *) VLIQS, "volume occupied by liquid+solid in m3"
!    write (1, *) VVAP, "volume occupied by gas in m3"
!    write (1, *) pm, "mixture molecular weight"
!    write (1, *) RATES(NCOMP_NCC+1)*86400, "reaction rate g/L d"
!    write (1, *) nliq, "liquid molar flow rate kmol/s"
!    write (1, *) m(5)*3600, "mass flow rates kg/h"
!    do i=1,NCOMP_NC
!    write(1,*) "Component concentration ", i, ": ", c(i)
!    end do
     write (1, *) fT, fIav, "kinetic factors"
     write (1, *) Iav, "Average light intensity"
!    write (1, *) (kalgae*c(NCOMP_NCC+1)+kd)*h
     do i=1,NCOMP_NCC
```

```
write(1,*) "Component molar fraction", i, ": ", X(i)
end do
write (1, *) STWORK_VL
    close(1,STATUS='keep')

RETURN
END
```

Appendix B - Excel calculations

I_0 [µmol m^{-2} s^{-1}]	Net photo.eff	Photo.eff	Total photo.eff
100	0.235	0.151	0.121
200	0.201	0.131	0.105
300	0.164	0.108	0.086
400	0.121	0.080	0.064

Table B.1. *Photosynthetic efficiencies vs I_0.*

Reactor depth [cm]	τ [d]	I_0 [µmol m^{-2} s^{-1}]	PAR [%]	Error PAR
15	0.5	300	0	0.00
15	0.9	300	7.75	0.29
15	1.33	300	7.73	0.31
15	4.6	300	3.43	0.05
15	1.33	120	9.25	3.28
15	1.33	150	11.65	0.69
15	1.33	300	8.63	0.28
15	1.33	600	8.65	0.47
15	1.33	1000	5.37	0.88
15	1.33	1250	3.73	0.17
15	1.33	1500	3.38	0.18
15	1.33	2700	1.42	0.05
15	1.33	3600	0.87	0.06

Table B.2. *Experimental Photosynthetic efficiencies vs I_0 and τ (Borella et al., 2021)*

I_0 [µmol m^{-2} s^{-1}]	V_L [m^3]
100	85850.9
200	50736.9
300	41483.3
400	40266.7

Table B.3. *Volume of liquid in the reactor vs I_0.*

I_0 [µmol m^{-2} s^{-1}]	Vol.prod [g L^{-1} d^{-1}]
100	0.672796
200	1.138426
300	1.389023
400	1.434439

Table B.4. *Volumetric productivity vs I_0.*

I_0 [µmol m^{-2} s^{-1}]	Area [ha]
100	366.48
200	211.16
300	170.92
400	164.82

Table B.5. *Area vs I_0.*

I_0 [µmol m^{-2} s^{-1}]	Power [kW]
100	102615.57
200	118251.70
300	143576.74
400	193837.09

Table B.6. *Power vs I_0.*

Area [ha]	Power [kW]
366.48	102615.57
211.16	118251.70
170.92	143576.74
164.82	193837.09

Table B.7. *Area vs Power*

Appendix C – Stream tables

	Feed	Sweet	Carb	Rec_3
Temperature [°C]	28	30.5	31	30.5
Pressure [bar]	2.5	2.5	2.5	2.5
Vapor fraction	1	1	0	0
Liquid fraction	0	0	1	1
Solid fraction	0	0	0	0
Total mass flow [kg h^{-1}]	5654.76	1265.77	$2.0044 \cdot 10^{6}$	$2 \cdot 10^{6}$
O_2	0	55.361	0.0596	55.43
CO_2	4400.96	0.0028	1.416	0.0033
CO	799.351	768.314	31.18	0.15
CH_4	297.553	281.196	16.49	0.14
H_2	93.731	90.613	3.13	0.012
N_2	41.2365	40.14	1.10	0.0028
Na_2CO_3	0	0	0	0
H_2O	21.9223	30.15	$1.95 \cdot 10^{6}$	$1.95 \cdot 10^{6}$
H_3O^+	0	0	$8.32 \cdot 10^{-6}$	$3.76 \cdot 10^{-7}$
Na^+	0	0	21761.5	21761.7
OH^-	0	0	7.78	174.35
HCO_3^-	0	0	12254.1	652.8
CO_3^{2-}	0	0	22356.8	2778.68
Biomass	0	0	0	0
Mass fractions				
O_2	0	0.044	$2.97 \cdot 10^{-8}$	$2.77 \cdot 10^{-5}$
CO_2	0.778	$2.28 \cdot 10^{-6}$	$7.067 \cdot 10^{-7}$	$1.64 \cdot 10^{-9}$
CO	0.141	0.60	$1.55 \cdot 10^{-5}$	$7.51 \cdot 10^{-8}$
CH_4	0.052	0.22	$8.23 \cdot 10^{-6}$	$6.87 \cdot 10^{-8}$
H_2	0.016	0.071	$1.56 \cdot 10^{-6}$	$5.93 \cdot 10^{-9}$
N_2	0.0073	0.032	$5.5 \cdot 10^{-7}$	$1.43 \cdot 10^{-9}$
Na_2CO_3	0	0	0	0
H_2O	0.004	0.024	0.972	0.975
H_3O^+	0	0	$4.15 \cdot 10^{-12}$	$1.88 \cdot 10^{-13}$
Na^+	0	0	0.010	0.010
OH^-	0	0	$3.88 \cdot 10^{-6}$	$8.72 \cdot 10^{-5}$
HCO_3^-	0	0	0.0061	0.00032
CO_3^{2-}	0	0	0.011	0.014
Biomass	0	0	0	0
Mole flow [kmol h^{-1}]	196.27	94.74	109630	109628
Volume flow [L min^{-1}]	32611.3	15949.1	32701.91	32636.8
pH			9.86	11.22

Table C.1. *Stream table for the absorber.*

	Liq	Vap	Carb
Temperature [°C]	30	30	31
Pressure [atm]	1	1	2.47
Vapor fraction	0	1	0
Liquid fraction	1	0	1
Solid fraction	0	0	0
Total mass flow [kg h^{-1}]	$2.0039 \cdot 10^6$	31.61	$2.0044 \cdot 10^6$
O_2	0.028	0.031	0.0596
CO_2	1.405	0.063	1.416
CO	12.55	18.63	31.18
CH_4	8.087	8.41	16.49
H_2	1.148	1.98	3.13
N_2	0.347	0.75	1.10
Na_2CO_3	0	0	0
H_2O	$1.94 \cdot 10^6$	1.73	$1.95 \cdot 10^6$
H_3O^+	$8{,}2 \cdot 10^{-6}$	0	$8.32 \cdot 10^{-6}$
Na^+	21761.5	0	21761.5
OH^-	7.42	0	7.78
HCO_3^-	12252.7	0	12254.1
CO_3^{2-}	22358.15	0	22356.8
Biomass	0	0	0
Mass fractions			
O_2	$1.40 \cdot 10^{-8}$	0.00099	$2.97 \cdot 10^{-8}$
CO_2	$7.015 \cdot 10^{-7}$	0.00197	$7.067 \cdot 10^{-7}$
CO	$6{,}26 \cdot 10^{-6}$	0.589	$1.55 \cdot 10^{-5}$
CH_4	$4.035 \cdot 10^{-6}$	0.266	$8.23 \cdot 10^{-6}$
H_2	$5.73 \cdot 10^{-7}$	0.062	$1.56 \cdot 10^{-6}$
N_2	$1.73 \cdot 10^{-7}$	0.0238	$5.5 \cdot 10^{-7}$
Na_2CO_3	0	0	0
H_2O	0.9718	0.0548	0.972
H_3O^+	$4.086 \cdot 10^{-12}$	0	$4.15 \cdot 10^{-12}$
Na^+	0.010	0	0.010
OH^-	$3.70 \cdot 10^{-6}$	0	$3.88 \cdot 10^{-6}$
HCO_3^-	0.0061	0	0.0061
CO_3^{2-}	0.011	0	0.011
Biomass	0	0	0
Mole flow [kmol h^{-1}]	109627,246793853	2.297	109630
Volume flow [L min^{-1}]	32692.02	952.46	32701.91
pH	9.87		9.86

Table C.2. *Stream table for flash 1.*

	Inlet	Outlet
Temperature [°C]	30	30
Pressure [bar]	1	1
Vapor fraction	0	0.00177
Liquid fraction	1	0.99703
Solid fraction	0	0.0012
Total mass flow [kg h^{-1}]	$2.0039 \cdot 10^{6}$	$2.0039 \cdot 10^{6}$
O_2	0.028	3509.74
CO_2	1.405	0.0102
CO	12.55	12.55
CH_4	8.087	8.087
H_2	1.148	1.148
N_2	0.347	0.347
Na_2CO_3	0	0
H_2O	$1.94 \cdot 10^{6}$	$1.95 \cdot 10^{6}$
H_3O^+	$8{,}2 \cdot 10^{-6}$	$3.68 \cdot 10^{-7}$
Na^+	21761.5	21761.50
OH^-	7.42	171.34
HCO_3^-	12252.7	645.18
CO_3^{2-}	22358.15	27776.90
Biomass	0	2400.46
Mass fractions		
O_2	$1.40 \cdot 10^{-8}$	0.00175
CO_2	$7.015 \cdot 10^{-7}$	$5.11 \cdot 10^{-9}$
CO	$6{,}26 \cdot 10^{-6}$	$6.26 \cdot 10^{-6}$
CH_4	$4.035 \cdot 10^{-6}$	$4.035 \cdot 10^{-6}$
H_2	$5.73 \cdot 10^{-7}$	$5.73 \cdot 10^{-7}$
N_2	$1.73 \cdot 10^{-7}$	$1.73 \cdot 10^{-7}$
Na_2CO_3	0	0
H_2O	0.9718	0.9719
H_3O^+	$4.086 \cdot 10^{-12}$	$1.84 \cdot 10^{-13}$
Na^+	0.010	0.01086
OH^-	$3.70 \cdot 10^{-6}$	$8.55 \cdot 10^{-5}$
HCO_3^-	0.0061	0.000322
CO_3^{2-}	0.011	0.0138
Biomass	$9 \cdot 10^{-8}$	0.00119
Mole flow [kmol h^{-1}]	109627.25	109653.04
Volume flow [L min^{-1}]	32692.02	79872.47
pH	9.87	11.23

Table C.3. *Stream table for the PBR.*

	Outlet	Vap2	Liq2
Temperature [°C]	30	30	30
Pressure [bar]	1	1	1
Vapor fraction	0.00177	1	0
Liquid fraction	0.99703	0	0.998
Solid fraction	0.0012	0	0.0012
Total mass flow [kg h^{-1}]	$2.0039 \cdot 10^{6}$	3555.93	$2.0039 \cdot 10^{6}$
O_2	3509.74	3447.85	61.9
CO_2	0.0102	0.0071	0.0032
CO	12.55	12.38	0.168
CH_4	8.087	7.93	0.153
H_2	1.148	1.135	0.0132
N_2	0.347	0.344	0.0032
Na_2CO_3	0	0	0
H_2O	$1.95 \cdot 10^{6}$	86.272	$1.95 \cdot 10^{6}$
H_3O^+	$3.68 \cdot 10^{-7}$	0	$3.684 \cdot 10^{-7}$
Na^+	21761.50	0	21761.506
OH^-	171.34	0	171.345
HCO_3^-	645.18	0	645.184
CO_3^{2-}	27776.90	0	27776.90
Biomass	2400.46	0	2399.64
Mass fractions			
O_2	0.00175	0.97	$3.093 \cdot 10^{-5}$
CO_2	$5.11 \cdot 10^{-9}$	$1.98 \cdot 10^{-6}$	$1.59 \cdot 10^{-9}$
CO	$6.26 \cdot 10^{-6}$	0.0035	$8.38 \cdot 10^{-8}$
CH_4	$4.035 \cdot 10^{-6}$	0.0022	$7.66 \cdot 10^{-8}$
H_2	$5.73 \cdot 10^{-7}$	0.00032	$6.61 \cdot 10^{-9}$
N_2	$1.73 \cdot 10^{-7}$	$9.68 \cdot 10^{-5}$	$1.59 \cdot 10^{-9}$
Na_2CO_3	0	0	0
H_2O	0.9719	0.024	0.973
H_3O^+	$1.84 \cdot 10^{-13}$	0	$1.84 \cdot 10^{-13}$
Na^+	0.01086	0	0.01087
OH^-	$8.55 \cdot 10^{-5}$	0	$8.56 \cdot 10^{-5}$
HCO_3^-	0.000322	0	0.00032
CO_3^{2-}	0.0138	0	0.0139
Biomass	0.00119	0	0.00119
Mole flow [kmol h^{-1}]	109653.04	114.05	109538.98
Volume flow [L min^{-1}]	79872.47	47238.75	32633.72
pH	11.23		11.23

Table C.4. *Stream table for flash 2.*

	Liq2	Biomass	Liquid
Temperature [°C]	30	30	30
Pressure [bar]	1	1	1
Vapor fraction	0	0	0
Liquid fraction	0.998	0.799	1
Solid fraction	0.0012	0.2001	0
Total mass flow [kg h^{-1}]	$2.0039 \cdot 10^{6}$	11990.01	$1.988 \cdot 10^{6}$
O_2	61.9	0.297	61.59
CO_2	0.0032	$1.53 \cdot 10^{-5}$	0.0032
CO	0.168	0.0008	0.167
CH_4	0.153	0.0007	0.153
H_2	0.0132	$6.35 \cdot 10^{-5}$	0.0132
N_2	0.0032	$1.53 \cdot 10^{-5}$	0.0032
Na_2CO_3	0	0	0
H_2O	$1.95 \cdot 10^{6}$	9348.37	1938228.04
H_3O^+	$3.684 \cdot 10^{-7}$	$1.76 \cdot 10^{-9}$	$3.67 \cdot 10^{-7}$
Na^+	21761.506	104.45	21657.05
OH^-	171.345	0.822	170.52
HCO_3^-	645.184	3.0969	642.088
CO_3^{2-}	27776.90	133.33	27643.57
Biomass	2399.64	2400.46	0
Mass fractions			
O_2	$3.093 \cdot 10^{-5}$	$2{,}47 \cdot 10^{-5}$	$3.097 \cdot 10^{-5}$
CO_2	$1.59 \cdot 10^{-9}$	$1.27 \cdot 10^{-9}$	$1.59 \cdot 10^{-9}$
CO	$8.38 \cdot 10^{-8}$	$6.71 \cdot 10^{-8}$	$8.397 \cdot 10^{-8}$
CH_4	$7.66 \cdot 10^{-8}$	$6.14 \cdot 10^{-8}$	$7.67 \cdot 10^{-8}$
H_2	$6.61 \cdot 10^{-9}$	$5.3 \cdot 10^{-9}$	$6.62 \cdot 10^{-9}$
N_2	$1.59 \cdot 10^{-9}$	$1.27 \cdot 10^{-9}$	$1.598 \cdot 10^{-9}$
Na_2CO_3	0	0	0
H_2O	0.973	0.779	0.975
H_3O^+	$1.84 \cdot 10^{-13}$	$1.47 \cdot 10^{-13}$	$1.844 \cdot 10^{-13}$
Na^+	0.01087	0.0087	0.010
OH^-	$8.56 \cdot 10^{-5}$	$6.86 \cdot 10^{-5}$	$8.576 \cdot 10^{-5}$
HCO_3^-	0.00032	0.00026	0.000323
CO_3^{2-}	0.0139	0.011	0.0139
Biomass	0.00119	0.20	0
Mole flow [kmol h^{-1}]	109538.98	525.78	109013.20
Volume flow [L min^{-1}]	32633.72	183.17	32450.54
pH	11.23		

Table C.5. *Stream table for the solid-liquid separator.*

	Feed	Make-up	Purge	Biomass
Temperature [°C]	28	35	31	30
Pressure [bar]	2.47	2.47	1	1
Vapor fraction	1	0	0	0
Liquid fraction	0	1	1	0.799
Solid fraction	0	0	0	0.2001
Total mass flow [kg h^{-1}]	5654.76	$2.10 \cdot 10^{5}$	198840.32	11990.01
O_2	0	0	6.16	0.297
CO_2	4400.96	0,00043	0.00032	$1.53 \cdot 10^{-5}$
CO	799.351	0	0.0167	0,0008
CH_4	297.553	0	0.0153	0,0007
H_2	93.731	0	0.00132	$6.35 \cdot 10^{-5}$
N_2	41.2365	0	0.00032	$1.53 \cdot 10^{-5}$
Na_2CO_3	0	0	0	0
H_2O	21.9223	204774.122	193822.80	9348.37
H_3O^+	0	$4.70 \cdot 10^{-8}$	$3.7 \cdot 10^{-8}$	$1.76 \cdot 10^{-9}$
Na^+	0	2270.4	2165.70	104.45
OH^-	0	20.95	17.05	0.822
HCO_3^-	0	75.17	64.21	3.0969
CO_3^{2-}	0	2889.35	2764.35	133.33
Biomass	0	0	0	2400.46
Mass fractions				
O_2	0	0	$3.097 \cdot 10^{-5}$	$2,47 \cdot 10^{-5}$
CO_2	0.778	$2.06 \cdot 10^{-9}$	$1.596 \cdot 10^{-9}$	$1.27 \cdot 10^{-9}$
CO	0.141	0	$8.397 \cdot 10^{-8}$	$6.71 \cdot 10^{-8}$
CH_4	0.052	0	$7.67 \cdot 10^{-8}$	$6.14 \cdot 10^{-8}$
H_2	0.016	0	$6.62 \cdot 10^{-9}$	$5.3 \cdot 10^{-9}$
N_2	0.0073	0	$1.59 \cdot 10^{-9}$	$1.27 \cdot 10^{-9}$
Na_2CO_3	0	0	0	0
H_2O	0.004	0.975	0.975	0.779
H_3O^+	0	$2.24 \cdot 10^{-13}$	$1.84 \cdot 10^{-13}$	$1.47 \cdot 10^{-13}$
Na^+	0	0,010	0.010	0.0087
OH^-	0	$9,97 \cdot 10^{-5}$	$8.57 \cdot 10^{-5}$	$6.86 \cdot 10^{-5}$
HCO_3^-	0	0,00036	0.000323	0.00026
CO_3^{2-}	0	0,0137	0.0139	0.011
Biomass	0	0	0	0.20
Mole flow [kmol h^{-1}]	196.27	11516.062	10901.32	525.78
Volume flow [L min^{-1}]	32611.3	3433.55	3245.054	183.17
pH				

Table C.6. *Stream table for loads and products*

Bibliography

Aghaalipour, E., Akbulut, A., & Güllü, G. (2020). Carbon dioxide capture with microalgae species in continuous gas-supplied closed cultivation systems. *Biochemical Engineering Journal*, **163**, 107741.

Asif, M., Suleman, M., Haq, I., & Jamal, S. A. (2018). Post-combustion CO2 capture with chemical absorption and hybrid system: current status and challenges. *Greenhouse Gases: Science and Technology*, **8**(6), 998-1031.

Aspen Plus V12.1 help.

Ban, Z. H., Keong, L. K., & Mohd Shariff, A. (2014). Physical absorption of CO2 capture: a review. *Advanced Materials Research*, **917**, 134-143.

Banerjee, S., & Ramaswamy, S. (2017). Dynamic process model and economic analysis of microalgae cultivation in open raceway ponds. *Algal research*, **26**, 330-340.

Barbera, E., Mio, A., Pavan, A. M., Bertucco, A., & Fermeglia, M. (2022). Fuelling power plants by natural gas: An analysis of energy efficiency, economical aspects and environmental footprint based on detailed process simulation of the whole carbon capture and storage system. *Energy Conversion and Management*, **252**, 115072.

Batac, C. C., Gathercole, N. S., Maravilla, A. F., & Beltran, A. B. (2020, April). Evaluation of different carbonate sources for bicarbonate-based integrated carbon capture and algae production system using Spirulina platensis. In IOP Conference Series: *Materials Science and Engineering* (Vol. **778**, No. 1, p. 012041). IOP Publishing.

Bernard, O., & Rémond, B. (2012). Validation of a simple model accounting for light and temperature effect on microalgal growth. *Bioresource technology*, **123**, 520-527.

A. Bertucco and E. Barbera, "Lecture notes, 2019-2020", Department of Industrial Engineering, University of Padova, 2019-2020

Blanken, W., Cuaresma, M., Wijffels, R. H., & Janssen, M. (2013). Cultivation of microalgae on artificial light comes at a cost. *Algal Research*, **2**(4), 333-340.

Borella, L., Ortolan, D., Barbera, E., Trivellin, N., & Sforza, E. (2021). A multiwavelength model to improve microalgal productivity and energetic conversion in a red-blue light emitting diodes (LEDs) continuous photobioreactor. *Energy Conversion and Management*, **243**, 114330.

Borhani, T. N. G., Azarpour, A., Akbari, V., Alwi, S. R. W., & Manan, Z. A. (2015). CO2 capture with potassium carbonate solutions: A state-of-the-art review. *International journal of greenhouse gas control*, **41**, 142-162.

Burger, J., Papaioannou, V., Gopinath, S., Jackson, G., Galindo, A., & Adjiman, C. S. (2015). A hierarchical method to integrated solvent and process design of physical CO 2 absorption using the SAFT-γ M ie approach. *AIChE Journal*, **61**(10), 3249-3269.

Paolo Canu, lecture notes, "Chemical Reaction Engineering", University of Padova, 2020-2021.

Da Rosa, A. P. C., Carvalho, L. F., Goldbeck, L., & Costa, J. A. V. (2011). Carbon dioxide fixation by microalgae cultivated in open bioreactors. *Energy Conversion and Management*, **52**(8-9), 3071-3073.

Chi, Z., Xie, Y., Elloy, F., Zheng, Y., Hu, Y., & Chen, S. (2013). Bicarbonate-based integrated carbon capture and algae production system with alkalihalophilic cyanobacterium. *Bioresource technology*, **133**, 513-521.

Chiaramonti, D., Prussi, M., Casini, D., Tredici, M. R., Rodolfi, L., Bassi, N., ... & Bondioli, P. (2013). Review of energy balance in raceway ponds for microalgae cultivation: Re-thinking a traditional system is possible. *Applied Energy*, **102**, 101-111.

Chiu, S. Y., Kao, C. Y., Huang, T. T., Lin, C. J., Ong, S. C., Chen, C. D., ... & Lin, C. S. (2011). Microalgal biomass production and on-site bioremediation of carbon dioxide, nitrogen oxide and sulfur dioxide from flue gas using Chlorella sp. cultures. *Bioresource technology*, **102**(19), 9135-9142.

Collodi, G., Wheeler, F. (2010). Hydrogen production via steam reforming with CO2 capture. *Chemical Engineering Transactions*, **19**, 37-42. Internal report.

A. R. Colta, "Effetto del rapporto di riciclo in fotobioreattori in continuo per la coltivazione di Arthrospira Maxima: composizione della biomassa e ottimizzazione del consumo di acqua e nutrienti.", work of thesis, Microalgae Laboratory, 2023.

da Rosa, G. M., Moraes, L., Cardias, B. B., & Costa, J. A. V. (2015). Chemical absorption and CO2 biofixation via the cultivation of Spirulina in semicontinuous mode with nutrient recycle. *Bioresource technology*, **192**, 321-327.

Daneshvar, E., Ok, Y. S., Tavakoli, S., Sarkar, B., Shaheen, S. M., Hong, H., ... & Bhatnagar, A. (2021). Insights into upstream processing of microalgae: A review. *Bioresource technology*, **329**, 124870.

Gris, B., Sforza, E., Vecchiato, L., & Bertucco, A. (2014). Development of a process for an efficient exploitation of CO2 captured from flue gases as liquid carbonates for Chlorella protothecoides cultivation. *Industrial & Engineering Chemistry Research*, **53**(43), 16678-16688.

Handler, R. M., Canter, C. E., Kalnes, T. N., Lupton, F. S., Kholiqov, O., Shonnard, D. R., & Blowers, P. (2012). Evaluation of environmental impacts from microalgae cultivation in open-air raceway ponds: Analysis of the prior literature and investigation of wide variance in predicted impacts. *Algal Research*, **1**(1), 83-92.

IEA. Net zero by 2050. A roadmap for the global energy sector 2021. 2021

Isa, F., Zabiri, H., Ng, N. K. S., & Shariff, A. M. (2018). CO2 removal via promoted potassium carbonate: A review on modeling and simulation techniques. *International Journal of Greenhouse Gas Control*, **76**, 236-265.

https://it.frwiki.wiki/wiki/Carbonate_de_sodium#Propri%C3%A9t%C3%A9s_physico-chimiques, visited on January 8, 2023.

https://fr.wikipedia.org/wiki/Fichier:Solubilite_Na2CO3.png, visited on January 8, 2023.

JRC Science for policy report. Global Energy and Climate Outlook 2019: Electrification for the low-carbon transition. 2020. https://doi.org/10.2760/ 58255.

JRC Photovoltaic Geographical Information System (PVGIS) - European Commission (europa.eu) – visited on April 10, 2022 and on January 8, 2023.

Katebah, M., & Linke, P. (2022). Analysis of hydrogen production costs in Steam-Methane Reforming considering integration with electrolysis and CO2 capture. *Cleaner Engineering and Technology*, **10**, 100552.

Knuutila, H., Juliussen, O., & Svendsen, H. F. (2010). Kinetics of the reaction of carbon dioxide with aqueous sodium and potassium carbonate solutions. *Chemical Engineering Science*, **65**(23), 6077-6088.

Könst, P., Mireles, I. H., van der Stel, R., van Os, P., & Goetheer, E. (2017). Integrated system for capturing CO2 as feedstock for algae production. *Energy Procedia*, **114**, 7126-7132.

Lee, J. H., Lee, D. W., Kwak, C., Kang, K., & Lee, J. H. (2019). Technoeconomic and environmental evaluation of sodium bicarbonate production using CO2 from flue gas of a coal-fired power plant. *Industrial & Engineering Chemistry Research*, **58**(34), 15533-15541.

Lee, B. J., Lee, J. I., Yun, S. Y., Hwang, B. G., Lim, C. S., & Park, Y. K. (2020). Methodology to calculate the CO2 emission reduction at the coal-fired power plant: CO2 capture and utilization applying technology of mineral carbonation. *Sustainability*, **12**(18), 7402.

Mona, S., Malyan, S. K., Saini, N., Deepak, B., Pugazhendhi, A., & Kumar, S. S. (2021). Towards sustainable agriculture with carbon sequestration, and greenhouse gas mitigation using algal biochar. *Chemosphere*, **275**, 129856.

Nguyen, L. N., Vu, M. T., Vu, H. P., Johir, M. A. H., Labeeuw, L., Ralph, P. J., ... & Nghiem, L. D. (2022). Microalgae-based carbon capture and utilization: A critical review on current system developments and biomass utilization. *Critical Reviews in Environmental Science and Technology*, 1-23.

Norahim, N., Yaisanga, P., Faungnawakij, K., Charinpanitkul, T., & Klaysom, C. (2018). Recent membrane developments for CO2 separation and capture. *Chemical Engineering & Technology*, **41**(2), 211-223.

Nwaoha, C., Beaulieu, M., Tontiwachwuthikul, P., & Gibson, M. D. (2018). Techno-economic analysis of CO2 capture from a 1.2 million MTPA cement plant using AMP-PZ-MEA blend. *International Journal of Greenhouse Gas Control*, **78**, 400-412.

Pastore, M., Primavera, A., Milocco, A., Barbera, E., & Sforza, E. (2022). Tuning the Solid Retention Time to Boost Microalgal Productivity and Carbon Exploitation in an Industrial Pilot-Scale LED Photobioreactor. *Industrial & Engineering Chemistry Research*, **61**(23), 7739-7747.

Pellegrini, L. A., De Guido, G., & Moioli, S. (2020). Design of the CO2 removal section for PSA tail gas treatment in a hydrogen production plant. *Frontiers in Energy Research*, **8**, 77.

Renon, H., & Prausnitz, J. M. (1968). Local compositions in thermodynamic excess functions for liquid mixtures. *AIChE journal*, **14**(1), 135-144.

Rigamonti, L., & Brivio, E. (2022). Life cycle assessment of methanol production by a carbon capture and utilization technology applied to steel mill gases. *International Journal of Greenhouse Gas Control*, **115**, 103616.

Ring, M. J., Lindner, D., Cross, E. F., & Schlesinger, M. E. (2012). Causes of the global warming observed since the 19th century. *Atmospheric and Climate sciences*, **2**(04), 401.

Salama, E. S., Kurade, M. B., Abou-Shanab, R. A., El-Dalatony, M. M., Yang, I. S., Min, B., & Jeon, B. H. (2017). Recent progress in microalgal biomass production coupled with wastewater treatment for biofuel generation. *Renewable and Sustainable Energy Reviews*, **79**, 1189-1211.

Subramanian, S., & Sayre, R. T. (2022). The right stuff; realizing the potential for enhanced biomass production in microalgae. *FRONTIERS IN ENERGY RESEARCH*, **10**.

Sayari, A., Belmabkhout, Y., & Serna-Guerrero, R. (2011). Flue gas treatment via CO2 adsorption. *Chemical Engineering Journal*, **171**(3), 760-774.

Sayre, R. (2020). Optimising the photosynthetic efficiency in plants and green algae for biomass production. *Biology*, **10.26904/RF**-133-7073.

Shen, M., Tong, L., Yin, S., Liu, C., Wang, L., Feng, W., & Ding, Y. (2022). Cryogenic technology progress for CO2 capture under carbon neutrality goals: A review. *Separation and Purification Technology*, **121734**.

Schulze, P. S., Barreira, L. A., Pereira, H. G., Perales, J. A., & Varela, J. C. (2014). Light emitting diodes (LEDs) applied to microalgal production. *Trends in biotechnology*, **32**(8), 422-430.

Shi, X., Mathew, A. S., Xu, Y., Yau, S. T., & Xu, G. (2022). Enhanced Growth of Microalgae and Production of Lipids via Electrostatically Controlled Photosynthesis. *ACS Sustainable Chemistry & Engineering*, **10**(35), 11459-11465.

Song, C., Liu, Q., Qi, Y., Chen, G., Song, Y., Kansha, Y., & Kitamura, Y. (2019). Absorption-microalgae hybrid CO2 capture and biotransformation strategy—A review. *International Journal of Greenhouse Gas Control*, **88**, 109-117.

Song, C., Liu, Q., Deng, S., Li, H., & Kitamura, Y. (2019). Cryogenic-based CO2 capture technologies: State-of-the-art developments and current challenges. *Renewable and Sustainable Energy Reviews*, **101**, 265-278.

Trentin, G., Barbera, E., Bertucco, A., & Sforza, E. (2020). Role of oxygen in tubular photobioreactors: Model-Based design and operating conditions to minimize productivity losses. *Chemical Engineering and Processing-Process Intensification*, **157**, 108151.

Wilberforce, T., Baroutaji, A., Soudan, B., Al-Alami, A. H., & Olabi, A. G. (2019). Outlook of carbon capture technology and challenges. *Science of the total environment*, **657**, 56-72.

X-Price Foundation- https://www.xprize.org/prizes/elonmusk/student-award-winners, visited on May 15, 2022.

Yamada, H. (2021). Amine-based capture of CO2 for utilization and storage. *Polymer Journal*, **53**(1), 93-102.

Zaimes, G. G., & Khanna, V. (2013). Microalgal biomass production pathways: evaluation of life cycle environmental impacts. *Biotechnology for biofuels*, **6**(1), 1-11.

Zhu, C., Chen, S., Ji, Y., Schwaneberg, U., & Chi, Z. (2022). Progress toward a bicarbonate-based microalgae production system. *Trends in Biotechnology*, **40**(2), 180-193.

Ziobrowski, Z., & Rotkegel, A. (2022). Comparison of CO2 separation efficiency from flue gases based on commonly used methods and materials. *Materials*, **15**(2), 460.

Ringraziamenti

Esprimere la gratitudine a parole mi è sempre risultato difficile, ma farò del mio meglio.

In primo luogo, desidero ringraziare il Professore Alberto Bertucco, di cui ho apprezzato l'entusiasmo per il proprio lavoro e la vicinanza durante la stesura della tesi. Grazie, perché ha saputo trasmettermi curiosità e passione per lo studio.

Un ringraziamento speciale va alla Professoressa Elena Barbera, che per un intero anno mi ha guidata nello sviluppo della tesi, senza mai tirarsi indietro di fronte alle mie richieste di aiuto. Grazie per la disponibilità al dialogo e per la vicinanza, soprattutto nei momenti di difficoltà. Grazie per l'infinita pazienza.

Vorrei ringraziare tutta la mia famiglia, che da sempre mi è stata accanto, nei momenti belli e in quelli difficili.

Ringrazio mia madre, per tutto l'amore che mi ha dato e che continua a darmi ogni giorno. Hai speso ogni fibra del tuo essere per rendermi la persona che sono oggi. Probabilmente non riuscirei, in poche righe, a descrivere tutta la gratitudine che provo, ma sappi che sei la mia roccia.

Grazie a tutti i miei zii e zie. Avete contribuito in modo speciale alla collezione di ricordi felici che porto con me e che spero di ampliare sempre più. In particolare, vorrei ringraziare zio Fernando, che mi ha sempre trattata al pari di una figlia. Grazie per tutti i caffè e le chiacchierate. Grazie perché so di poter sempre contare sul tuo supporto.

Desidero poi ringraziare tutti i miei cugini. Essendo figlia unica, siete i fratelli che non ho mai avuto. Nonostante i tenori di vita diversi e la lontananza fisica, sappiate che siete sempre nei miei pensieri. Un pensiero speciale va a Flora, sempre pronta a sostenermi e ad offrirmi la sua spalla, e a Checca, che mi ha insegnato a prendere la vita con ironia. Grazie per esserci sempre state.

Ringrazio poi i miei nipotini, Lorenzo e Serena. Mi avete regalato tante gioie e spero di potervi accompagnare nei vostri percorsi di vita. Siate sempre felici.

Vorrei ringraziare tutti i miei amici.

Matilde, non bastano le parole a descrivere il nostro rapporto. Semplicemente, sono grata per averti incontrata. Grazie per la complicità, per l'intesa. Grazie perché so che, ogni volta che tendo una mano, incontro sempre la tua.

Michela, la nostra amicizia è nata per puro caso, tra i banchi di scuola. Grazie per avermi chiesto di sedermi accanto a te, perché da allora ci siamo legate indissolubilmente.

Ringrazio le mie amiche di sempre. Carmela, Anna e Stefania. Quante corse in bici e quanti pomeriggi trascorsi dietro ad un pallone. Mi auguro che la spensieratezza sia sempre parte del legame che ci unisce e che, anche quando la vita dirama le nostre strade, possiamo sempre e comunque ritrovarci.

Ringrazio di cuore le mie colleghe e amiche Maria Concetta, Chiara e Lory. Nonostante vi abbia estenuate, tra ansie e apprensioni, non avete mai rinunciato ad incoraggiarmi e ad aiutarmi. La distanza non ci ha permesso di vivere appieno questi anni universitari, ma sono certa che recupereremo.

Grazie agli amici che non vedo e sento tutti i giorni, ma che sento sempre vicini: Ilenia, Riccardo, Caterina e Giulia. Abbiamo iniziato assieme il percorso universitario ed anche se abbiamo intrapreso percorsi diversi, ci attendono ancora tanti caffè da prendere assieme.

Desidero ringraziare le mie coinquiline: Marina, Melissa, Alice, Giulia e Milena. Grazie per tutte le chiacchierate e per aver condiviso con me un pezzetto di vita. Sono stata davvero fortunata a conoscere persone come voi.

Infine, ringrazio Carmine, l'amore della mia vita. Sei la prova che, anche dagli eventi peggiori che la vita possa propinare, può nascere qualcosa di bello. Sei stato una ventata di aria fresca, nel momento in cui credevo di soffocare. Sappi che non c'è nulla di più dolce che perdermi nei tuoi occhi. Ti amo.